Spontaneous CP violation in the Next-to-Minimal Supersymmetric Standard Model

Thesis submitted to the University of Glasgow
for the degree of Doctor of Philosophy

June 2000

Alessandro Usai

Department of Physics and Astronomy
University of Glasgow

Abstract

In this thesis we will investigate CP violation within the Next-to-Minimal Supersymmetric Standard Model (NMSSM).

The study of the violation of the CP symmetry is relevant for several reasons. The origin of CP symmetry violation observed experimentally in the kaon system and nowhere else, is still uncertain and under active investigation. Also, and perhaps more intriguing, CP violation is a necessary ingredient of explanations of baryogenesis: supersymmetric theories allow for several sources of CP violation, whether explicit or not, therefore guaranteeing the necessary amount of CP violation. In fact, there are potentially so many CP violating phases, that it is an issue whether supersymmetry is compatible with the tight experimental constraints on the electron and neutron electric dipole moments.

In particular we will concentrate on the study of Spontaneous CP Violation (SCPV), where the vacuum is CP non conserving. In the Standard Model, although the Electroweak symmetry is spontaneously broken, SCPV cannot occur, as at least two Higgs doublets are needed. Also, within the simplest extension of the Standard Model, the Minimal Supersymmetric Standard Model, SCPV, although possible in principle, is ruled out experimentally.

Here we will show a detailed analysis of possible SCPV under general assumptions within the NMSSM. The implications of this are also addressed both for experiments at high energy colliders and also at low energy for the neutron and electron electric dipole moments when the CP violating phases are large. We have considered these phases as arbitrary parameters, and have studied the consequences as a function of the amount of CP violation present.

In chapter 1 and 2 we briefly review the MSSM and the NMSSM.

In chapter 3 we review the literature on SCPV, in both models, as a comparison. We also discuss the assumptions and formalism which will be used extensively in the following analysis.

In chapter 4 we discuss weak SCPV [1] and its possible experimental consequences. The study of this scenario will effectively constitute the main aim of this work.

In chapter 5 we present a thorough numerical analysis of SCPV both weak and not, over a vast area of the parameter space. The chapter also includes a discussion of the Higgs sector when CP is not violated, and when it is violated explicitly.

In chapter 6 we address the issue of whether SCPV within the NMSSM is experimentally testable with emphasis on the weak SCPV case.

In chapter 7 we then discuss the constraints coming from the neutron and electron electric dipole moments, which are relevant when SCPV is not weak.

We then summarise our overall conclusions.

---

[1]'Weak' means 'with small CP violating phases'. Except in chapter 5, we are considering only CP violation in the Higgs sector, not in strong interactions.

Contents

Chapter 1

Minimal Supersymmetric extension of the Standard Model

This first chapter is devoted to an introduction of the Minimal Supersymmetric extension of the Standard Model (MSSM) and the formalism involved.

We will not discuss the theoretical background involved in supersymmetry and refer to [1] [2] [3] [4] [5] for a thorough discussion of the subject.

1.1 MSSM

The MSSM is the simplest supersymmetric extension of the Standard Model (SM).

The first difference from the SM is that we need not less than two chiral superfields H_1, H_2 to give mass to the down and up generations of quarks, meaning in turn that two Higgs doublets have to be considered, whereas in the SM one Higgs doublet is enough.

The superpotential of the MSSM is

$$W = \mu \epsilon_{ij} H_1^i H_2^j + W_{l'} \tag{1.1}$$

where H_1 and H_2 are the two Higgs doublets,

$$H_1 = \begin{pmatrix} H_1^{0*} \\ -H_1^- \end{pmatrix} \quad H_2 = \begin{pmatrix} H_2^+ \\ H_2^0 \end{pmatrix} \tag{1.2}$$

$\epsilon_{12} = -\epsilon_{21} = 1$, $\epsilon_{11} = \epsilon_{22} = 0$, and W_F contains the Yukawa terms

$$W_F = \epsilon_{ij}(f H_1^i \tilde{L}^j \tilde{R} + f_1 H_1^i \tilde{Q}^j \tilde{D} + f_2 H_2^j \tilde{Q}^i \tilde{U}) \tag{1.3}$$

where f_i are the Yukawa coupling constants.

As it is, supersymmetry forbids the appearance of H_1^* and H_2^*; on the other hand gauge invariance forbids the appearance of couplings like $H_1 Q U$ where Q is the quark doublet and U is the quark singlet. Consequently no up-quark mass can be generated if H_2 is not present. It is clear that a charged Higgs boson will be present in the theory too.

It should be noted that many other terms can in theory be present in the superpotential, which, however, violate explicitly the baryon or lepton numbers; these terms are phenomenologically hard to handle, so that it is customary to omit them on the basis of a so called R-symmetry invariance, according to which particles have R-charge equal to +1, whereas s-particles have a R-charge equal to -1. This in turn means that a lightest stable s-particle has to be present, with possible consequences for the amount of dark matter in the Universe.

Supersymmetry has to be broken as otherwise particles and s-particles would have the same mass, which is clearly against the experimental evidence. Supersymmetry is assumed to be broken spontaneously at a certain scale M_S, although the details of how this happens are still a matter of discussion. It is for this reason that we introduce extra terms which explicitly break supersymmetry without impinging on the renormalizability of the resulting lagrangian. This means that the couplings of these terms have to be soft, that is to say of positive dimension lower than four as all the dimension four terms have to respect supersymmetry.

The resulting expression for the effective potential, which also includes the SUSY soft-breaking terms, is then the following

$$V = \frac{g^2}{8} \left(4 \, |H_1^* H_2|^2 - 2 \, (H_1^* H_1)(H_2^* H_2) + \tag{1.4}$$

$$+(H_1^\star H_1)^2 + (H_2^\star H_2)^2 \Big) +$$

$$+\frac{g'^2}{8} \left(H_2^\star H_2 - H_1^\star H_1 \right)^2 +$$

$$+\mu^2 \left(H_1^\star H_1^i + H_2^\star H_2^i \right) + V_{SB}$$

where V_{SB}, containing all the possible the soft-breaking terms, is

$$V_{SB} = m_1^2 \left(H_1^\star H_1 \right) + m_2^2 \left(H_2^\star H_2 \right) - \left(m_{12}^2 \, \epsilon_{ij} \, H_1^i H_2^j + h.c. \right)$$

where m_1, m_2, m_{12} have dimensions of mass.

It should be noted that we are implicitly ignoring the contribution of W_F to the effective potential on the basis that we assume the s-quark and s-lepton fields not to acquire a vacuum expectation value (vev), so that the colour and lepton numbers remain unbroken. This assumption will be held throughout the whole of this work.

We have spontaneous breaking of the electro-weak symmetry (SBEWS) once the neutral Higgs bosons fields acquire vevs

$$< H_1 > = \begin{pmatrix} v_1 \\ 0 \end{pmatrix} \quad < H_2 > = \begin{pmatrix} 0 \\ v_2 \end{pmatrix} \tag{1.5}$$

with v_1, $v_2 > 0$ so that we define $\tan\beta = \frac{v_2}{v_1}$ with $0 \le \beta \le \pi/2$. The fields ϕ_1^- and ϕ_2^+ are assumed not to take a vev as otherwise electric charge number violation would occur.

Note that the vevs are taken to be real; this, as we will see in the forthcoming chapters, means that no spontaneous CP violation is assumed. A problem of naturalness arises as, for the SBEWS to occur, μ is required to be ≤ 1 TeV while at the same time there is no reason why it should not be of the order of the unification scale ($\sim 10^{16}$ GeV); this is part of the so called μ puzzle, which we will discuss more extensively in connection with the Next-to-Minimal Supersymmetric Model (NMSSM).

The μ-term can always be reabsorbed in the redefinition of the soft terms m_1^2 and m_2^2; these on the other hand can be traded for v_1 and v_2 through the minimising conditions imposed on the effective potential, to insure that at (v_1, v_2) the effective potential has a stationary point;

this will of course need to be a minimum [1] for the SBEWS to occur. We have the resulting spectrum of three neutral and one charged Higgs bosons [2]

$$m_{A^0}^2 = M_{H^+}^2 - M_W^2 \tag{1.6}$$

$$m_{H^0,h^0}^2 = \frac{1}{2}\left(m_{A^0}^2 + m_Z^2 \pm \sqrt{(m_{A^0}^2 + m_Z^2)^2 - 4\,m_Z^2\,m_{A^0}^2\,cos^2 2\beta}\right) \tag{1.7}$$

where A^0 is the pseudoscalar, h^0, H^0 are scalars (H^0 being the heavier of the two), $M_{H^\pm}^2$ is the mass of the charged Higgs boson, and α, the mixing angle, is given by the relations

$$cos2\alpha = cos2\beta\left(\frac{m_{A^0}^2 - m_Z^2}{m_{H^0}^2 - m_{h^0}^2}\right) \tag{1.8}$$

$$sin2\alpha = -sin2\beta\left(\frac{m_{H^0}^2 + m_{h^0}^2}{m_{H^0}^2 - m_{h^0}^2}\right). \tag{1.9}$$

We see that $M_{H^\pm} \geq M_W$, $m_{H^0} \geq m_Z$, $m_{A^0} \geq m_{h^0}$ and $m_{h^0} \leq m|cos2\beta| \leq M_Z$ with $m = min(M_Z, m_{A^0})$, that is to say at the tree level the charged Higgs boson has to be heavier than M_W whereas the lightest neutral Higgs boson has to be lighter than M_Z; on the other hand the other neutral Higgs bosons can be quite heavy.

It is important to note that the picture now outlined holds only at the tree level, and is substantially changed once radiative corrections are added, either using Renormalization Group equations (RGE) or adding corresponding loop corrections to the effective potential, so that the MSSM is not yet ruled out by the data (see [7]). We will discuss more extensively the issue of radiative corrections in the next chapters.

---

[1]In the MSSM a minimum will automatically be also absolute; this is not the case for the NMSSM, as we will see in the forthcoming pages.

[2]For a discussion of the expansion of the neutral Higgs fields in term of the physical fields we refer to the Appendix C.

Chapter 2

The Next-to-Minimal Supersymmetric Standard Model (NMSSM)

2.1 Introduction

The NMSSM is an extension of the MSSM, where a singlet field under the gauge group $SU(3) \times SU(2) \times U(1)_{em}$ is added to the superpotential. The motivations for so extending the MSSM are several:

1) A possible solution for the so called μ-puzzle.

2) The upper bound on the lightest Higgs boson in the MSSM makes it reachable in the near future by LHC, so that if no evidence is found an alternative model will be needed.

3) NMSSM allows for Spontaneous CP Violation (SCPV), as we will discuss in the forthcoming pages, this in turn having possible far reaching consequences for CP violation as observed in the Kaon system, and for baryogenesis.

In the MSSM the superpotential contains the term $\mu H_1 H_2$. As already mentioned in the first chapter, the parameter μ can be in principle of the order M_{Planck} although a value of the order of the soft masses, responsible for the supersymmetry breaking, is required for the electroweak symmetry breaking to occur at the right energy scale of around

200 GeV, so that a hierarchy problem arises.

In the NMSSM μ can be traded for the coupling of the singlet scalar field to H_1 and H_2, the two Higgs doublets, so that a term such as $\lambda N H_1 H_2$ is present in the superpotential instead[10]: the soft breaking terms can then induce a vev for the field N of the right order of magnitude. A self coupling term of the form $k N^3/3$ has to be present in the model in order to break the unwanted Peccei-Quinn symmetry

$$N \to N e^{i\theta} , H_1 H_2 \to H_1 H_2 e^{-i\theta}$$

which is spontaneously broken once the Higgs fields take their vacuum expectation values, hence giving rise to an unwanted axion.

2.2 NMSSM

The most general form of the superpotential, with no terms violating the baryon and lepton numbers, is[8]

$$W = \lambda\epsilon_{ij} H_1^i H_2^j N + \mu\epsilon_{ij} H_1^i H_2^j - r N + \frac{1}{2}M N^2 + \frac{1}{3}k N^3 + W_F \quad (2.1)$$

where

$$W_F = \epsilon_{ij}(f H_1^i \tilde{L}^j \tilde{R} + f_1 H_1^i \tilde{Q}^j \tilde{D} + f_2 H_2^j \tilde{Q}^i \tilde{U}) \quad (2.2)$$

is the term giving rise to the Yukawa interactions, f, f_1 and f_2 are the corresponding Yukawa coupling constants and $\epsilon_{12} = -\epsilon_{21} = 1$, $\epsilon_{11} = \epsilon_{22} = 0$; H_1^i, H_2^j are the components of the Higgs doublets

$$H_1 = \left(\begin{array}{c} H_1^{0\star} \\ -H_1^- \end{array} \right) \quad H_2 = \left(\begin{array}{c} H_2^+ \\ H_2^0 \end{array} \right) \quad (2.3)$$

N is the singlet field, $\tilde{L}$ ($\tilde{R}$) and $\tilde{Q}$ ($\tilde{D}$) are respectively the $SU(2)$ weak doublet (singlet) lepton and quark superfields; and k, λ, μ, r, M are parameters (λ and k in particular are dimensionless) which we assume for the moment to be real[1]. Making a shift in the N field, the parameter M in the superpotential can be put equal to zero without loss of

---

[1] This simply means that we do not introduce as yet any explicitly CP violating phases.

generality.

The dimensionful terms in μ and r give rise to a hierarchy problem. We will not discuss in this work the μ-puzzle and so will keep the μ term because it explicitly violates the Z_3 symmetry, with important consequences for SCPV, as we will discuss later. We are in fact interested in the Higgs spectrum and the differences related to the presence of μ.

The scalar potential is a Hermitian function given by [8]

$$V = \frac{1}{2}\left(D^a D a + (D')^2\right) + F_i^* F_i \tag{2.4}$$

where

$$F_i = \frac{\partial W}{\partial A_i} \tag{2.5}$$

$$D^a = \frac{1}{2}\, g\, A_i^*\, \sigma_{ij}^a\, A_j \tag{2.6}$$

$$D' = \frac{1}{2}\, g'\, y_i\, A_i^*\, A_i + \xi \tag{2.7}$$

with A_i indicating all the scalar fields of the theory and y_i their weak hypercharges: H_1 with $y_1 = -1$, H_2 with $y_2 = 1$ and N with $y_3 = 0$. We assume that the parameter ξ is equal to zero.

We now once again introduce extra terms which explicitly break supersymmetry without affecting the renormalizability of the resulting lagrangian (see the first chapter) and the number of which will be bigger than in the MSSM. The resulting effective potential, which also includes the susy soft-breaking terms, is then the following

$$V = \frac{g^2}{8}\left(4\,|H_1^* H_2|^2 - 2\,(H_1^* H_1)\,(H_2^* H_2)+ \right. \tag{2.8}$$

$$\left. +(H_1^* H_1)^2 - (H_2^* H_2)^2\right) +$$

$$+\frac{g'^2}{8}\left(H_2^* H_2 - H_1^* H_1\right)^2 + \left(\lambda\,\epsilon_{ij}\, H_1^i\, H_2^j\, N^{*2} + h.c.\right)+$$

$$+\lambda\mu(N + h.c.)(H_1^* H_1 + H_2^* H_2) + \mu^2\left(H_1^* H_1^i + H_2^* H_2^i\right) +$$

$$+|\lambda\, H_1^i\, H_2^j \epsilon_{ij} - r + k\, N^2|^2 + \lambda^2\left(H_1^* H_1^i + H_2^* H_2^i\right) N^* N + V_{SB}$$

where V_{SB}, containing all the possible the soft-breaking terms, is

$$V_{SB} = m_1^2 \left(H_1^* H_1 \right) + m_2^2 \left(H_2^* H_2 \right) - \left(m_{12}^2 \, \epsilon_{ij} \, H_1^i \, H_2^j + h.c. \right) + \quad (2.9)$$

$$+ m_3^2 \, N^* N + \left(m_5^2 \, N^2 + h.c. \right) + \left(m_4 \, \epsilon_{ij} \, H_1^i \, H_2^j \, N + (1/3) \, m_6 \, N^3 + h.c. \right).$$

However, if the susy breaking scale does not coincide with the electro-weak symmetry breaking one, then the quartic couplings in the effective potential may be determined using the RGE [2].
The resulting effective potential is then

$$V = \frac{1}{2} \, Y_1 (H_1^* H_1)^2 + \frac{1}{2} \, Y_2 (H_2^* H_2)^2 + \quad\quad (2.10)$$

$$+ (Y_3 + Y_4)(H_1^* H_1)(H_2^* H_2) - Y_4 \, |H_1^* H_2|^2 +$$

$$+ (Y_5 \, H_1^* H_1 + Y_6 \, H_2^* H_2) N^* N + (Y_7 \, \epsilon_{ij} \, H_1^i \, H_2^j \, N^{*2} + h.c.) +$$

$$+ Y_8 (N^* N)^2 + \lambda \mu (N + h.c.)(H_1^* H_1 - H_2^* H_2) + \mu^2 \left(H_1^* H_1 + H_2^* H_2 \right) +$$

$$+ V_{SB}$$

where Y_i, i=1,8 are related to the parameters of the superpotential, λ and k, and the gauge couplings; for exact supersymmetry they are:

$$g_1 = g' \; , \; g_2 = g \quad\quad\quad (2.11)$$

$$Y_1 = Y_2 = \frac{1}{4} \left(g^2 + g'^2 \right), \;\; Y_3 = \frac{1}{4} \left(g'^2 - g^2 \right), \;\; Y_4 = \lambda^2 - \frac{1}{2} g'^2$$

$$Y_5 = Y_6 = \lambda^2 \, , \;\; Y_7 = \lambda \, k \, , Y_8 = k^2 \; .$$

The RGE for the Y_i coefficients will in general include quark as well as squark contributions. However, the squarks will not contribute if their masses are bigger than the SUSY breaking scale as in this case they decouple. Furthermore, if a small value of $\tan\beta$ (i.e. ≈ 1) is taken, then the contribution of the bottom quark and squark can be safely ignored compared to the corresponding top and stop ones.
Another way of including radiative corrections is to consider the one loop corrections to the effective potential, taking the values of Y_i equal

---

[2] We have used in particular the RGE of the two doublets model, as we will see in more detail in the next chapter.

to those at the scale where exact supersymmetry holds. This method is particularly suitable if many particles with different mass scales are considered.

In the supergravity inspired models a simple form of SUSY breaking potential is assumed at the SUSY breaking scale, and then the soft masses are also fixed through the RGE [11]. The soft masses are run down to low energies starting from the common values m_0 and A_0 at the unification scale. In this way once we fix m_0 we also fix all the soft masses at low energy. The same can be done both for the soft masses in the Higgs sector and squarks sectors; in the latter case there is a constraint on the value of the tri-linear coupling at the unification scale (A_0) [12][13] coming from the requirement that the minimum of the effective potential be such as not to break the charge and colour charge symmetries. This can be simply imposed to be the case if one assumes that the squark and charged Higgs fields have always vacuum expectation values equal to zero; we rely throughout this work on this assumption.

The RGE of the soft masses are mixed with those of the gauge coupling, Yukawa coupling constants, λ and k parameters. The gaugino masses and μ are not coupled to the soft masses but only to the gauge coupling constants.

In this work we assume a more conservative approach: we take all the soft masses as independent and free to take any value, positive or negative, at the electro-weak scale, as the form of the soft masses is assumed not to change, unlike the parameters Y_i. This in a way makes predictions more difficult as they will be dependent on more parameters.

Chapter 3

SCPV in the NMSSM

3.1 Introduction

SCPV arises when the lagrangian before the electro-weak symmetry breaking is CP invariant whereas the vacuum is not, so that CP violating phases will emerge once the Higgs fields and/or any of the singlet fields take their vacuum expectation values [15].

If the effective potential were to be invariant under such discrete symmetry transformations before the spontaneous breaking of the electroweak symmetry, then afterwards the discrete symmetry would be spontaneously broken too, so that there would be regions of the universe with different vacuum states. Among these regions domain walls would form whose energy density becomes bigger than the energy density of matter as the Universe expands, in contrast with what we observe today. This is the well known domain walls problem and is unavoidably present when any discrete symmetry is spontaneously broken and so also when the CP symmetry is spontaneously broken [16], under the assumption that symmetry restoration does occur at high temperature. A possible way to lift the vacua degeneracy, so that no domain walls arise, has been shown in [17]; another possibility is that an explicit CP violating phase is also present.

It is well known that SCPV cannot occur in the SM as any phase on the vev can be removed by a rotation of the Higgs field. This then led to the analysis of SCPV within the two Higgs doublets model, where

indeed SCPV is feasible. However, in this model problems arise related
to flavour changing neutral currents as well as electric charge number
violation, which occurs when after SSB the $U(1)$ symmetry of electro-
dynamics is broken (see [7], [14]).

Within the MSSM SUSY guarantees the absence of flavour changing
neutral currents as well as that the vacuum does not violate the electric
charge number. However, at the tree level SCPV cannot occur due to
the residual influence of SUSY itself, which hinders the presence of

$$\lambda_5 \left[\left(H_1^\dagger H_2 \right)^2 + \left(H_2^\dagger H_1 \right)^2 \right]$$

(the effective potential in the two Higgs doublets model instead does
contain the above term), this in turn constraining the phase associated
to one of the vevs of the two neutral Higgs fields to be equal to either
zero or multiples of π (just one phase can be present, as the other one
can always be rotated away).

This is only true at the tree level though as when radiative corrections
are added on a $\delta\lambda_5$ can be generated, so that SCPV is then possible
in the MSSM too [14]. However, it was pointed out in [18] that SCPV
in the MSSM leads to the presence of a too light pseudoscalar neutral
Higgs boson, in agreement with the Georgi-Pais theorem [19], so that
experimentally the scenario is ruled out (we will discuss this theorem
and its extension in 4.2).

3.2   SCPV within NMSSM

In this section we discuss SCPV in the NMSSM.

If we take the vacuum expectation values (v.e.v.) of H_i^0 $(i = 1, 2)$ and
N to be dependent on a phase then SCPV may occur.

Indeed it has been shown by [9] that this is the case even for exact
SUSY and at the tree level if Z_3 symmetry violating terms are present
in the effective potential. A general Z_n discrete transformation, with n
an integer number, transforms a generic field ϕ in the effective potential
such that

$$\phi \to e^{i 2\pi/n} \phi.$$

If on the other hand a Z_3 symmetry is imposed on the effective potential then SCPV is not possible, as shown in [21].

In the field dependent effective potential those terms in r and $\lambda\mu$ are Z_3 symmetry violating together with the terms in m_5 and m_{12}. There are no other possible Z_n symmetries except for a possible Z_2 symmetry which is violated by the terms in $\lambda\mu$, m_4 and m_5.

The papers reviewed give a wide idea about the phenomenological implications of the scenario, keeping an eye to our analysis, which we describe in the next chapters. In all the papers no Z_3 symmetry violating terms are considered (and so $\mu=0$), contrary to what we do, so that the analysis we will present in the next chapters is more general. The main conclusion which can be drawn is that the scenario is feasible and of strong interest, especially in view of the LHC advent.

In the NMSSM with the Z_3 symmetry imposed SCPV can still be triggered by radiative corrections both at zero and finite temperature[22] [23][24][25], although at zero temperature the problem of a small mass for the lightest neutral Higgs boson reappears, as in the MSSM.

In [25] the stops and top contributions to the one-loop part of the effective potential are taken into account and the induced changes to the Higgs bosons mass matrices considered. The masses of the stops are taken to be degenerate. For the scenario to be feasible very heavy stops are required, with a mass of the order of 3 TeV and so beyond the reach of LHC, in order to have the lightest neutral Higgs boson being as heavy as possible. Furthermore, strong constraints on the value of $\tan\beta$, λ and A_λ/A_k are required, where A_λ, A_k are soft scalar masses (the corresponding terms in V_{soft} are $\lambda A_\lambda H_1 H_2 N$ and $\frac{k A_k}{3} N^3$). The charged Higgs boson mass is

$$M_{H\pm}^2 = M_W^2 + (3r - 1)\lambda^2 v_0^2 \tag{3.1}$$

where in this formula $r = A_\lambda/A_k$. From the requirements for the sub-determinants of the neutral Higgs mass matrix to be positive together with the condition for the minimum of the potential to break the CP symmetry the following constraint is obtained

$$0 < (4r - 1)\lambda^2 < \frac{1}{2}\frac{M_Z^2}{v_0^2}(\sqrt{1 + \Delta} - 1) \tag{3.2}$$

where Δ comes from the radiative corrections.

An upper bound on the charged Higgs mass of about 110 GeV results which, although not ruled out directly [26], [27], is far below the lower limit obtained indirectly by [28].

However, the same analysis has been carried out in [29] without assuming the squarks to be degenerate, and the conclusions found there are quite different from [25]. The off-diagonal elements of the squark mass matrices contribute this time to the Δ term in [25]. It is found that the off-diagonal elements increase with v_3 so that $M_{H^\pm}$ can take much bigger values, namely around 700 GeV, for squark masses around 3 TeV, and so far beyond any present experimental upper bound.

In [30] a Z_3 conserving NMSSM superpotential is considered and the RG equations of the two Higgs doublets model for the parameters Y_i used, together with the constraints on the λ and k parameters coming from the requirements that perturbation theory holds up to the unification scale[31]. The SUSY scale is taken to be 1 TeV and 10 TeV. The resulting radiative corrections to the tree level quartic terms allow the Higgs bosons mass matrix to be positive definite so that real masses for the neutral Higgs bosons can arise, unlike the case when the SUSY breaking scale is equal to 100 GeV. The corresponding bound on the lightest and second lightest Higgs bosons masses have been obtained as a function of $\tan\beta$ and it is found that the mass of the lightest Higgs boson m_{h_1} is such that $m_{h_1} < 20$ GeV for a SUSY breaking scale equal to either 1 TeV or 10 TeV. In particular they find in both cases that m_{h_1} gets smaller as $\tan\beta$ increases, so that the highest value of m_{h_1} is found when $\tan\beta$ is small. The bounds are clearly well below the current experimental limits shown in [27], although the singlet component in the lightest neutral Higgs field can be dominant.

Also, $M_{H^\pm}$ is found to be smaller than 110 GeV for a SUSY breaking scale of 10 TeV, and 95 GeV for a SUSY breaking scale of 1 TeV respectively. For $\tan\beta$ equal to 2-3 $M_{H^\pm}$ has an upper bound equal to about 90 GeV for both the cases. These bounds are in disagreement with the indirect experimental bounds established by [28], although not yet ruled out directly [26].

In [39] the same authors present an analogous analysis where the one-loop corrections to the parameters Y_i are added, the superpotential being just the same as in [30]. For the one-loop corrections only t

and b quarks and squarks are considered, all the other contributions being negligible. High values of tanβ can now be considered and it is found that certain intervals of tanβ are experimentally excluded. This can be assessed thanks to the assumption of m_{h_1} being 90 percent singlet and 95 percent respectively. As in [30] the danger of too a low bound on $M_{H\pm}$ arises again, although this time is less severe. This is because adding the one-loop corrections changes significantly the resulting charged Higgs boson mass, namely $M_{H\pm} < 115$ GeV for SUSY breaking scale of 1 TeV without one- loop corrections against $M_{H\pm} < 140$ GeV with the one-loop corrections whereas for the lightest Higgs boson mass we have $m_{h_1} < 90$ GeV without the one-loop corrections and still the same once the one-loop corrections are added as these have no significant effect on the neutral Higgs bosons mass matrix. This is to be compared with what happens when one naively adds up to the tree level effective potential the one-loop corrections coming from top and stops: in this case in fact the mass bound on m_{h_1} is shifted upwards[29] [1].

In the next section the NMSSM model and the relevant notation used are introduced.

3.3   SCPV: a model

We will study in the following pages SCPV in the NMSSM at the tree level including those terms which violate the Z_3 and Z_2 symmetry. We do so because the μ-term and other soft terms can influence the resulting mass spectrum and allow more possibilities for SCPV.

After the electro-weak symmetry breaking the scalar potential is the following real function

$$V = \frac{1}{2}(Y_1\, v_1^4 + Y_2\, v_2^4) + (Y_3 + Y_4)\, v_1^2 v_2^2 + (Y_5\, v_1^2 + Y_6\, v_2^2)\, v_3^2 + \qquad (3.3)$$

$$+2\, Y_7\, v_1\, v_2\, v_3^2\, cos(\theta_1 + \theta_2 - 2\theta_3) + Y_8\, v_3^4 +$$

---

[1]It is not always to be expected that quantum corrections should increase the masses at the tree level; in fact it is found in the MSSM (and no SCPV) that the second-loop corrections tend to decrease the mass bound rather than increase it [43], [44].

$$+\mu^2 \left(v_1^2 + v_2^2\right) + 2\,\lambda\,\mu\left(v_1^2 + v_2^2\right) v_3\, cos(\theta_3)\ |$$

$$+m_1^2\, v_1^2 + m_2^2\, v_2^2 + m_3^2\, v_3^2 + 2\, m_5\, v_1\, v_2\, v_3\, cos(\theta_1 + \theta_2 + \theta_3) + \frac{2}{3} m_6\, v_3^3\, cos(3\theta_3) -$$

$$-2\, m_{12}^2\, v_1\, v_2\, cos(\theta_1 + \theta_2) + 2\, m_4^2\, v_3^2\, cos(2\theta_3)\ .$$

We are for the moment assuming a generic SUSY breaking scale, as discussed in the first section.

At the minimum we must have $v_1^2 + v_2^2 = (174\,GeV)^2$ in order to get the correct values for the masses of the $W^\pm$ and Z vector bosons. As it is, the potential allows for a redefinition of the phases such that without loss of generality we can take $\theta_2 = 0$. SCPV will occur if at the minimum θ_1 and/or $\theta_3 \neq n\pi$.

Besides the soft-breaking masses, we then have the following variables: $tan\beta = \frac{v_2}{v_1}$, v_3, θ_1, θ_3, μ, λ and k. The Y_i coefficients are determined through the RGE, which are the subject of the next subsection.

3.4 RG equations and the λ and k parameters

In this work we used the one loop RGE of the two doublets model, which are the following:

$$16\,\pi^2\, \frac{\partial Y_i}{\partial t} = f_i\,,\ i = 1,\cdots,8 \tag{3.4}$$

where $t = ln\left(\frac{Q}{100\,GeV}\right)$ where Q is the renormalization point and the $f_i\, i = 1,\cdots,8$ coefficients are given in the appendix A.

The RGE for the gauge coupling constants and the top Yukawa coupling constant are respectively, at the one loop order

$$16\,\pi^2\, \frac{\partial g_i}{\partial t} = -c_i\, g_i^3 \tag{3.5}$$

where $g_2 = g'$, $g_1 = g$,

$$c_1 = -7\,,\ \ c_2 = 3\,,\ \ c_3 = 7 \tag{3.6}$$

and

$$16\,\pi^2\,\frac{\partial h_t}{\partial t} = h_t\,(\frac{9}{2}\,h_t^2 - \frac{17}{12}\,g_1^2 - \frac{9}{4}\,g_2^2 - 8g_3^2) + \frac{1}{2}\,h_t\,h_b^2 \qquad (3.7)$$

$$16\,\pi^2\,\frac{\partial h_b}{\partial t} = h_b\,(\frac{9}{2}\,h_b^2 + \frac{1}{2}h_t^2 - \frac{5}{12}\,g_1^2 - \frac{9}{4}\,g_2^2 - 8g_3^2)\,. \qquad (3.8)$$

The bottom quark contribution can be ignored for small values of $\tan\beta$. The relationship among the Y_i ($i = 1 \cdots 8$) coefficients and the gauge coupling constants, λ and k parameters of the superpotential for exact supersymmetry are, as we have already seen, the following:

$$Y_1 = Y_2 = \frac{1}{4}\,(g_1^2 + g_2^2)\,, \quad Y_3 = \frac{1}{4}\,(g_2^2 - g_1^2)\,, \quad Y_4 = \lambda^2 - \frac{1}{2}\,g_2^2 \qquad (3.9)$$

$$Y_5 = Y_6 = \lambda^2\,, \quad Y_7 = \lambda k \quad Y_8 = k^2\,.$$

The values of the coupling constants at the electro-weak scale are

$$g_1 = 0.358\,, \quad g_2 = 0.651\,, \quad g_3 = 1.218\,. \qquad (3.10)$$

It has been shown by [31] that if perturbation theory is to be valid up to the unification scale then the λ and k parameters have to have values in the following ranges

$$|k| \leq 0.63\,, \quad |\lambda| \leq 0.87 \qquad (3.11)$$

with roughly

$$\lambda^2 + k^2 \leq 1. \qquad (3.12)$$

This is still true when SCPV is considered as the RG equations for λ and k do not change[2].

The procedure is then the following: once the SUSY breaking scale Q is fixed, the gauge coupling constants are run from the known values at the electro-weak scale up to Q; the Y_i coefficients at the scale Q are then determined and the RGE are run down to obtain the Y_i coefficients at the electro-weak scale.

Before ending this subsection some remarks are required.

We are allowed to use the two doublets RGE between the electro-weak

---

[2]For a further discussion of the λ and k parameters see [34] and [37].

scale and the SUSY breaking scale as long as stops are heavier than the
SUSY breaking scale itself, otherwise their contribution would not be
negligible. However squarks cannot be too heavy as otherwise the Higgs
bosons would get too large contributions from loop diagrams involving
squarks so that for a SUSY breaking scale higher than 1 TeV the full
RGE should be taken in order to allow stops with a mass around one
TeV or less.

In principle we should include the b quark contribution too, although
this will be certainly smaller that the t quark contribution.

3.5   Mass spectrum

The mass matrix for the neutral Higgs bosons can be easily calculated
from the field dependent potential as

$$M_{ij}^2 = \frac{\partial V}{\partial A_i \partial A_j} \ (i,j = 1,6) \tag{3.13}$$

where A_i are this time the real and imaginary parts of the neutral fields,
namely H_1^0, H_2^0 and N. The resulting symmetric mass matrix will be
field dependent.

At the minimum of the potential its eigenvalues will then be the squared
masses of the neutral Higgs bosons.

For the SCPV case there is mixing between the scalar 3x3 mass matrix
S and the pseudo scalar 3x3 one PS, that is to say the mixing matrix
MX will not be equal to the zero matrix:

$$M^2 = \left(\begin{array}{cc} S & MX \\ MX & PS \end{array} \right). \tag{3.14}$$

We are here taking the imaginary part of H_2^0 and H_1^0 as independent
fields, which is the reason why the mass matrix squared is 6x6, whereas
in the unitary gauge, taking the imaginary parts to be respectively
$\cos\beta\, A$ and $\sin\beta\, A$, with A a neutral scalar field the mass matrix squared
is 5x5 with no Goldstone boson (see Appendix C). In general M^2 has
to be diagonalised numerically. The resulting spectrum consists of one
Goldstone boson and five massive neutral Higgs bosons, the Goldstone

boson being purely in the pseudo-scalar part when CP is conserved.

The charged Higgs mass matrix squared can be diagonalised analytically because it is a 4x4 matrix which is in turn equivalent to two 2x2 equal matrices. The spectrum consists of a Goldstone boson and a massive charged one with mass $M_{H\pm}$ given by the expression.

$$M^2_{H\pm} = -Y_4 \, v_0^2 + (-Y_7 \, v_3^2 \, cos(\theta_1 - 2\,\theta_3) + m^2_{12} \, cos(\theta_1) - \quad (3.15)$$

$$-m_5 \, v_3 \, cos(\theta_1 + \theta_3)) \, \frac{1}{sin\beta \, cos\beta}.$$

This relation is only valid at the tree level.

An important point is that requiring $M^2_{H\pm} > 0$ is a necessary condition for the minima of the effective potential to conserve electric charge.

The neutralino mass matrix is a 5x5 one (see Appendix B) so that this too has to be diagonalised numerically. In general all the five eigenstates will be massive.

To obtain the neutralino masses the absolute value squared of the mass matrix has to be calculated, that is to say $M_n \, M^\dagger_n = |M_n|^2$; we then diagonalise numerically the hermitian matrix so obtained and take the square root of the eigenvalues.

The chargino mass matrix is a 2x2 one (see Appendix B), and again the two eigenstates are in general massive.

The chargino masses can be obtained in the same way as described for the neutralino with the difference that the diagonalisation procedure can be carried out analytically.

The neutral Higgs bosons, neutralino and chargino mass matrices at the tree level are shown in the appendix B under the assumption of the most general superpotential, a generic SUSY scale and independent soft masses.

Once the mass matrices have been diagonalised the resulting masses have to be checked against the current experimental lower limits as there is yet no evidence of any supersymmetric particle.

3.6   Search of the parameter space

The large number of parameters in the NMSSM renders at first sight any numerical analysis problematic. It is clear that to vary independently all the soft-masses as well as $\tan\beta$, v_3, θ_1, θ_3, μ, λ and k would result in an extremely lengthy analysis. Things do not look so bad though if one notices that we are not interested in all the parameter space but only in those regions where the scalar potential has a minimum, which we will then check to see whether it is an absolute one or not. For a point in the five-dimensional space v_1, v_2, v_3, θ_1, θ_3 to be a minimum the necessary but not sufficient condition is that the following equations be satisfied

$$\frac{\partial V}{\partial \theta_1} = 2\,v_3\,m_5\,sin(\theta_1 + \theta_3) - (2\,m_{12}^2\,sin(\theta_1) - \qquad (3.16)$$

$$-2\,Y_7\,v_3^2\,sin(\theta_1 - 2\theta_3) = 0$$

$$\frac{\partial V}{\partial \theta_3} = 4\,m_4^2\,v_3^2\,sin(2\theta_3) + 2\,m_6\,v_3^3\,sin(3\theta_3) - \qquad (3.17)$$

$$-4\,Y_7\,v_1\,v_3^2\,v_2\,sin(\theta_1 - 2\theta_3) +$$

$$+2\,m_5\,v_1\,v_2\,v_3\,sin(\theta_1 + \theta_3) + 2\,v_0^2\mu\,v_3\,k\,sin(\theta_3) = 0$$

$$\frac{\partial V}{\partial v_i} = 0\,,\, i = 1, 2, 3.$$

Imposing the first two equations we fix m_5 and m_4, whereas the last three equations fix m_1^2, m_2^2 and m_3^2 respectively. We can then make sure that these equations are always satisfied by simply fixing five of the soft-masses through the five minimising equations themselves. Furthermore we can trade m_{12}^2 for $M_{H^\pm}$ once we impose the equation (3.15), so that

$$m_{12}^2 = (M_{H^\pm}^2 + Y_4\,v_0^2)\,sin(\theta_1 + \theta_3)\,\frac{sin\beta\,cos\beta}{sin(\theta_3)} - Y_7\,v_3^2\,\frac{sin(3\theta_3)}{sin(\theta_3)} \quad (3.18)$$

As we do not know the value of the charged Higgs mass $M_{H^\pm}$ this has to be varied too, but it can be done within a range above the current experimental upper limit [26], [28], so that we are in this way able to optimise the procedure. Furthermore, we implicitly look for electric

charge symmetry conserving minima as we always require $M_{H^{\pm}}^2 > 0$.

We choose starting values for m_6, $M_{H^{\pm}}$, μ, λ, k. Once this is done the Y_i $(i = 1, \cdots 7)$ can be determined through the RGE once the supersymmetry breaking scale is fixed. We also choose starting values for $\tan\beta$, v_3, θ_1, θ_3, namely the values at which we want our potential to have a minimum. As the chosen point might be a point of maximum or inflection an iterative numerical search is required. A minimum is signaled by the fact that the eigenvalues of the mass matrix squared of the neutral Higgs bosons are all positive at the point.

Numerical searches in other parts of the parameter space are necessary to ensure that the prescribed vevs correspond to a global minimum.

We will discuss in chapter 4 an analytical as well as numerical study of the neutral Higgs boson mass matrix.

Chapter 4

Weak SCPV within the NMSSM

4.1 Introduction

In this chapter we discuss SCPV when the CP violating phases are small. The issue of how small these phases have to be for the results shown in the forthcoming pages to hold will be discussed in the next chapter, where a numerical analysis is shown.

In the second section we present a general result which has the status of a theorem and which can be compared with the Georgi-Pais theorem [19].

In the third section we explicitly refer to the NMSSM and discuss the theorem of section two within the context of the model.

4.2 A general result

In this section we present a general result [20] for those models where SCPV can occur at the tree level.

Our result is a variant of the Georgi-Pais theorem [19], which discusses the conditions under which radiative corrections can break a discrete symmetry, which is apparently conserved at the tree level. A massless scalar field is required to be present in the CP conserving theory, which

acquires a small mass once radiative corrections are added and the CP symmetry spontaneously broken.

The argument relies on the smallness of the radiative corrections, which in turn allows a Taylor expansion around the CP violating minimum. The key step in the proof is the equation

$$\sum_k \frac{\partial^2 V}{\partial \phi_j \partial \phi_k} \left((U\delta\lambda)_k - \delta\lambda_k \right) = 0 \qquad (4.1)$$

where $V(\phi)$ is the field dependent scalar potential, ϕ_j are spinless meson fields, the vector λ is the value of ϕ at which the minimum of the scalar potential occurs, U is the CP symmetry operator and $\delta\lambda$ is the change due to radiative corrections. $U\lambda = \lambda$ if there is no spontaneous symmetry breaking, and from the above expression it is immediately clear that if the mass matrix $\frac{\partial^2 V}{\partial \phi_j \partial \phi_k}$ is not singular the relation $U\delta\lambda = \delta\lambda$ holds and no SCPV occurs. On the other hand if a massless particle is present in the unbroken theory then the mass matrix is singular and we can have SCPV due to the radiative corrections. The massless mode will gain a small mass as a result of the radiative corrections. It is this mechanism which produces the light scalar when SCPV is induced in the MSSM or NMSSM with Z_3.

This theorem still holds if Goldstone bosons are present in the model, as the transformation $\delta\lambda$ can be chosen orthogonal to the Goldstone-boson subspace.

As stated in the paper the key assumption for the theorem to work is that the spontaneous symmetry breaking is perturbative.

We will now show[20] with a similar argument that if SCPV is weak, that is to say the CP violating phases attached to the vevs are small, then there is in the model a quasi massless scalar particle. The smallness of the CP violating phases is this time the key assumption, as the smallness of the quantum corrections to the tree level effective potential was in [19].

Refering to the scalar potential in the NMSSM, for small CP violating phases the potential has two nearby minima at the points

$$\underline{\epsilon}_1 = (v_1, v_2, v_3, v_1\theta_1, v_3\theta_3) \qquad (4.2)$$

$$\underline{\epsilon}_2 = (v_1, v_2, v_3, -v_1\theta_1, -v_3\theta_3).$$

If we then perform a Taylor expansion

$$(\underline{c}_2 - \underline{c}_1)_j \frac{\partial^2 V}{\partial \phi_j \partial \phi_i}\Big|_{\underline{c}_1} \approx \frac{\partial V}{\partial \phi_i}\Big|_{\underline{c}_2} - \frac{\partial V}{\partial \phi_i}\Big|_{\underline{c}_1} = 0 - 0 \qquad (4.3)$$

so that the mass matrix squared of the Higgs bosons is singular and a massless particle results as a consequence. This is clearly only an approximation although at the limit for the CP violating phases going to zero this will be exactly true. In the limit of the CP violating phases going to zero the mass matrix is block diagonal and $(\underline{c}_2 - \underline{c}_1)$ is an eigenvector of the pseudo-scalar block.

This result is general and so the issue arises of whether this scenario is in agreement with the experimental bounds on the lightest Higgs boson mass. We will discuss this extensively in chapter 6.

4.3 Weak SCPV within the NMSSM

We have seen in the previous section that a light eigenmode arises when SCPV is weak, and that this eigenmode is to be found in the CP odd sector, which almost decouples from the CP even sector as the phases get smaller and smaller. We show here an analysis of the CP odd mass matrix and its corresponding eigenvalues and eigenvectors. The CP odd part of the 6x6 matrix can in fact be assumed to be decoupled to first approximation if the CP phases are small enough, as the off-diagonal block elements of the mass matrix squared are proportional to $\sin\theta_i$, $i = 1, 3$. Considering the CP odd 3x3 matrix (see appendix B), if we add to the elements of the first column those of the second one multiplied by v_2/v_1 we obtain a zero column, corresponding to a Goldstone boson, so that the matrix is reduced to a 2x2 one, which can be written as

$$\begin{pmatrix} \frac{A}{\sin\beta\cos\beta} & \frac{v_0}{v_3} B \\ \frac{v_0}{v_3} B & C \end{pmatrix}. \qquad (4.4)$$

where A is the (5,4) element of the whole 6x6 mass matrix, B is equal to $(6,4)\frac{v_2}{v_3}$, and C is equal to the (6,6) element.

The expressions for m_1^2, m_2^2, m_3^2, m_4^2, obtained from 3.6, and m_5 and

m_{12}^2, given in 3.16, 3.17 respectively, have then to be substituted into the matrix elements. For this 2x2 matrix we just have to consider m_4^2, m_5 and m_{12}^2.

As we are interested in the eigenvalues of the mass matrix at the minimum, the v_i, i=1,3 and θ_1, θ_3 in the matrix and those in the minimising equations fixing the soft masses above and in the expression of m_{12}^2 are the same.

Because we are explicitly interested in the case with small CP violating angles, we can take Taylor expansions of the trigonometric functions in the expressions of m_5, m_6 and m_{12}^2. We consider three regimes, namely when θ_1 is negligible compared to θ_3, when the opposite is true, and when the two phases are of the same order.

In general, if $\theta_1 \ll \theta_3$ the eigenvector

$$(\underline{e}_2 - \underline{e}_1)_j \approx (0,0,0,0,0,2v_3\theta_3) \tag{4.5}$$

is in the pseudoscalar singlet part of the mass matrix, i.e. the lightest neutral Higgs boson is singlet. Likewise, if $\theta_1 \gg \theta_3$ the lightest neutral Higgs boson is doublet.

In particular, the equations for m_{12}^2, m_4^2 and m_5 are once again just the equations (3.18), (3.16), (3.17); they will be, for the three regimes, the following:

Case(a) $\theta_1 \ll \theta_3$

$$m_{12}^2 = \left(M_{H^\pm}^2 + Y_4\, v_0^2\right) sin\beta\, cos\beta + 3\, Y_7\, v_3^2 \tag{4.6}$$

$$m_5 = 2\, Y_7\, v_3 \tag{4.7}$$

$$m_4^2 = -\left(6\, m_6\, v_3^3\, \theta_3 + 8\, Y_7\, v_1\, v_3^2\, v_2\, \theta_3 + \right. \tag{4.8}$$

$$\left. +2\, m_5\, v_1\, v_2\, v_3\, \theta_3 + 2\, \mu\, v_0^2\, v_3\, k\, \theta_3\right)/\left(8\, v_3^2\, \theta_3\right)$$

Case(b) $\theta_3 \ll \theta_1$

$$m_{12}^2 = \left(M_{H^\pm}^2 + Y_4\, v_0^2\right) sin\beta\, cos\beta\frac{\theta_1}{\theta_3} + 3\, Y_7\, v_3^2 \tag{4.9}$$

$$m_5 = m_{12}^2\, /v_3 - Y_7\, v_3 \tag{4.10}$$

$$m_4^2 = -\left(-4\, Y_7\, v_1\, v_3^2\, v_2\, \theta_1 + 2\, m_5\, v_1\, v_2\, v_3\, \theta_1\right)/\left(8\, v_3^2\, \theta_3\right) \tag{4.11}$$

and

Case(c) $\theta_1 \sim \theta_3$

$$m_{12}^2 = \left(M_{H\pm}^2 + Y_4\,v_0^2\right)(k+1)\,sin\beta\,cos\beta + 3\,Y_7\,v_3^2 \qquad (4.12)$$

$$m_5 = m_{12}^2\,k\,/(v_3(k+1)) - Y_7\,v_3\,(k-2)/(k+1) \qquad (4.13)$$

$$m_4^2 = -\left(2\,m_6\,v_3^3\,\theta_3 - 4\,Y_7\,v_1\,v_3^2\,v_2\,(k-2)\theta_3\right)+ \qquad (4.14)$$

$$+2\,m_5\,v_1\,v_2\,v_3\,(k+1)\theta_3 + 2\,\mu\,v_0^2\,v_3\,k\,\theta_3\Big)\,/(8\,v_3^2\,\theta_3).$$

These equations are exactly the ones required so that the 2x2 matrix, remnant of the CP odd 3x3 mass matrix, has a zero eigenvalue. Taking the whole 6x6 mass matrix, this will be a small eigenvalue, rather than a zero one, as the elements coupling the CP even to the CP odd sectors are very small but non zero.

The first three equations imply that the elements C and B are zero, but $A \neq 0$, so that the light particle will be almost completely in the N sector; the second set will imply that A and B are zero, but $C \neq 0$ so that the massless particle will be almost exclusively in the $H_1 H_2$, sector, whereas for the third set

$$\frac{AC}{sin\beta cos\beta} - \frac{v_0^2}{v_3^2}B^2 = 0$$

and the particle will be a mixture of Higgs fields and the singlet field. Furthermore, in the case $\theta_3 << \theta_1$ the equation for m_{12} and the equation for m_5 and m_4 can be combined to give an upper bound on the mass of the charged Higgs boson M_{H^+}

$$M_{H\pm}^2 = -Y_4\,v_0^2 = M_W^2 - \lambda^2 v_0^2 < M_W^2\,. \qquad (4.15)$$

So for the case where the lightest Higgs boson is almost completely in the H_1, H_2 sector, that is to say for θ_3 negligible compared to θ_1, $M_{H\pm}$ can be at most equal to M_W. However, the value of $M_{H=}$ can increase significantly if the stop quark contribution in the one-loop corrections to the mass matrix is considered.

This result should be compared to the MSSM case, where at the tree

level $M^2_{H^\pm} = M^2_W + M^2_{A^0}$ and $M_{H^\pm} = M_W$ when the lightest pseudoscalar is massless. In the NMSSM, in the CP conserving case and no mixing in the pseudoscalar sector, we instead have

$$M^2_{H^\pm} = M^2_W - \lambda^2 v^2_0 + M^2_{A^0} \qquad (4.16)$$

where $M^2_{A^0}$ is the mass of the lightest pseudoscalar. For weak SCPV and the $\theta_3 \gg \theta_1$ case, the lightest pseudoscalar is singlet, and $M^2_{A^0}$ in eq.(4.16) is now the mass of the second lightest pseudoscalar, which is in the $H_1 H_2$ sector. We will see more explicitly in the next section how big the mass of the lightest Higgs boson as a function of the CP violating phases really is.

4.3.1 N field importance

Using the transformation outlined in the Appendix C it is possible to get rid of the Goldstone boson within the mass matrix so that the physical eigenvectors of the five neutral Higgs fields can be obtained. We can then, assuming weak SCPV such that the even and odd parts of the mass matrix decouple, obtain the N field content in the lightest neutral Higgs boson eigenstate analytically due to the fact that this is going to be a pseudoscalar. In particular the N field percentage in the lightest pseudoscalar eigenvector is

$$N\% = \frac{100\, v^2_3\, \theta^2_3}{v^2_0\, sin^2\beta\, cos^2\beta\, \theta^2_1 + v^2_3\, \theta^2_3}. \qquad (4.17)$$

Note that this formula does not depend on the choice of $\theta_2 = 0$ and can be obtained easily from the 2x2 psuedoscalar mass matrix.

We see that $N\%$ can be made small either assuming $\theta_3 \ll \theta_1$, as we have already seen in the previous pages, or taking small values of v_3.

For high values of v_3 such that v_0 can be neglected, the N field percentage will be independent of θ_3 and v_3 and equal to 100 (i.e. 100% decoupling) whereas for small values of v_3 this will not be the case. Even for moderate vevs the $N\%$ tends to be high, e.g. $\tan\beta=1$, $v_3 = v_0$, $\theta_1 = \theta_3$,

$$\frac{N\%}{100} = \frac{v^2_0\theta^2}{v^2_0\theta^2/4 + v^2_0\theta^2} = \frac{4}{5}$$

or $\tan\beta=2$, $v_3 = 2\,v_0$, $\theta_1 = \theta_3$,

$$\frac{N\%}{100} = \frac{4\,v_0^2}{v_0^2\,4/25 + 4\,v_0^2} = \frac{25}{26}.$$

This feature of the model is crucial as far as a possible experimental detection of the pseudoscalar is concerned. We will discuss this issue in more detail in chapter 6.

Chapter 5

Neutral Higgs bosons spectrum within the NMSSM

5.1   Introduction

We study in this chapter the neutral Higgs bosons mass spectrum numerically, focusing on the SCPV case.

As far as SCPV is concerned, several issues will be addressed: we will first discuss the mass of the lightest neutral Higgs boson as well as the role played by the various parameters within the model.

We will show how the parameter space is populated when the CP violating phases are small, particularly in connection with the study of the minima of the effective potential and the likely occurrence of metastable solutions for the SBEWS (spontaneous breaking of the electro-weak symmetry), which is typical of the NMSSM.

We discuss the mass of the second lightest neutral Higgs boson and the close relation between the lightest and second lightest neutral Higgs boson masses.

For comparison, we discuss the mass spectrum in the cases of CP conservation and also of explicit CP violation. Finally we summarise our results.

5.2   Lightest neutral Higgs boson with SCPV

In this section we discuss the behaviour of the neutral Higgs bosons
when the CP violating phases are varied. Because of the many param-
eters, this requires a numerical analysis.

We have seen in the previous chapter that if the CP violating phases
are small, there must be a light Higgs boson. We show here that the
upper bound on the lightest Higgs boson mass decreases proportionally
to the angles. Very roughly $m_{h_1} \approx 500\,\theta_1$ GeV where $\theta_1 < 0.1$ rad.
In particular we fix θ_1 to a starting value and then vary θ_3 from zero
to twice the value of θ_1, so that now a plot of the mass of the lightest
neutral Higgs mass as a function of θ_3 can be made.

It must be emphasized that the chosen interval over which θ_3 is varied
is such that the $\theta_1 << \theta_3$ regime is not covered. We will postpone its
discussion until section 5.3.1 as in this regime the values of λ and k
play a crucial role.

For each value of θ_3 10^5 random configurations are generated for the in-
dependent variables which are left in the potential, that is to say $\tan\beta$,
v_3, m_6, μ, $M_{H^\pm}$. The parameters λ and k are given fixed values.

The neutral Higgs boson mass matrix is then diagonalised for each set
so generated, and those 100 sets which give the highest values for m_{h_1}
stored. The procedure is repeated for each value of θ_3 in the range.

The parameters are randomly varied within the limits shown in Table
5.1.

The chosen values for h_t and the range of $\tan\beta$ are such as to account
for the top quark mass, which is around 174 GeV (see [40] for a discus-
sion of the relevant top quark mass). Two ranges for the charged Higgs
boson mass have been chosen; the 55-200 GeV interval is rather wider
than the most recent experimental lower bound coming from LEP [26]
according to which $M_{H^+} \geq 69$ GeV; however, it is interesting to see
what the resulting neutral Higgs bosons spectrum is for such a light
$M_{H\pm}$, given that in the small CP violating phases regime, $\theta_3 << \theta_1$
implies $M_{H^\pm} < M_W$; note also that this range evades the experimen-
tal lower bound of arounf 250 GeV, coming from the process $b \to s\gamma$,
which applies in a general two Higgs doublets model [28], but can be
avoided in supersymmetric models by cancellation between diagrams
with particles and s-particles in the loops.

Table 5.1: Ranges within which the parameters are randomly varied.

$tan\beta$	v_3	m_6	M_H^+	
2-3	10-510 GeV	-500-500 GeV	55-200 GeV , 200-800 GeV	
μ	λ	k	h_t	
-500-500 GeV	0.5	0.5	1.05	

The second interval, 200-800 GeV is a conservative one and shows the dependence of m_{h_1} on $M_{H\pm}$, or effectively v_3, when $v_3 > v_0$ that is to say v_3 (see eq. (3.15)).

We diagonalize the neutral Higgs boson mass matrix squared numerically: its eigenvalues are required to be positive in order for the effective potential to have a minimum at the chosen point in the $(v_1, v_2, v_3, \theta_1, \theta_3)$ space. The minima so found are in general local, and so metastable. This is an important point, which we will discuss in more detail in 5.4. Note that, unless explicitly stated, the same randomly generated couplings in the effective potential are taken; the consequence is that in the small phases regime the same sets which give the upper bound for a certain value of θ_1 will do so when θ_1 is ten times bigger, until eventually the phases are big enough that the light pseudoscalar theorem does not hold anymore. We found that the lightest neutral Higgs boson mass is directly proportional to θ_1 in the small phases regime. This procedure does not affect the mass bounds as long as saturation is achieved, i.e. the mass bounds do not increase any more with the number of iterations, and indeed for the sake of studying the behaviour of m_h as a function of the phases it is perfectly acceptable. However, different seeds for generating the random numbers have to be taken when absolute minima are looked for, as we will see in 5.4.

We show in Fig. 5.1, 5.2, 5.3, 5.4 plots so obtained for $\theta_1 = 1$, 0.1, 0.01, 0.001 rad respectively. The SUSY scale is in all the graphs assumed to be 1 TeV.

Fig. 5.1 shows the maximum value which the lightest neutral Higgs boson mass can take in this case, i.e. ≈ 120 GeV for the $M_{H\pm} = 200 - 800$ GeV and below 100 GeV for $M_{H\pm} = 55 - 200$ GeV; these limits change slightly when the λ and k parameters are varied. The $\theta_1 = 1$ rad case

evades the theorem of 4.2 as the CP violating phases are big, so that the lightest neutral Higgs boson will be CP even as well as CP odd. The other figures show the corresponding upper limits when we reduce the CP violating phases.

It is clear that m_{h_1} gets smaller and smaller when θ_1 is reduced (θ_3 being reduced accordingly too), in agreement with the analysis of 4.2. For θ_3 negligible compared to θ_1, $M_{H^\pm} < M_W$ at tree level, as we have discussed in the previous section (eq. (4.15). This is true whether or not θ_1 is small, so that in all the graphs of Fig. 5.1,5.2, 5.3, 5.4 for the case $M_{H^\pm} = 200 - 800$ GeV we see an abrupt interruption of the curve. m_{h1} falls down as θ_3 approaches smaller and smaller values compared to the value of θ_1 because the fewer parameter sets give real eigenvalues for the neutral Higgs bosons mass matrix: the values of $M_{H^\pm}$ are in fact required to be close to 200 GeV, which is the lowest limit allowed for the range in which the mass of the charged Higgs boson is randomly varied. Eventually values of $M_{H^\pm}$ smaller than 200 GeV will be required, and then it is not longer possible to get real eigenvalues for the neutral Higgs boson mass matrix, so the curve stops abruptly. The same fall takes place for the interval $M_{H^\pm} = 55 - 200$ GeV, because for smaller values of θ_3 a smaller region of the parameter space is available, although the curve does not stop abruptly, as the charged Higgs boson mass is allowed to take values below M_W.

We can see this explicitly in the Fig. 5.5, 5.6, 5.7, 5.8 where the lightest neutral Higgs boson mass is this time plotted as a function of $M_{H^\pm}$, and θ_1, θ_3 are given fixed values, with θ_3 always equal to $0.01\theta_1$, so that we are in the regime (b) of 4.3. For $M_{H^\pm} > M_W$ GeV, the eigenvalues of the neutral Higgs boson mass matrix are in general complex. For small values of θ_3 it is in principle necessary to consider the one-loop correction to the mass matrix of the charged Higgs boson, as the correction is significant [29]. However, in this region the lightest neutral Higgs boson is almost completely in the $H_1 H_2$ sector, as in the MSSM, so that for $\theta_1 < 0.1$ rad it is ruled out by experiment [26].

Two important points should be stressed.

For the case with $M_{H^\pm} = 55 - 200$ GeV the number of sets which give real eigenvalues for the mass matrix is in general smaller than for the case $M_{H^\pm} = 200 - 800$ GeV. This is due to the fact that taking small
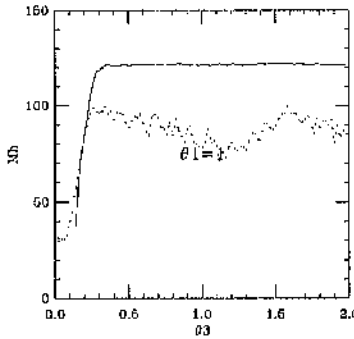
Figure 5.1: $\theta_1=1$ rad, SUSY breaking scale=1 TeV. Upper bound in GeV on the lightest neutral Higgs mass. $M_{H^+}=200$-800 GeV (continuous line) and $M_{H^\pm}=55$-200 GeV (dotted line).
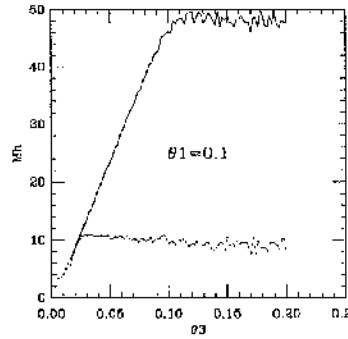
Figure 5.2: $\theta_1=0.1$ rad, same as in Fig. 5.1.
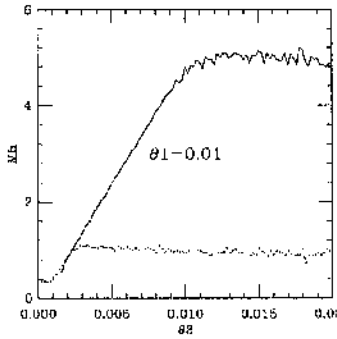
Figure 5.3: $\theta_1=0.01$ rad, same as in Fig. 5.1.
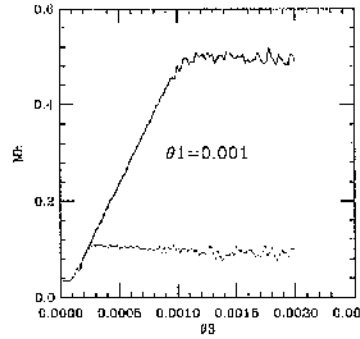
Figure 5.4: $\theta_1=0.001$ rad, same as in Fig. 5.1.

values of $M_{H^\pm}$ implies having small values of v_3 and in this region of the parameter space the number of sets giving real eigenvalues for the mass matrix is suppressed; this is to be expected because in the limit of a zero v_3 and no Z_3 symmetry violating terms in the effective potential, we reobtain the MSSM , within which SCPV cannot occur at the tree level. This is also the reason why when radiative corrections are included a bigger number of sets is in general available.

Also, in the small phases regime increasing θ_3 means in general lowering the number of sets available, whatever the range within which $M_{H^\pm}$ is varied. We will discuss this in more detail when we will discuss the search for absolute minima.

In our approximate mathematical analysis we have not said how small the CP violating phases have to be for the theorem of 4.2 to hold; the only condition is that the phases be small enough for the mixing elements in the neutral Higgs boson mass matrix squared to be negligible compared to the elements of both the 3x3 scalar and the 2x2 pseudoscalar blocks respectively. Therefore for fixed phases some regions of the parameters space will satisfy the theorem conditions whereas some others will not, rendering a numerical analysis necessary.

The picture does not change if we vary the SUSY breaking scale, as can be seen in the Fig. 5.9, 5.10, 5.11, 5.12 in which the SUSY breaking scale is taken equal to 174 GeV, while otherwise being the same analysis with the same ranges and values for λ and k as in Fig. 5.1, 5.2, 5.3, 5.4. Also shown are similar curves but where the number of randomly generated sets for each value of θ_3 (taking ten values of it, rather than one hundred as before) is taken to be equal to 1 million and for each value of θ_3 a different seed for the randomly generated sets is taken. Saturation is not completely achieved and a bigger number of iterations is required; this is specially true for the case of Fig. 5.9 where the depletion for $\theta_3 \approx 1\,rad$ in the case $M_{H^\pm} = 55 - 200$ GeV is clearly due to the reduced number of sets which give positive eigenvalues for the neutral Higgs boson mass matrix.

Comparing Fig. 5.9 with Fig. 5.1 we see that the mass bound is approximately 10% higher in the 1 TeV SUSY breaking case, which includes radiative corrections using 1-loop RG equations. These increase the bound on the scalar component of m_{h_1}. In the Z_3 CP conserving case,
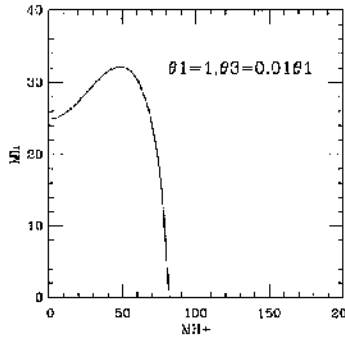
Figure 5.5: SUSY breaking scale=174 GeV. Upper bound on the lightest neutral Higgs mass as a function of $M_{H^\pm}$. $\theta_1=1$ rad, $\theta_3 = 0.01\theta_1$.
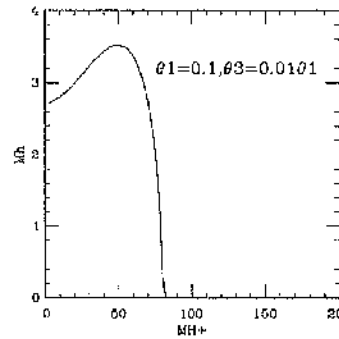

Figure 5.6: Same as in Fig. 5.5, but with $\theta_1=0.1$ rad.
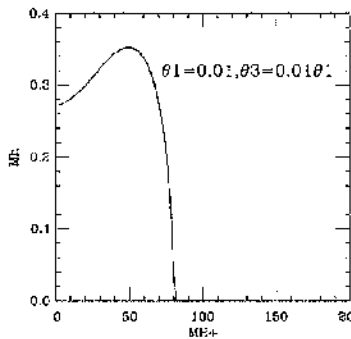
Figure 5.7: Same as in Fig. 5.5, but with $\theta_1=0.01$ rad.
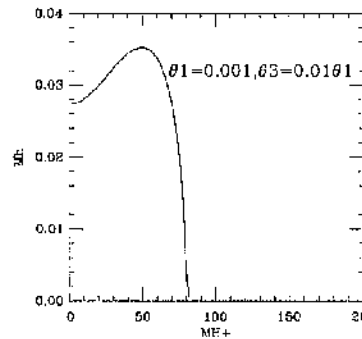
Figure 5.8: Same as in Fig. 5.5, but with $\theta_1=0.001$ rad.

the lightest neutral Higgs boson is in the scalar sector, and its mass at
the one loop order is ([7] where m_{h^0} is the lightest neutral Higgs boson
mass)

$$m_{h^0}^2 \leq M_Z^2 \left(cos^2 2\beta + \frac{2\,\lambda^2\,cos^2\theta_W}{g^2}\,sin^2 2\beta \right) \qquad (5.1)$$

so that bigger values of λ give a higher upper bound on m_{h^0}. Also, the
RGE increase the $M_Z^2 cos^2 2\beta$ contribution, which is the reason why for
$\theta_1 = 1 rad$ the upper bounds on m_{h_1} are higher for a SUSY scale equal
to 1 TeV, than those for a SUSY scale equal to 174 GeV.
However, λ and k are constrained to be such that $\lambda^2 + k^2 < 1$ (see 3.4)
and the RGE depend on λ and k in a way that too small values of k,
corresponding to bigger values of λ, upset the minima of the effective
potential, so that no real eigenvalues can be found, as we will discuss in
5.6 for the case of no SCPV. This is also the reason why in general our
upper bounds for big CP violating phases are lower than those which
can be found in the literature, where one-loop terms are added to the
effective potential, so that λ can be maximised. Moreover, we do not
include stop contributions, which also contribute in raising the upper
bounds. A comparison of the various upper bounds for $M_{H^\pm}$=55-200
GeV and $M_{H^\pm}$=200-800 GeV clearly shows that for the latter interval
much higher bounds are obtained (the $\theta_1 = 1$ rad case is an exception
as we are not in the small CP violating phases regime). As we will
see in section 5.4, this is due to the fact that higher values of $M_{H^\pm}$
mean higher values of v_3 and consequently higher values of m_{h_1}, as for
small CP violating phases the lightest neutral Higgs boson is (almost
completely) CP odd and mostly N field, so that its mass increases with
v_3.
It should be noted that for $M_{H^\pm} = 55 - 200$ GeV and values of $\theta_3 \approx \theta_1$
small the number of parameters giving real eigenvalues of the neutral
Higgs boson mass matrix is much reduced due to the requirement that
$M_{H^\pm} > M_W$; however, even if the number of iterations is increased,
the lightest neutral Higgs boson mass does not change significantly, as
saturation is indeed achieved.
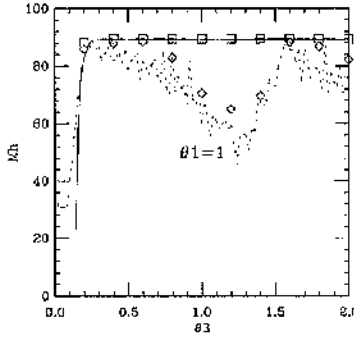
Figure 5.9: $\theta_1 = 1$ rad, SUSY breaking scale=174 GeV. Upper bound on the lightest neutral Higgs mass. $M_{H^\pm}$=200-800 GeV (continuous line) and $M_{H^\pm}$=55-200 GeV (dotted line) for 10^5 iterations, and for 10^6 iterations (squares and diamonds) and ten values of θ_3.
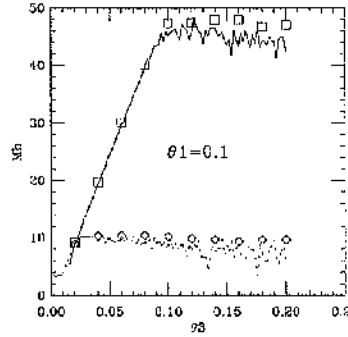
Figure 5.10: Same as in Fig. 5.9 but for θ_1=0.1 rad.
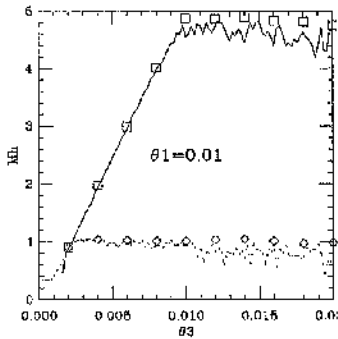
Figure 5.11: Same as in Fig. 5.9 but for θ_1=0.01 rad.
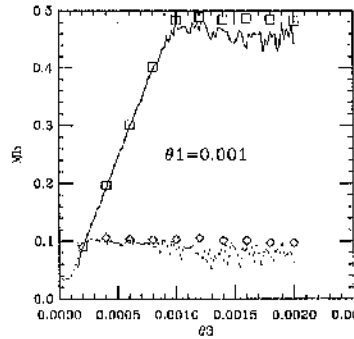
Figure 5.12: Same as in Fig. 5.9 but for θ_1=0.001 rad.
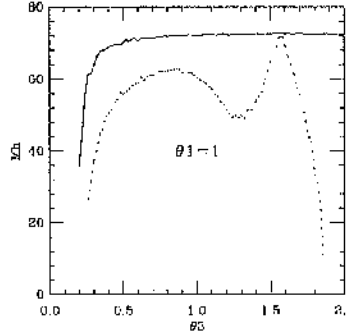
Figure 5.13: $\theta_1 = 1$ rad, SUSY breaking scale=174 GeV. Upper bound on the lightest neutral Higgs boson mass for $k = 0.65$ and $\lambda = 0.1$; $m_6 = 0$ (dotted line) and varied randomly (continuous line). $M_{H^\pm}$=200-800 GeV.
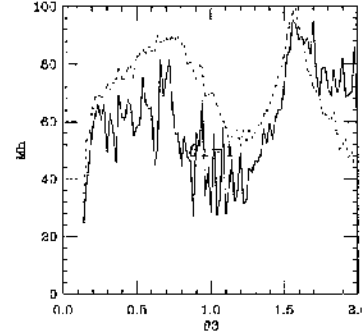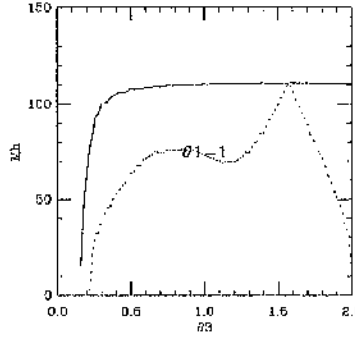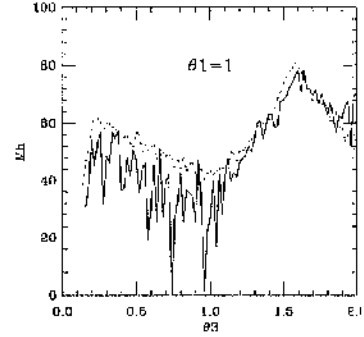
Figure 5.14: $\theta_1 = 1$ rad, SUSY breaking scale=174 GeV. Upper bound on the lightest neutral Higgs boson mass for $k = 0.1$ and $\lambda = 0.65$; $m_6 = 0$ (dotted line) and varied randomly (continuous line). $M_{H^\pm}$=200-800 GeV.

5.3 λ and k influence

So far we have always taken λ and k fixed to starting values at the SUSY breaking scale, within the ranges allowed by the requirement that perturbation theory still holds up to the unification scale ($\lambda^2 + k^2 < 1$, eq. (3.11)).

We now show in Fig. 5.13, 5.14 the same graphs as in Fig. 5.9, but this time with starting values for λ and k respectively equal to 0.1, 0.65 and vice versa. The parameters are once again randomly varied within the ranges shown in Tab. 1 (continuous line) and with m_6 fixed equal to zero (dotted line).

We see that when m_6, the N^3 term coefficient, is fixed to zero different values of λ and k do not cause a great difference in the final graphs, whereas when m_6 is allowed to be different from zero the case when k is small shows a jagged curve which is almost always beneath the corresponding one for $m_6 = 0$. We understand this as being due to the fact that when k is small and m_6 is different from zero, the potential is

more likely to be unstable with respect to the variable v_3 so that many more sets are rejected because of the occurrence of complex eigenvalues, and the upper bound on the lightest neutral Higgs boson mass is correspondingly lower than for $m_6 = 0$. This also explains why the curve is jagged. On the other hand for $k = 0.65$ the curve for $m_6 = 0$ is always beneath the one where m_6 is taken to be different from zero, as it should be because now the potential is safe from instabilities with respect to v_3.

The conclusion is that for the diagrams with $k = 0.1$ the saturation has not been achieved and many more iterations are required, because of the smaller number of good sets available. In Fig. 5.16, 5.15 we show the same graphs as in Fig. 5.14, 5.13 but for a SUSY scale equal to 1 TeV; once again the picture does not change. However, we notice that the radiative corrections for the case with $k = 0.1$ imply a lower bound on m_h than for the same case for a SUSY scale equal to 174 GeV: this is understood by the fact that the RGE make the effective potential unstable.

In Fig. 5.17 we show the same graph as in Fig. 5.16 but this time allowing for a number of random iterations equal to one million, so ten times bigger than in the other diagrams. It can be seen that this time saturation is achieved.

5.3.1   The $\theta_1 << \theta_3$ regime analysis

As we already said, we have so far not considered numerically the $\theta_3 >> \theta_1$ regime. We did so because for this case the λ and k parameters play an important role, as we will see.

Setting $\theta_1 = 0$ and taking the values $\lambda = k = 0.5$, we found no real eigenvalues for any values of θ_3. The reason for this has to do with the chosen values of λ and k. We show in Fig. 5.18, 5.19, 5.20, 5.21 m_{h_1} as a function of λ for $\theta_1 = 0$ and θ_3 equal respectively to 1, 0.1, 0.01, 0.001 rad. The value of k is chosen so that $\lambda^2 + k^2 = 1$ and the SUSY breaking scale is taken equal to 174 GeV. In any case for small values of θ_1 (namely $\theta_1 \approx 0.1, 0.01, 0.001$ rad) the RGE do not change significantly the resulting bounds. It is clear that in all the cases a value of λ smaller than the corresponding value of k is required in order

Figure 5.15: $\theta_1 = 1$ rad, SUSY breaking scale=1 TeV. Upper bound on the lightest neutral Higgs boson mass for $k = 0.65$ and $\lambda = 0.1$; $m_6 = 0$ (dotted line) and varied randomly (continuous line). $M_{H^\pm}$=200-800 GeV.

Figure 5.16: $\theta_1 = 1$ rad, SUSY breaking scale=1 TeV. Upper bound on the lightest neutral Higgs boson mass for $k = 0.1$ and $\lambda = 0.65$; $m_6 = 0$ (dotted line) and varied randomly (continuous line). $M_{H^\pm}$=200-800 GeV.
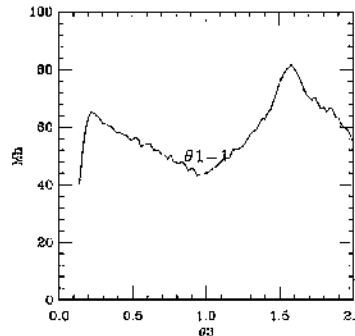
Figure 5.17: $\theta_1 = 1$ rad, SUSY breaking scale=1 TeV. Upper bound on the lightest neutral Higgs boson mass for $k = 0.1$ and $\lambda = 0.65$; m_6 is varied randomly. The number of iterations is equal to 1 million. $M_{H^\pm}$=200-800 GeV.
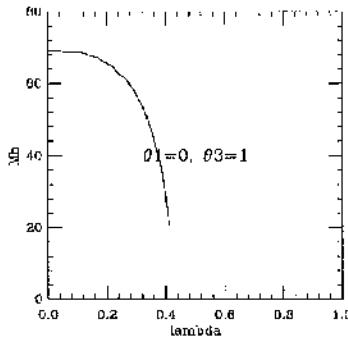
Figure 5.18: $\theta_1 = 0$, $\theta_3 = 1$ rad, SUSY breaking scale=174 GeV and $M_{H^\pm} = 55\text{-}200$ GeV. Upper bound on the lightest neutral Higgs mass as a function of λ.
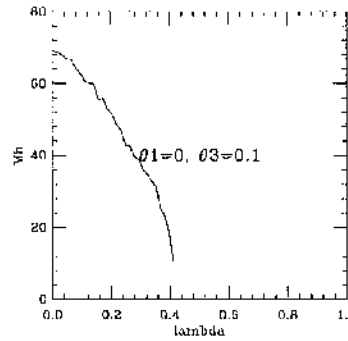
Figure 5.19: Same as in Fig. 5.18, but with $\theta_3 = 0.1$ rad.
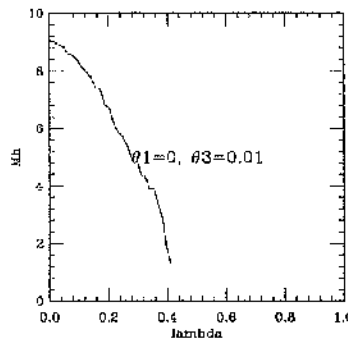
Figure 5.20: Same as in Fig. 5.18, but with $\theta_3 = 0.01$ rad.
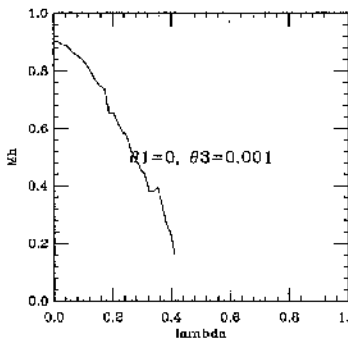
Figure 5.21: Same as in Fig. 5.18, but with $\theta_3 = 0.001$ rad.

for the eigenvalues of the neutral Higgs bosons mass matrix to be real. We explain this as due to the requirement of having the singlet field N decoupled from the $H_1 H_2$ sector, as otherwise the pseudoscalar could not be completely singlet. In fact, λ and m_4 are the parameter which determines the size of the interaction between the two Higgs doublets sector and the singlet field N.

5.4 The parameter space and absolute minima

In this section we analyse the parameter space in more detail as an introduction to the issue of how likely it is that weak SCPV local minima are also absolute ones. We will in particular show the interplay between the various parameters in the effective potential and the CP violating phases. Such a numerical study is required, as in general within the NMSSM deeper minima can be present than those which break the electro-weak symmetry and so also when SCPV is considered. For each minimum a numerical analysis is therefore required to establish whether the effective potential has deeper minima [1].

5.4.1 The parameter space

So far we have just studied numerically the neutral Higgs bosons masses. The condition that the mass squared are positive implies that the effective potential has a minimum, in general local, at the point so found in the space $(v_1, v_2, v_3, \theta_1, \theta_3)$. However, the effective potential may have deeper minima elsewhere. Unfortunately, producing upper bounds on the masses while at the same time ensuring that the minima found are absolute ones requires expensive numerical minimization of the effective potential. Some care is then required in choosing the region of the parameter space for this analysis. In particular the effective potential (eq.(3.3)) in the case of positive m_6 often has deeper minima for large values of v_3 and $\theta_3 = \frac{\pi}{3}$, because of the term $\frac{2}{3}m_6 v_3^3 cos(3\theta_3)$ in the effective potential. Consequently, those minima found for $m_6 > 0$ are likely

---

[1] We are of course assuming that the present electro-weak vacuum is stable.

to be only local. Incidentally we found that for m_6 varied between -500 and 500 [2], m_{h_1} is in fact higher for positive values of m_6.

The important parameters when searching for absolute minima are found to be μ and m_6; it is therefore important to understand in what part of the space μ-m_6 the sets giving real eigenvalues of the neutral Higgs boson mass matrix really are.
So far we have been discussing only mass upper bounds, and only those parameters which gave the highest value of m_{h_1} for each value of θ_1 and θ_3 were selected for numerical minimization of the effective potential. However, this means that the resulting sets may turn out to be predominantly in a certain region of the space μ-m_6. This is indeed the case, as we can see in Fig. 5.22, 5.23 (to save time, unless stated otherwise, θ_3 is given just 10 values rather 100) where m_6 is plotted against μ for the case $M_{H^\pm}$=200-800 GeV, SUSY scale equal to 174 GeV and $\theta_1 = 0.001$ rad (all the other parameters being as in Tab. 5.1): in particular, in Fig. 5.22 only the sets giving the upper bounds are considered whereas in Fig. 5.23 all the sets giving the highest value of m_h for each value of the N field fraction $|a_5|^2$, where a_5 is the imaginary part component of the N field in the normalised eigenvector [3] of m_{h_1} are considered (this is done for each value of θ_1 and θ_3).
In this way we make sure to have sets corresponding to high as well as low content of the N field.
The squares and crosses refer to the points respectively for the first half of values of θ_3 and for the second one, going from the lowest to the highest one.
It is clear that in both the figures the sets giving the mass upper bounds are localised preferably in the region where $m_6 > 0$; in fact, for higher values of $M_{H^\pm}$ (which means higher values of v_3) decoupling is stronger, which in turn favours positive values of m_6, for which the potential is more likely to have a minimum with respect to v_3, as can be seen from

---

[2]It should be remembered that m_6 is a dimensionful quantity with dimension [GeV]. The minus sign is allowed within the effective potential as well as the positive sign.

[3]Note that the eigenvectors are normalised to one. Note also that when the theorem of 4.2 does not hold anymore, the N field fraction will be given by $|a_3|^2 + |a_5|^2$.

$\frac{\partial^2 V}{\partial v_3^2} > 0$ [4]. By decoupling we mean the lightest neutral Higgs boson being completely a singlet, which requires either the N field and two Higgs doublet sectors being not connected, or v_3 much bigger than $v_0 = 174$ GeV, so that the singlet field predominates. The latter condition can be effectively relaxed as even for small values of v_3 (of the same order of v_0) the N field can predominate, as can be inferred by the formula (4.17). This will be discussed furthermore in the next chapter, when the singlet field percentage in the eigenvector of the lightest neutral Higgs boson is shown.

It is worth emphasizing further the fact that high values of $M_{H^\pm}$ imply high values of v_3. In our analysis, once $M_{H^\pm}$ and v_3 are given, then m_{12}^2 is given too; however, a high value for $M_{H^\pm}$ together with a small value for v_3 will most likely result in a value for m_{12} such that the potential does not have a minimum anymore.

Another feature visible from the graphs is that μ takes preferably negative values and that in the case of decoupling m_6 negative means that μ is negative too [5] (this turns out to be true in general, although the opposite is certainly false).

On the other hand, taking the range $M_{H^\pm} = 55 - 200$ GeV decoupling is not enhanced anymore and consequently one has sets with positive as well as negative values of m_6, as can be seen in Fig. 5.24 which is to be compared to Fig. 5.23. However, one also notices that negative values of m_6 predominate for $\theta_3 > \theta_1$ and vice versa for positive values of m_6; this also explains why the range with $-500 < m_6 < 500$ gives more sets than the range with $-500 < m_6 < 0$ for the first half of the θ_3 interval whereas for the second half the number of sets for the two cases is almost the same (only those sets with $m_6 < 0$ being allowed), as can be seen in Fig. 5.25 [6] (the parameters are as in Tab.

---

[4] That it is not just the sets giving the highest values of m_{h_1} to have positive values of m_6 can be inferred looking at Fig. 5.30, where $-500 < m_6 < 0$, and 5.27, which gives the total number of sets with real m_{h_i}.

[5] This is only true when small CP violating phases are considered; for big phases, μ can be positive together with m_6 being negative; it seems that this happens preferentially for $\theta_3 > \theta_1$.

[6] The number of sets which give real m_{h_i} is bigger than the number of sets plotted in Fig. 5.24 where just those sets which give the highest values of m_{h_i} are plotted.

5.1 with $M_{H^\pm} = 55 - 200$ GeV and SUSY breaking scale equal to 174 GeV) where the crosses are for $-500 < m_6 < 500$ and the diamonds are for $-500 < m_6 < 0$ [7] (similar graphs are obtained for the cases with $\theta_1 = 0.01, 0.1$ rad respectively).

The way to understand the behaviour outlined requires the following observation:

the soft term m_{12}^2 is in general positive for $\theta_3 > \theta_1$; this threatens to destabilize the potential, so that a reduction of v_3 is required, the net effect being that the upper bound on $M_{H^\pm}$ can still be saturated. For $\theta_3 < \theta_1$, m_{12}^2 can be either positive or negative, depending on the allowed values of $M_{H^\pm}$ and v_3; for high values of v_3 (which means bigger values of m_h) negative values of m_{12}^2 will result.

We then have that for $\theta_3 < \theta_1$, v_3 will be preferably high (compatibly with the range within which $M_{H^\pm}$ is varied) whereas for $\theta_3 > \theta_1$, v_3 will be smaller. The parameter μ has the opposite behaviour to m_{12}^2.

We can understand what we have seen so far in the following way:

a) High values of $M_{H^\pm}$ (decoupling)

Bigger values of v_3 (greater than v_0) at the potential minimum $\Rightarrow$ the N field fraction is high and almost independent of θ_3 and v_3 $\Rightarrow m_6 > 0$ preferred and bigger values of m_h result; for $\theta_3 < \theta_1$, m_{12}^2 can be both positive and negative; for $\theta_3 > \theta_1$, m_{12}^2 becomes positive and increases with v_3; this then requires v_3 to decrease slightly, in order to suppress the effect of m_{12}^2 on the effective potential. $M_{H^\pm}$ is seen to take all possible values allowed, no matter what the values of θ_3 are; high values of $M_{H^\pm}$ are preferred as higher values of m_h are obtained. m_6 takes preferably positive values, no matter what θ_3 is, as v_3 is always quite big (see case b for comparison).

b) Low values of $M_{H^\pm}$ (incomplete decoupling)

---

[7] It is worth mentioning that if saturation were achieved than for $\theta_3 > \theta_1$ the crosses and the diamonds should coincide; nontheless, the mass upper bounds change insignificantly.

Very low values of v_3 required for the potential to have a minimum
$\Rightarrow$ the N field fraction is low and increases with θ_3 and v_3 [8].
For $\theta_3 > \theta_1$ m_{12}^2 becomes positive and increases with v_3; this then
requires v_3 to decrease in order to suppress the effect of m_{12}^2 on the
effective potential, the values falling down quite sharply due to the low
values of $M_{H^\pm}$. $M_{H^\pm}$ is seen to take all possible values allowed, no
matter what the values of θ_3 are; high values of $M_{H^\pm}$ are preferred
as higher values of m_h are obtained. The resulting N field percentage
for mass upper bound is independent of θ_3, as we will see in the next
chapter.

When v_3 sharply decreases, so do m_1^2 and m_2^2, which go from posi-
tive values to negative ones; on the other hand m_3^2, m_4^2 and m_5 remain
positive and increase, so that for the potential to have a minimum with
respect to θ_3, m_6 has to take negative values.
So we have that high values of v_3 (i.e. $\theta_3 < \theta_1$) imply $m_6 > 0$ whereas
low values of v_3 (i.e. $\theta_3 > \theta_1$) imply $m_6 < 0$.

Fig. 5.25 tells us that the number of sets for $-500 < m_6 < 500$ is
bigger than for the case $-500 < m_6 < 0$ because in the former case
m_6 can be either positive or negative, the number of sets with $m_6 > 0$
being much higher. Also shown is the case for $-500 < m_6 < 500$, with
$\lambda = 0.1$ and $k = 0.65$, where decoupling is much enhanced (because of
the smallness of λ) and the number of sets can then increase with θ_3.

The case $\theta_1 = 1$ rad, where the theorem certainly does not hold
anymore, is shown in Fig. 5.26; the increase in the number of sets after
$\theta_3 = 1$ rad is explained by the fact that the sum of the CP violating
phases exceeds $\pi/2$: in fact, after $\theta_3 = \pi/2$ the number of sets declines
and the picture for small values of θ_3 is reproduced.
Analogous graphs are shown in Fig. 5.27, 5.28 for the case $M_{H^\pm} =$
$200 - 800$ GeV for $\theta_1 = 0.001$ rad and $\theta_1 = 1$ rad respectively. De-
coupling is this time enhanced, so that for $0 < m_6 < 500$ we expect
fewer cases than for $-500 < m_6 < 500$ because only those sets with m_6
close to zero will give real m_{h_i}. This is confirmed by the correspond-
ing graphs of Fig. 5.29, 5.30, 5.31 and 5.32 where again m_6 is plotted

---

[8]See the formula (4.17).
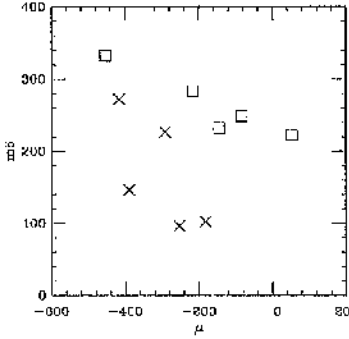
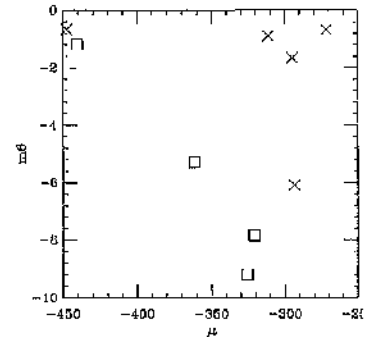Figure 5.22: SUSY breaking scale=174 GeV. $M_{H^\pm}$=200-800 GeV and -500 < m_6 < 500. m_6 plotted against μ for the case θ_1=0.001 rad and $\theta_3 = 0 - 2\theta_1$. The points correspond to the sets which give the final mass upper bounds (see the Text); squares are for $\theta_3 = 0 - \theta_1$ and crosses are for $\theta_3 = \theta_1 - 2\theta_1$.
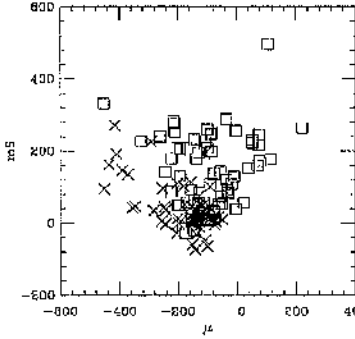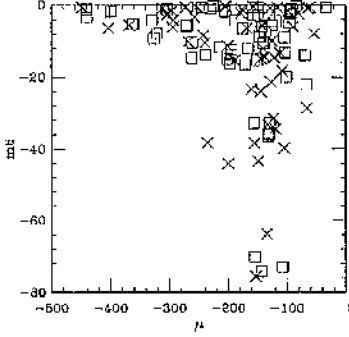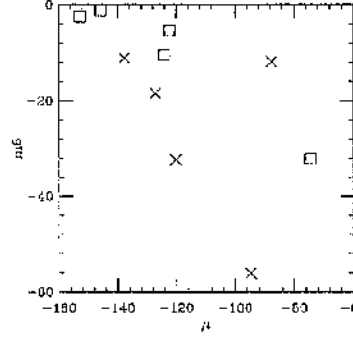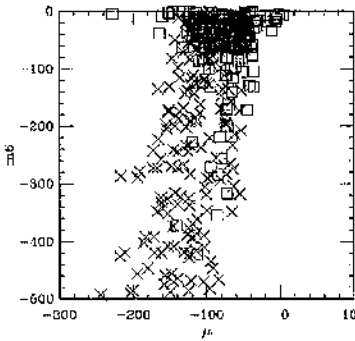

Figure 5.23: SUSY breaking scale=174 GeV. $M_{H^\pm}$=200-800 GeV and $-500 < m_6 <$ 500. m_6 plotted against μ for the case θ_1=0.001 rad and $\theta_3 = 0 - 2\theta_1$. The points correspond to the sets which give the highest values of m_h for each value of $|a_5|^2$ (see the Text); squares are for $\theta_3 = 0 - \theta_1$ and crosses are for $\theta_3 = \theta_1 - 2\theta_1$.
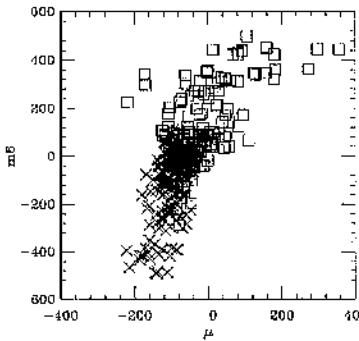
Figure 5.24: SUSY breaking scale=174 GeV. $M_{H^\pm}$=55-200 GeV and $-500 < m_6 < 500$. m_6 plotted against μ for the case θ_1=0.001 rad and $\theta_3 = 0 - 2\theta_1$. The points correspond to the sets which give the highest values of m_h for each value of $|a_5|^2$ (see the Text); squares are for $\theta_3 = 0 - \theta_1$ and crosses are for $\theta_3 = \theta_1 - 2\theta_1$.
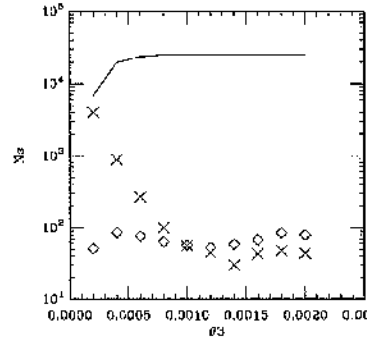
Figure 5.25: SUSY breaking scale=174 GeV. $M_{H^\pm}$=55-200 GeV. Number of sets (Ns) with real m_{h_4} plotted against θ_3 for the case θ_1=0.001 rad. Crosses are for $-500 < m_6 < 500$ and diamonds are for $-500 < m_6 < 0$. The case for $-500 < m_6 < 500$ and $\lambda = 0.1$ and $k = 0.65$ is also shown (continuous line).
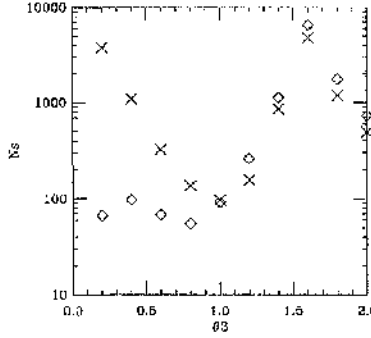
Figure 5.26: SUSY breaking scale=174 GeV. M_{H^-}=55-200 GeV. Number of sets (Ns) with real m_{h_i} plotted against θ_3 for the case θ_1=1 rad. Crosses are for $-500 < m_6 < 500$ and diamonds are for $-500 < m_6 < 0$.
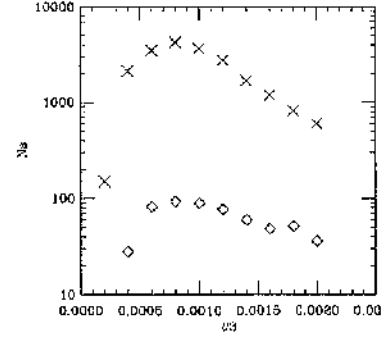
Figure 5.27: SUSY breaking scale=174 GeV. M_{H^+}=200-800 GeV. Number of sets (Ns) with real m_{h_i} plotted against θ_3 for the case θ_1=0.001 rad. Crosses are for $-500 < m_6 < 500$ and diamonds are for $-500 < m_6 < 0$.
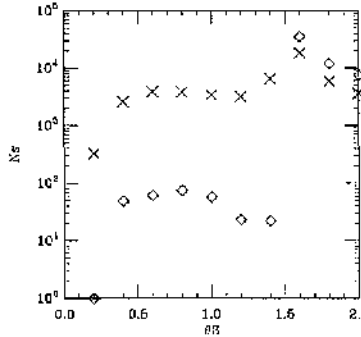
Figure 5.28: SUSY breaking scale=174 GeV. M_{H^-}=200-800 GeV. Number of sets (Ns) with real m_{h_i} plotted against θ_3 for the case θ_1=1 rad. Crosses are for $500 < m_6 < 500$ and diamonds are for $-500 < m_6 < 0$.

Figure 5.29: SUSY breaking scale=174 GeV. $M_{H^\pm}$=200-800 GeV and $-500 < m_6 < 0$. m_6 plotted against μ for the case θ_1=0.001 rad and $\theta_3 = 0 - 2\theta_1$. The points correspond to the sets which give the final mass upper bounds (see the Text); squares are for $\theta_3 = 0 - \theta_1$ and crosses are for $\theta_3 = \theta_1 - 2\theta_1$.

Figure 5.30: SUSY breaking scale=174 GeV. $M_{H^\pm}$=200-800 GeV and $-500 < m_6 < 0$. m_6 plotted against μ for the case θ_1=0.001 rad and $\theta_3 = 0 - 2\theta_1$. The points correspond to the sets which give the highest values of m_h for each value of $|a_5|^2$ (see the Text); squares are for $\theta_3 = 0 - \theta_1$ and crosses are for $\theta_3 = \theta_1 - 2\theta_1$.

Figure 5.31: SUSY breaking scale=174 GeV. $M_{H^\pm}$=55-200 GeV and $-500 < m_6 < 0$. m_6 plotted against μ for the case θ_1=0.001 rad and $\theta_3 = 0 - 2\theta_1$. The points correspond to the sets which give the final mass upper bounds (see the Text); squares are for $\theta_3 = 0 - \theta_1$ and crosses are for $\theta_3 = \theta_1 - 2\theta_1$.

Figure 5.32: SUSY breaking scale=174 GeV. $M_{H^\pm}$=55-200 GeV and $-500 < m_6 < 0$. m_6 plotted against μ for the case θ_1=0.001 rad and $\theta_3 = 0 - 2\theta_1$. The points correspond to the sets which give the highest values of m_h for each value of $|a_5|^2$ (see the Text); squares are for $\theta_3 = 0 - \theta_1$ and crosses are for $\theta_3 = \theta_1 - 2\theta_1$.

against μ.

Finally it should be noticed that increasing the SUSY breaking scale to 1 TeV does not change the picture we have outlined.

5.4.2 Absolute minima

The mass bounds shown in the previous sections correspond to local minima of the effective potential. We now check that some points can be found which correspond to absolute minima and give rather similar curves, though computer time limitations make these bounds statistically weaker.

What we have seen in 5.4.1 is important as far as the search for absolute minima is concerned; in fact, as we have mentioned before, positive high values of m_6 are likely to give rise to local minima only, so that we do not expect to find any absolute minima in this region.

Coming now to the method we used in the search for absolute minima, we repeated the same analysis we performed when looking for the mass upper bounds on m_{h_1}, but this time storing for each value of θ_3 those 100 sets which gave the 100 highest values for m_{h_1}; we then minimised the effective potential in the hope that for each value of θ_3 a set could be found among the 100 stored whose corresponding minimum of the effective potential happened to be an absolute one, starting with the sets with highest corresponding values of m_{h_1} and going downward.

This method has the advantage of being very fast, assuming that some sets which give absolute minima are to be found. However, the curves so obtained are no longer mass upper bounds, unless very close to the real upper bounds (where the minima are in general local). This is because the absolute minima have been found for only a subset of the parameter space. Other sets could give absolute minima with higher masses, but these would of course be below the local minima bounds.

It should be noticed that if a set is found to give rise to a local minimum only, this means that there are values of the vevs and the phases different from the ones chosen for which the potential has a deeper minimum. This is equivalent to saying that the absolute minimum occurs for the same set of soft terms but a different values of $\tan\beta$, v_3, θ_1 and θ_3, assuming that the absolute minimum so found is CP violating. However, one should then check the resulting mass spectrum: although this can

in principle be done the procedure is not suitable for an understanding of the mass bounds themselves.

We have found that the search was unsuccessful for $M_{H^\pm} = 200 - 800$ GeV, as expected, due to the fact that all the sets (namely those one hundred sets which give the highest values of m_h for each value of θ_3) have high positive values of m_6 and v_3, no matter what the SUSY scale is. However, solutions with $M_{H^\pm} = 200 - 800$ GeV were found taking $m_6 = 0$, and with $M_{H^+} = 55 - 200$ GeV and any m_6.
In Fig. 5.33, 5.34, 5.35, 5.36 the continuous lines show the lightest neutral Higgs boson mass as a function of θ_3 (θ_3 is varied 100 times) for $\theta_1 = 1, 0.1, 0.01, 0.001$ rad respectively, for a SUSY scale equal to 1 TeV and for m_6 set equal to zero; the dotted lines show instead the same bounds where the minima have been checked to be absolute ones. Analogous graphs with $-500 < m_6 < 0$ can be easily obtained.

It is important to assess in which area of the parameter space absolute minima are more likely to be found. This of course requires a big number of absolute minima in the first place. We have repeatedly performed the analysis described in the previous pages for both SUSY scales of 1 TeV and 174 GeV and for both the ranges of $M_{H^\pm}$ of Tab. 5.1. We assume that for $\theta_1 = 0.001, 0.01$ rad all the parameter space we have considered is certainly within the small CP violating phases regime (we have in fact verified that in all the numerical analysis for these values of θ_1 the lightest neutral Higgs boson eigenvector was to a very good degree pseudoscalar), so that we will just consider those absolute minima found for these value of θ_1, with θ_3 being varied as usual between 0 and $2\theta_1$.
We show in Fig. 5.37 m_6 against μ for those sets whose corresponding minimum was an absolute one for $\theta_1 = 0.001, 0.01$ rad; in particular the sets correspond to $m_6 = 0$, $-500 < m_6 < 0$ as well as $-500 < m_6 < 500$, the latter one for small values of $M_{H^\pm}$ only. Note that the points with $\theta_3 < \theta_1$ correspond to high values of v_3 and vice versa.
We have also looked for absolute minima for small CP violating phases in the case where μ is set equal to zero: no absolute minima could be found among the 100 sets stored for each value of θ_3; a more detailed analysis, choosing fixed values for θ_3 and increasing the number of sets
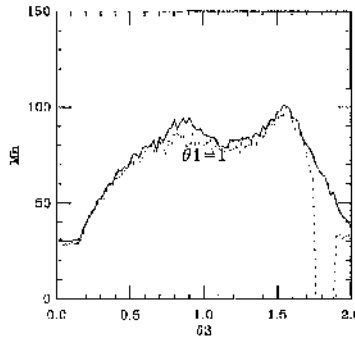
Figure 5.33: $\theta_1=1$ rad, SUSY breaking scale$=1$ TeV. Upper bound on the lightest neutral Higgs mass for $m_6=0$ (continuous line) and corresponding curve for which the minima are absolute ones (dotted line). $M_{H^\pm}=55\text{-}200$ GeV.
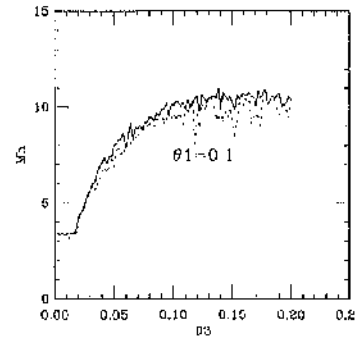
Figure 5.34: Same as in Fig. 5.33, but with $\theta_1=0.1$ rad.
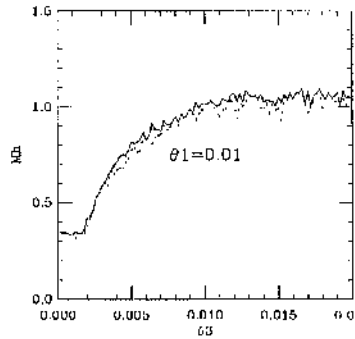
Figure 5.35: Same as in Fig. 5.33, but with $\theta_1=0.01$ rad.
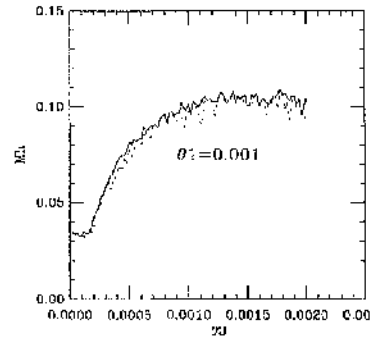
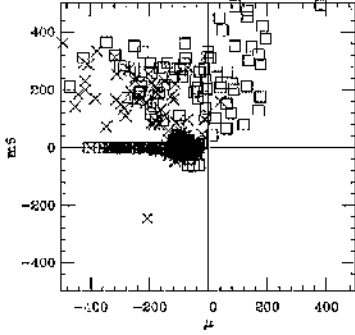Figure 5.36: Same as in Fig. 5.33, but with $\theta_1=0.001$ rad.

Figure 5.37: m_6 plotted against μ. The sets are for $\theta_1 = 0.001$, 0.01 rad and absolute minima are found. Notice that no absolute minima could be found for $\mu = 0$, but only for small μ.
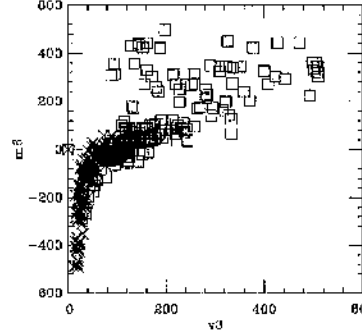
Figure 5.38: SUSY breaking scale=174 GeV. $M_{H\pm} = 55\text{-}200$ GeV and $-500 < m_6 < 500$. m_6 plotted against v_3 for the case $\theta_1 = 0.001$ rad and $\theta_3 = 0 - 2\theta_1$. The points correspond to the sets which give the highest values of m_h for each value of the N field fraction; squares are for $\theta_3 = 0 - \theta_1$ and crosses are for $\theta_3 = \theta_1 - 2\theta_1$.
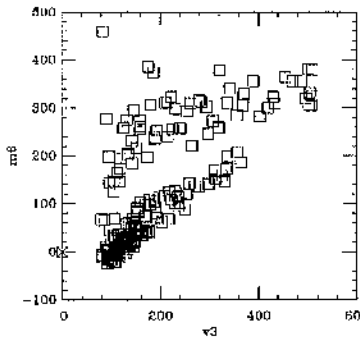
Figure 5.39: SUSY breaking scale=174 GeV. $M_{H\pm} = 55\text{-}200$ GeV and $-500 < m_6 < 500$ and $\mu = 0$. m_6 plotted against v_3 for the case $\theta_1 = 0.001$ rad and $\theta_3 = 0 - 2\theta_1$. The points correspond to the sets which give the highest values of m_h for each value of the N field fraction; squares are for $\theta_3 = 0 - \theta_1$ and crosses are for $\theta_3 = \theta_1 - 2\theta_1$.

from 100 to 10000 gave also no positive results. We also tried setting $m_6 = 0$, but once again no absolute minima could be found. Furthermore, the absolute minima eventually found were all CP conserving.

As an example of the difference setting μ equal to zero makes as far as populating the parameter space is concerned, we show in Fig. 5.38 and 5.39 the case where $M_{H\pm} = 55 - 200$ GeV and the SUSY breaking scale is 174 GeV, with μ set equal to zero in the latter one: m_6 is plotted against v_3 for all the sets giving the highest m_h for $|a_5|$ between 0 and 1 (100 values were taken). We see that this time, although decoupling is disfavoured, m_6 does not take negative values when $\theta_3 \geq \theta_1$ as v_3 does not decrease with θ_3: this is due to the fact that $|m_{12}|$ can now be bigger without destabilizing the effective potential.

We also notice that very few cases are to be found for $\theta_3 > \theta_1$ and that the number of sets is generally higher for small values of $M_{H\pm}$.

However, this alone does not explain the unsuccessful search for absolute minima.

5.5   Second lightest neutral Higgs boson

So far we have discussed the lightest neutral Higgs bosons in the case of SCPV. However, we have not said anything about the resulting masses of the other neutral Higgs bosons. This is quite important as far as the experimental detection of any such particles is concerned, as we will see in more detail in the next chapter.

We show in Fig. 5.40, 5.41, 5.42 the second lightest neutral Higgs boson and the second lightest pseudoscalar as a function of $M_{H\pm}$ for $\theta_1 = \theta_3 = 0.1$, 0.01, 0.001 rad respectively. The unfixed parameters are varied randomly within the ranges given in Tab. 5.1.

Those sets which give the heaviest possible lightest neutral Higgs boson are kept, and the resulting eigenvalues and eigenvectors of the neutral Higgs boson mass matrix stored. It is clear from the graphs that the second lightest pseudoscalar is much heavier than the second lightest neutral Higgs boson, which is then in the CP even sector.

We once again are allowed to speak of the CP odd and even sectors as if separate because we are in the small CP violating phases regime.

In Fig. 5.43, 5.44, 5.45 the same graphs are shown but this time as a function of v_3, with $M_{H^\pm}$ randomly varied between 200 and 800 GeV. We see that the second pseudoscalar is much heavier than the second lightest neutral Higgs boson; furthermore, its mass rises with v_3 due to the high percentage of the N field in the eigenvector (see chapter 4) until eventually it stops rising due to the fact that $M_{H^\pm}$ has reached the upper edge of the interval within which it is randomly varied. In fact, from the expression for charged Higgs boson mass (3.15) we see that $M_{H^\pm}$ rises together with v_3 for fixed θ_1 and θ_3.

On the other hand, the second lightest neutral Higgs boson mass seems not to depend either on v_3 or on $M_{H^\pm}$. This is due to the fact that the corresponding eigenvector is to be found predominantly in the H_1, H_2 sector for values of v_3 ($M_{H^\pm}$) comparable or bigger than v_0.

So we have found that for big values of v_3 or $M_{H^\pm}$ one of the eigenvectors of the 3x3 CP even part of the neutral Higgs boson mass matrix will decouple and become predominantly singlet, whereas the other two eigenvectors will be predominantly in the H_1, H_2 sector, therefore reproducing the picture we have in the MSSM [9].

This of course refers to those sets giving the upper bound on the lightest neutral Higgs boson only. However, bigger values of v_3 correspond to bigger values of m_h, so that in this case the second lightest neutral Higgs boson will be predominantly doublet in general.

However, as far as the experimental testing of the model is concerned, it is also important to see how big the sum of the lightest and second lightest neutral Higgs bosons, i.e. $m_A + m_{h_1}$ can be, rather than single neutral Higgs bosons masses themselves (we will discuss the issue of the experimental testability of the model in chapter six). The relevant graphs are shown in Fig. 5.46, 5.47, 5.48, 5.49 for the range $M_{H^\pm} = 55 - 200$ GeV, and in Fig. 5.50, 5.51, 5.52, 5.53 for the range $M_{H^\pm} = 200 - 800$ GeV.

We note that for small phases $m_A + m_h$ has a bound of the order of 100 GeV, but can be much greater for large phases.

The other scalar neutral Higgs bosons can in general be quite heavy,

---

[9] We observe that this is not true if we take for example $M_{H^\pm}$ between 55 and 200 GeV; in this case in fact the second lightest neutral Higgs boson eigenvector will contain a non negligible content of the N field.
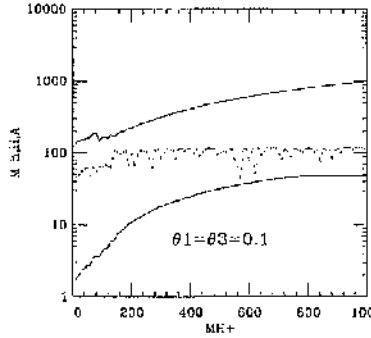
Figure 5.40: $\theta_1 = \theta_3 = 0.1$ rad, SUSY breaking scale=174 GeV. Lightest neutral Higgs boson (short dashed line), second lightest neutral Higgs boson (dotted line) and second lightest pseudoscalar (continuous line) masses as a function of $M_{H^\pm}$.
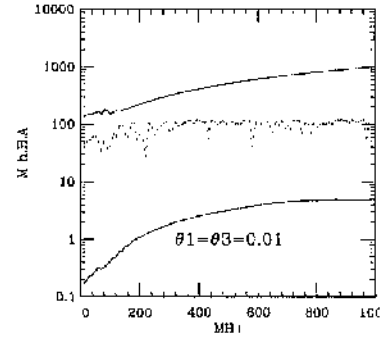
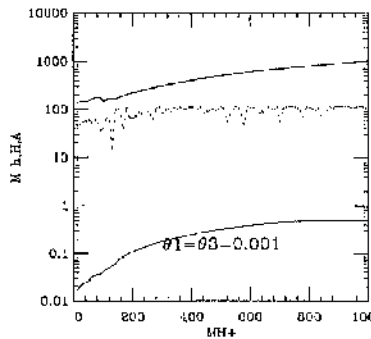Figure 5.41: Same as in Fig. 5.40, but with $\theta_1 = 0.01$ rad.

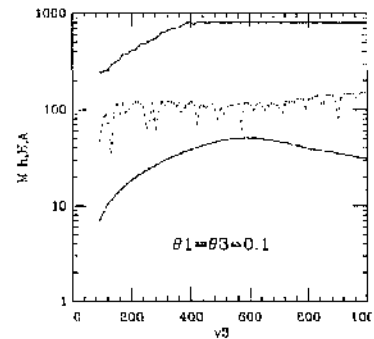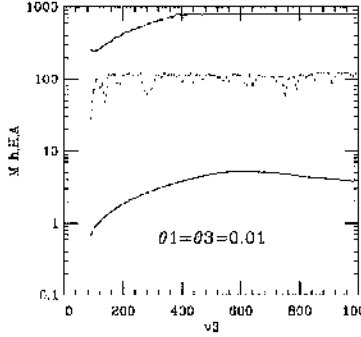Figure 5.42: Same as in Fig. 5.40, but with $\theta_1 = \theta_3 = 0.001$ rad.

Figure 5.43: SUSY breaking scale=174 GeV. Lightest neutral Higgs boson (short dashed line), second lightest neutral Higgs boson (dotted line) and second lightest pseudoscalar (continuous line) masses as a function of v_3, for $\theta_1 = \theta_3 = 0.1$ rad.

Figure 5.44: Same as in Fig. 5.43, but with $\theta_1 = \theta_3 = 0.01$ rad.
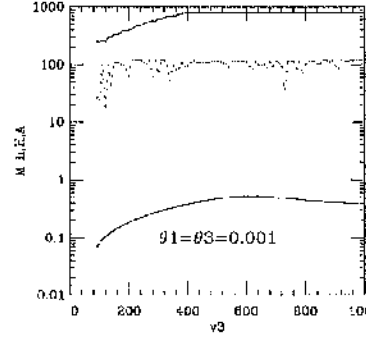
Figure 5.45: Same as in Fig. 5.43, but with $\theta_1 = \theta_3 = 0.001$ rad. v_3, for different values of $\theta_1 = \theta_3$,

like the second pseudoscalar.

5.6 Higgs spectrum when CP is conserved

We show in this section the upper bound on the lightest neutral Higgs boson and the corresponding second lightest one for the case when no SCPV is assumed, as a comparison with the results shown in the previous section. In this case the angles θ_1, θ_3 are exactly zero and no light pseudoscalar is needed, as in the case when the angles are non zero and small.

Once again the parameters are randomly varied and the values of λ and k fixed as in table 1; m_4 and m_{12}^2 are also varied randomly, as they cannot be fixed through the equations (3.13) and (3.14) anymore, as they are satisfied identically when $\theta_1 = \theta_3 = 0$, m_5 can still be traded for $M_{H^\pm}$.

The lightest and second lightest neutral Higgs bosons can be CP odd or CP even, according to whether big or small values for $M_{H^\pm}$ are taken; in the latter case the two pseudoscalars will be the heaviest of the five neutral Higgs bosons. However, it should be noted that as far as the lightest neutral Higgs boson mass is concerned, the upper bound on it
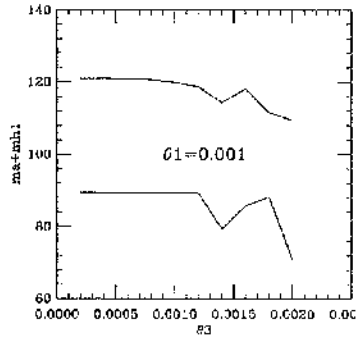
Figure 5.46:
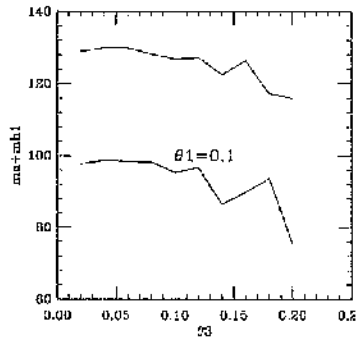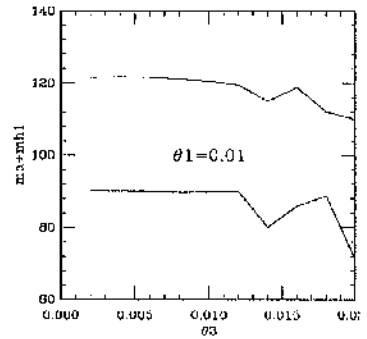
Figure 5.47:

Figure 5.48:
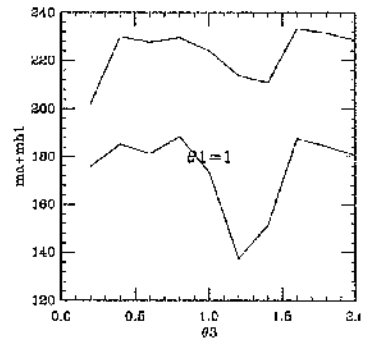
Figure 5.49: $M_{H^\pm}$=55-200 GeV. $m_A + m_{H_1}$ as a function of θ_3. SUSY breaking scale=174 GeV (lower line) and 1 TeV (higher line). Different values of θ_1 are taken, Fig. 5.46, 5.47, 5.48.
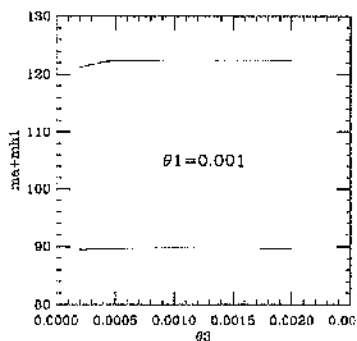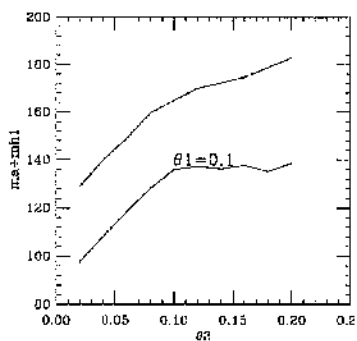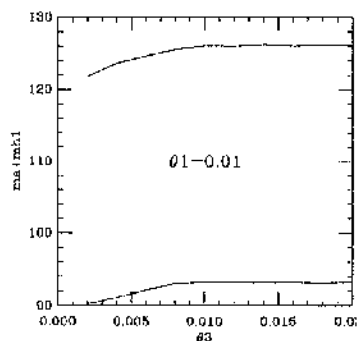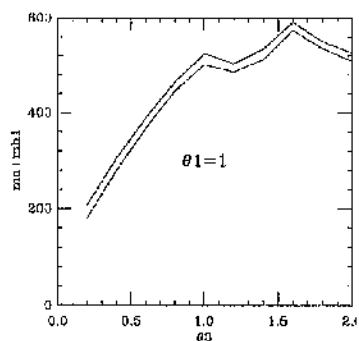
Figure 5.50:

Figure 5.51:

Figure 5.52:

Figure 5.53: $M_{H^\pm}=200\text{-}800$ GeV. $m_A+m_{H_1}$ as a function of θ_3. SUSY breaking scale=174 GeV (lower line) and 1 TeV (higher line). Different values of θ_1 are taken, Fig. 5.50, 5.51, 5.52.

is basically independent of $M_{H^\pm}$, contrary to when SCPV is considered. In Fig. 5.54, 5.55 the lightest and second lightest neutral Higgs boson masses are plotted as a function of $M_{H^\pm}$ and $\tan\beta$ is restricted to the interval 2-3, so that the b quark contribution to the RGE can be safely ignored.

In Fig. 5.56, 5.57 we show the lightest neutral Higgs boson mass as a function of $\tan\beta$ with the b quark contribution to the RGE taken into account (see Appendix A) for the case when $\lambda = k = 0.5$. In particular the restriction on the value of h_b so that perturbation theory still holds up to the unification scale is such that for the SUSY breaking scale equal either to EWSBS or to 1 TeV, $|h_b| \leq 1.0$.

In Fig. 5.58 and 5.59 λ and k are varied to give as high as possible a value for m_{h_1} assuming that perturbation theory still holds up to the unification scale [37], and taking a value of k at the energy scale of M_Z equal to 0.3.

The resulting graph of λ as a function of $\tan\beta$ is shown in Fig. 5.60. The upper bounds show in this case a clear maximum for small values of $\tan\beta$, as it should be expected from eq. (5.1) and in agreement with [37]. However, we are using the RGE approach rather than the one loop potential one, so that for too small values of k (required to achieve as big as possible values for λ) the RGE are such that the Y_8 (see 3.4) quartic term can become negative, thus making the potential unstable and rendering local minima more unlikely, as can be seen by the graph of Fig.5.61 where m_{h_0} is plotted as a function of $\tan\beta$ for $k = 0$, a SUSY breaking scale equal to 1 TeV (continuous line) and $M_{H^\pm} = 200 - 800$ GeV (the range in which $M_{H^\pm}$ is varied is not so important). It appears that the upper bound does not show a maximum anymore, and in fact the curve is for small values of $\tan\beta$ lower than the corresponding one for a SUSY breaking scale equal to 174 GeV (dotted line) when the RGE are not important, and always lower than the corresponding curve for a SUSY breaking scale equal to 1 TeV and $k = 0.3$, contrary to what should normally be the case.
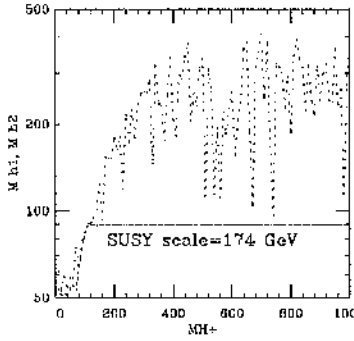
Figure 5.54: No SCPV, SUSY breaking
scale=174 GeV.Lightest neutral Higgs boson (short dashed line) and second lightest neutral Higgs boson (dotted line) masses as a function of $M_{H\pm}$.
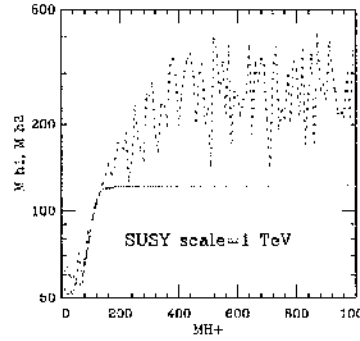

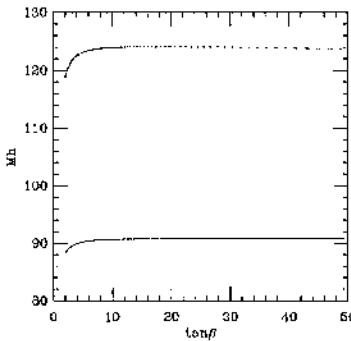Figure 5.55: No SCPV, SUSY breaking scale=1 TeV, same as in Fig. 5.54.

Figure 5.56: No SCPV. Upper bound on the lightest neutral Higgs mass as a function of $\tan\beta$ for $M_{H\pm}$=55-200 GeV and SUSY breaking scale equal to 174 GeV (continuous line) and 1 TeV (dotted line), for $\lambda = k = 0.5$.
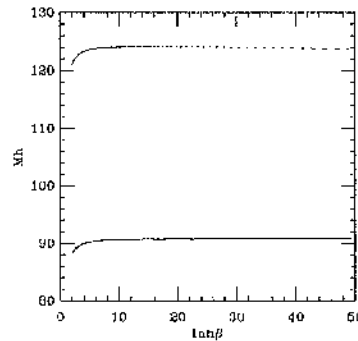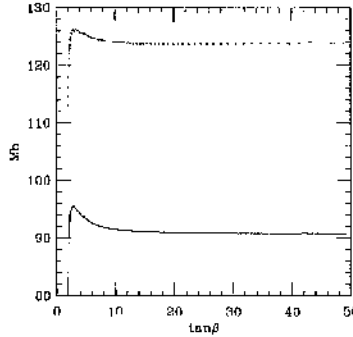

Figure 5.57: Same as in Fig. 5.56, but for $M_{H\pm}$=200-800 GeV.

Figure 5.58: No SCPV. Upper bound on the lightest neutral Higgs mass as a function of $\tan\beta$ for $M_{H^\pm}$=55-200 GeV and SUSY breaking scale equal to 174 GeV (continuous line) and 1 TeV (dotted line) $k = 0.3$ and λ which varies as a function of $\tan\beta$ (see the text).
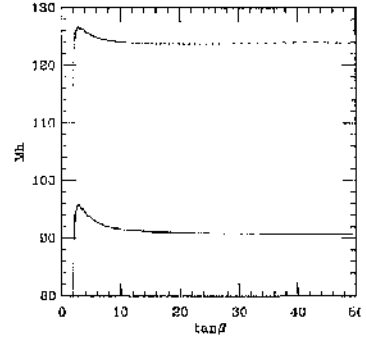

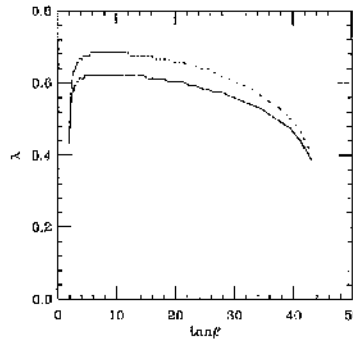Figure 5.59: same as in Fig. 5.58, but for $M_{H^\pm}$=200-800 GeV.

Figure 5.60: λ as a function of $\tan\beta$ for $k = 0.3$ (continuous line) and k=0 (dotted line).
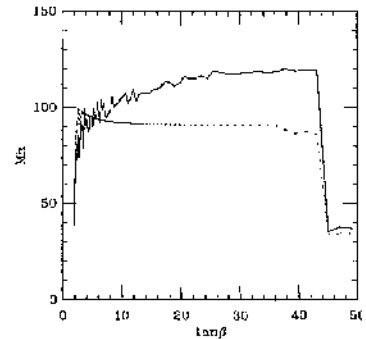

Figure 5.61: No SCPV. Upper bound on the lightest neutral Higgs mass as a function of $\tan\beta$ for $M_{H^\pm} = 200-800$ GeV and SUSY breaking scale equal to 174 GeV (dotted line) and 1 TeV (continuous line) $k = 0$ and λ which varies as a function of $\tan\beta$ (see the text).

5.7 Explicit CP violation

5.7.1 Introduction

So far we have discussed SCPV within the NMSSM as the only source of CP violation. However, CP violation can also be explicit.

There are two possible ways to break the CP symmetry explicitly, namely we can take complex Yukawa coupling constants (see [29]), so that the CP violation will not be in the Higgs sector, and/or we can take some of the parameters in the field dependent effective potential to be complex, so that new CP violating phases are introduced in the Higgs sector (in general some of these phases can be rotated away).

We will in particular analyse in this chapter the second possibility only. It must be emphasized that the vacuum is required to be CP violating as otherwise the potential is unstable (see [29]), so that the analysis of the previous chapter still holds. However, unlike the SCPV case, weak explicit CP violation does not require a light neutral pseudoscalar.

The analysis of explicit CP violation is motivated by the fact that it may represent a possible solution to the domain walls problem; an explicit CP violating phase can in fact lift the degeneracy of the vacua.

We will see in the next section what explicit CP violating phases we have in the NMSSM, and what the neutral Higgs mass spectrum looks like in the presence of these new phases.

5.7.2 NMSSM and explicit CP violation

Within the NMSSM, there are several parameters which can be in principle complex, therefore inducing explicit CP violation. We can in fact have complex μ, λ, k and r which are the parameters in the superpotential, as well as the soft-breaking masses corresponding to these parameters, namely m_{12}^2, m_4, m_5. In particular m_{12} can be taken to be real without loss of generality[8]. So far we treated m_5 and m_4 as real independent parameters; however, these soft mass terms are often written as $\lambda A_\lambda N H_1 H_2$ and $k A_k N^3$ where A_λ and A_k have dimensions of mass. In this notation λ, k and A_i can all be complex, which corresponds to taking m_4 and m_5 complex too. Nonetheless, these soft-masses can be taken as real without loss of generality as we can rotate

away their phases redefining the fields N and $H_1\, H_2$.

We are then left with three terms only, namely, for a SUSY scale equal to the EWSB scale

$$\lambda\, k^\star\, H_1\, H_2\, N\, +\, h.c \tag{5.2}$$

because of λ and k being complex, together with the terms

$$(\mu^\star\, \lambda\, N\, +\, h.c)\, (H_1^\star\, H_1\, +\, H_2^\star\, H_2) \tag{5.3}$$

and

$$r\, \lambda^\star\, N^{2\star} + h.c. \quad . \tag{5.4}$$

We then have three explicitly CP violating phases, namely θ_{exp1}, θ_{exp2} and θ_{exp3} associated to the the three terms above

$$\lambda\, k^\star = |\lambda\, k|\, e^{-i\,\theta_{exp1}} \tag{5.5}$$

$$\mu^\star\lambda = |\mu\,\lambda|\, e^{-i\,\theta_{exp2}} \tag{5.6}$$

$$r\,\lambda^\star = |r\,\lambda|\, e^{-i\,\theta_{exp3}}. \tag{5.7}$$

For a generic SUSY scale the product $\lambda\, k$ is Y_7, so that this will have a phase attached to it. The RGE are not changed by the introduction of this new phase, as they simply fix the coefficients of the gauge sector of the effective potential, which cannot but be real.

The charged Higgs boson mass can still be taken as an independent parameter; however, the corresponding expression for $M_{H^\pm}$ is now different

$$M_{H^\pm}^2 = \left(m_{12}\, sin(\theta_3) - Y_7\, v_3^2\, sin(3\theta_3 + \theta_{exp1})\right) / \tag{5.8}$$

$$(sin(\theta_1 + \theta_3)\, sin\beta\, cos\beta) - Y_4\, v_0^2.$$

Let us for the moment consider just one explicitly CP violating phase, i.e. θ_{exp1}. We want to see what changes the introduction of θ_{exp1} brings to the picture we discussed in the previous chapter. Now in fact the degeneracy of the two CP odd vacua is lifted, so that Georgi-Pais like theorem does not hold anymore.

We show in the Fig. 5.62, 5.63 the upper bound on the lightest neutral Higgs boson mass as a function of θ_{exp} for fixed values of $\theta_1 = \theta_3$ equal to respectively 0.001, 0.01 rad, and θ_{exp1} varied between -0.0001 and -0.01 rad. The sign difference is necessary because otherwise no

solutions are to be found for θ_{exp1} comparable to θ_1, θ_3. Unless otherwise specified, all the parameters are varied randomly within the same ranges as in Tab. 1.

We see that upper bound on M_h is larger in Fig. 5.62 as compared to 5.63: this is because in the former case the explicit phase in comparable to the phases attached to the vevs whereas in the latter case the explicit phase is much smaller and therefore the small phases regime still holds to some extent.

In Fig. 5.64, 5.65 we show the same graphs but this time for $\theta_1 = \theta_3$ equal to respectively 0.1 and 1 rad. From the Fig. 5.62, 5.63 we see that as θ_{exp} goes to zero, the weak SCPV scenario we discussed before is resumed, and the mass of the lightest neutral Higgs boson, which is in the CP odd sector, falls down. In the last two figures instead, the behaviour is different as $\theta_1 = \theta_3$ is quite big, especially in the fourth one. Here for θ_{exp1} going to zero m_h does not fall down, as this time we are not in the small phases regime, as confirmed also by the fact the lightest neutral Higgs boson is not this time mainly pseudoscalar.

Let us now consider the case where all the possible explicitly CP violating phases are considered. We show in Fig. 5.66, 5.67, 5.68, 5.69 the same graphs as in Fig. 5.62, 5.63, 5.64, 5.65 but this time with θ_{exp1}, θ_{exp2} and θ_{exp3} varied randomly between $-\pi/2$ and $\pi/2$. The saturation of the graphs has this time required 1 million random iterations.

Because we are plotting an upper bound on the mass of the lightest neutral Higgs boson, big explicitly CP violating phases will be preferred when θ_1 and θ_3 are small, as in this way the degeneracy between the CP connected vacua is lifted and a big value for m_h is allowed.

5.7.3   Summary

We have briefly addressed the issue of explicit CP violation within the NMSSM, for the case where small SCPV phases are concerned. This has important implications as far as baryogenesis and the domain wall problem are concerned. We have shown that explicit CP violating phases do alter the picture we outlined in the previous chapters, as expected. Experimentally it is going to be quite difficult to differentiate between explicit and spontaneous CP violation; even if the lightest neutral Higgs boson is quite heavy, therefore excluding the weak SCPV
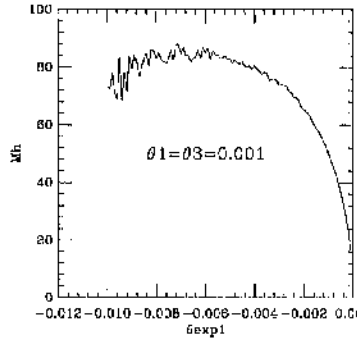
Figure 5.62: $\theta_1 = \theta_3 = 0.001$ rad, SUSY breaking scale=174 GeV and $M_{H^\pm}$=200-800 GeV. Upper bound on the lightest neutral Higgs mass as a function of θ_{exp1}.
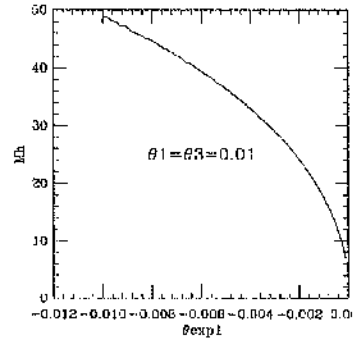

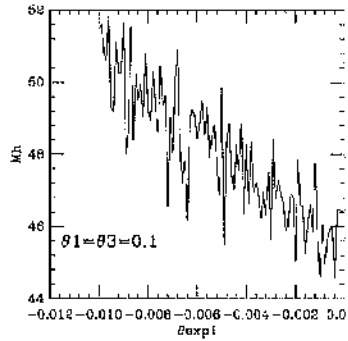Figure 5.63: Same as in Fig. 5.62, but with $\theta_1 = \theta_3$=0.01 rad.

Figure 5.64: Same as in Fig. 5.62, but with $\theta_1 = \theta_3$=0.1 rad.
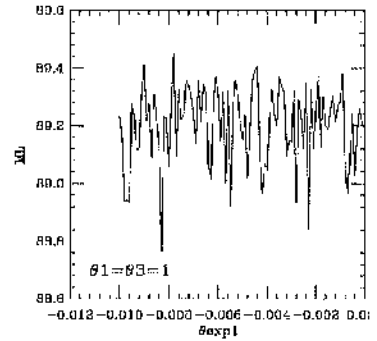

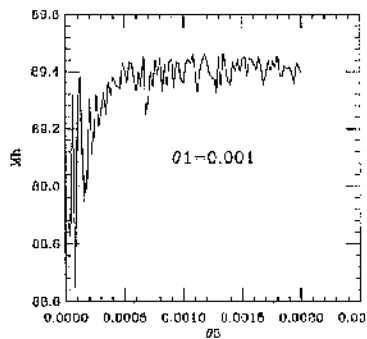Figure 5.65: Same as in Fig. 5.62, but with $\theta_1 = \theta_3$=1 rad.

Figure 5.66: θ_{cxp1}, θ_{cxp2}, θ_{cxp3} are varied randomly. SUSY breaking scale=174 GeV and $M_{H^\pm}$=200-800 GeV. Upper bound on the lightest neutral Higgs mass.
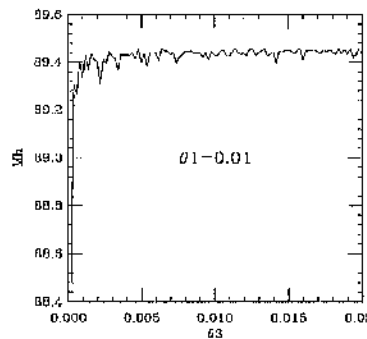

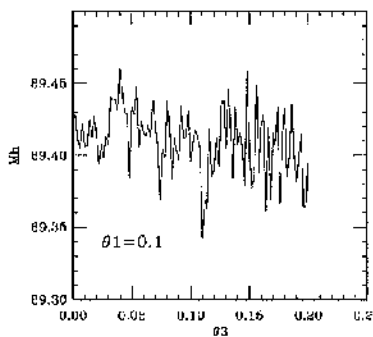Figure 5.67: Same as in Fig. 5.66, but with θ_1=0.01 rad.

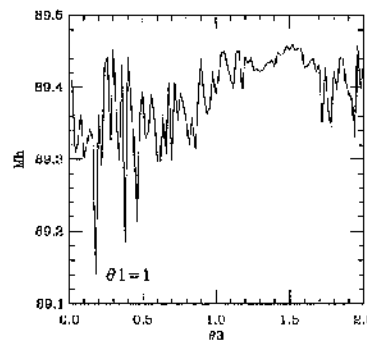Figure 5.68: Same as in Fig. 5.66, but with θ_1=0.1 rad.

Figure 5.69: Same as in Fig. 5.66, but with θ_1=1 rad.

scenario, one may still argue about the possibility of explicit CP violating phases being present.

However, any CP violating phase in the model will contribute to the electric and neutron dipole moments, and so possibly be in contradiction with the experimental bounds. We will address this issue in chapter 7.

5.8   Summary of the chapter

We have seen that weak SCPV implies the presence of a light pseudoscalar, and have studied in detail the corresponding mass spectrum for the three scenarios outlined in chapter 4.

We have discussed the role of λ and k and their importance for the mass bounds on m_A for the case $\theta_3 >> \theta_1$.

The parameter space has also been studied in detail together with the discussion of the absolute minima of the effective potential, and the relevant parameters for the mass bounds shown. We have found in particular that for weak SCPV, all the solutions for $\mu = 0$ were local, the absolute ones being CP conserving.

For weak SCPV the second lightest neutral Higgs boson is scalar, and predominantly doublet if $M_{H^\pm}$ is large.

When CP is conserved, the lightest neutral Higgs boson is scalar, and λ and k play an important role in the case of radiative corrections to the tree level bounds on m_h being considered.

Finally, we have also considered the explicit CP violation case, and seen that this time when the phases attached to the vevs are small no light pseudoscalar is present, because the degeneracy of the vacua is lifted, as should be expected.

Chapter 6

Search for the SUSY spectrum

6.1 General review

It is important to establish whether any of the neutral Higgs bosons for the case of SCPV with small CP violating phases, can be observed experimentally in the future. At present, in SM and MSSM only, lower bounds for neutral Higgs boson for the former one and for the lightest scalar and pseudoscalar in the MSSM for the latter one, exist. In particular, within the SM the neutral Higgs boson is heavier than 107.9 GeV with 95% confidence level, whereas for the MSSM the current limit is 88.3 GeV for the neutral scalar Higgs boson, and 88.4 GeV for the neutral pseudoscalar Higgs boson, with 95% confidence level [26]. For the MSSM the picture is more complicated as there are three neutral Higgs bosons which may be detected. This is obviously also true for the NMSSM, with the further complication of a fourth and fifth neutral Higgs boson, and the continuous presence of the singlet field, which does not couple to gauge bosons, quarks and leptons and thus renders detection more difficult than in the MSSM.

The hadron colliders and the $e^+ e^-$ colliders exploit different channels as suitable for the detection of Higgs bosons so that a specific analysis for each is required[7].

If CP is conserved, scalar and pseudoscalar neutral Higgs bosons will

not mix and according to the range of masses allowed they will decay
into different channels.

Let us observe first that within the electro-weak theory pseudoscalars
do not couple to a pair of vector bosons, so that the process

$$Z^* \to Z + A \tag{6.1}$$

does not occur. This is clearly true only when CP is an exact symmetry.
However, the same process involving scalars is possible

$$Z^* \to Z + S \tag{6.2}$$

(see Fig.6.1) and is the main search channel at LEP. In fact Z+S can ide-
ally be produced up to $\sqrt{s} = 190$ GeV centre of mass energy. The scalar
so produced will then decay into the heaviest fermion anti-fermion pair
kinematically allowed. For the case of the scalar decaying into a pair
of bottom anti-bottom quarks the observation of the process requires
b-tagging.

We can also have the production of a scalar as the result of the decay
of a real Z (see Fig.6.2)

$$Z \to S_i + Z^* \to S_i + l^+ l^- \tag{6.3}$$

if the process is kinematically allowed. The resulting branching ratio
must be lower than the experimental upper bound on the corresponding
process in the SM, namely

$$Z \to h^0 + l^+ l^-. \tag{6.4}$$

As far as the pseudoscalars are concerned, processes like

$$Z \to S_i + A_j \tag{6.5}$$

can take place, if kinematically allowed.

Even if not kinematically allowed for a real Z, this process is still pos-
sible via a virtual Z

$$Z^* \to S_i + A. \tag{6.6}$$

As already said, within the MSSM a lower bound of 88.4 GeV on the
mass of the lightest pseudoscalar exists[26]. This limit does not apply

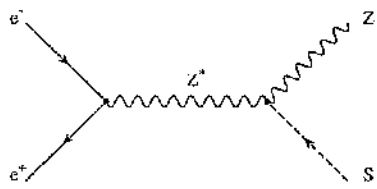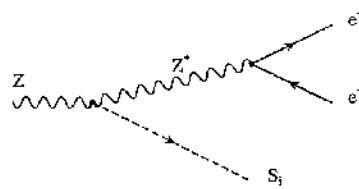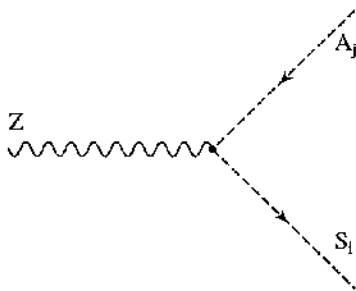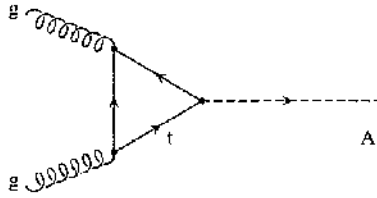Figure 6.1:

Figure 6.2:

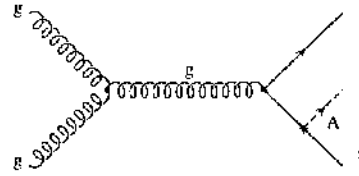Figure 6.3:

Figure 6.4:   Figure 6.5:

to the NMSSM because of the presence of the singlet field. In fact, within the MSSM at the tree level m_h is fixed when m_A and $\tan\beta$ are given, and the couplings obey the sum rule

$$g^2_{ZZS} + g^2_{ZSA} = \left(g^2_{ZZS}\right)^{SM} \tag{6.7}$$

so that the two processes of eq.(6.2), (6.5) are complementary; this is the way employed to determine experimental lower bounds on m_A and m_h within the MSSM. However, within the NMSSM m_h and m_A are independent, so that the two processes cannot be compared with the corresponding ones of the MSSM.

As far as a hadron collider is concerned, a scalar or pseudoscalar neutral Higgs boson can be produced through gg, WW/ZZ fusion (Fig. 6.4, where the case of gluon fusion to give a pseudoscalar is shown)

$$gg \to q\bar{q}\,A\,(S) \tag{6.8}$$

where q can be either a b quark or t quark, or through the Yukawa process of Fig. 6.5.

As far as the vector-vector fusion production is concerned, the coupling with the scalar in the MSSM will only be a fraction of the SM one, as the coupling is shared by the two scalars h^0, H^0. Neutral Higgs bosons can also be produced via Yukawa type diagrams similar to Fig. 6.5, where this time a virtual Z couples to a pair of fermions, i.e. $b\bar{b}$ (the top quark is too heavy to be produced at LEP2), with subsequent radiation

of a Higgs boson, which can then decay to a pair of $b\bar{b}$. This process is important for high values of $\tan\beta$ only, when h_t is not negligible; through this process a neutral Higgs boson as heavy as 180 GeV is kinematically accessible at LEP2. We will not include this contribution in the forthcoming numerical analysis as we will restrict to small values of $\tan\beta$.

6.2 The N field role in the weak SCPV regime

The above discussion applies only when in the Higgs sector the CP symmetry is exactly conserved. However, the experimental analysis is very close to the one delineated above.

Unfortunately, the content of the singlet field in the eigenvectors of the five neutral Higgs bosons of the NMSSM reduces all the couplings when compared to the MSSM ones. This in turn means that, because of the absence at the tree level of VV coupling for the pseudoscalar, this particle will be extremely difficult to observe. On the other hand, things are not so bad if one looks for scalar neutral Higgs bosons rather than pseudoscalars, as in this case the production through vector boson fusion is possible.

For small values of v_3 (or $M_{H\pm}$) such that no decoupling in the CP even sector occurs, the eigenvectors will contain a certain amount of the N field, so that any production will be reduced [1]. We will now discuss in detail how difficult it is to detect the pseudoscalar Higgs boson, i.e. how much weaker the coupling really is.

More precisely, we already know from the formula (4.17) (true assuming weak SCPV so that decoupling of the scalar and pseudoscalar sectors occurs) that, contrary to what could have been thought naively, the light pseudoscalar Higgs boson is predominantly singlet in most of the parameter space, so that indeed its coupling will be very much affected. We can see this explicitly by plotting the N field components of the

---

[1] Notice that the mass of the lightest neutral Higgs boson (which is CP odd) takes its maximum for a value of v_3 such that the decoupling occurs, so that rejecting such cases means having an even lighter mass for the pseudoscalar.

lightest and second lightest neutral Higgs bosons for the cases of Fig. 5.2, 5.3, 5.4 (a similar picture is obtained for a SUSY scale equal to 174 GeV) as a function of θ_3, for the two ranges $M_{H\pm}$=55-200 GeV and $M_{H\pm}$=200-800 GeV, as shown in Fig. 6.11, 6.9, 6.7 for the former range, and 6.10, 6.8, 6.6 for the latter one (ten values of θ_3 have been taken.

We show in Fig. 6.13, 6.15, 6.17 and 6.12, 6.14, 6.16 the corresponding graphs when the SUSY breaking scale is equal to 174 GeV. In the range $M_{H\pm}$=200-800 GeV the second lightest neutral Higgs boson is in the H_1, H_2 sector, as in the MSSM, whereas for the range $M_{H\pm}$=55-200 GeV this is not true anymore, as the decoupling does not occur due to the constrained values of $M_{H\pm}$, which in turn imposes an upper constraint on the allowed values of v_3.

Again we stress that the upper bounds on m_h we have discussed in chapter 5 correspond to a high content of the N field in the eigenvector of the lightest neutral Higgs boson itself; this is to be expected as according to the formula (4.17) the eigenvector of the pseudoscalar Higgs boson tends to be mostly N field, and this is confirmed numerically in the region of the parameter space discussed.

6.3   Numerical analysis

6.3.1   Experimental constraints

We have repeated the same numerical analysis as in the previous chapter, where we obtained the mass bounds on m_h for small CP violating phases as a function of θ_3 for fixed values of θ_1, but this time imposing experimental cuts on the randomly generated samples of sets of parameters.

The imposed experimental constraints are those coming from LEP1 on the on-shell Z boson decays and from LEP2 on the processes of eq. (6.1), (6.2), (6.6).

The constraint on the charged Higgs sector is explicitly imposed by our choice of $M_{H\pm}$ as an independent parameter. $M_{H\pm}$ in turn has to be heavier than 69 GeV, according to [26] where a direct lower limit is cited. As explained in 3.5, we also have prediction for chargino and
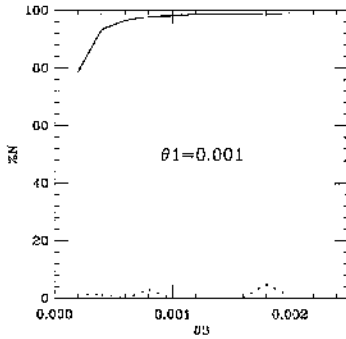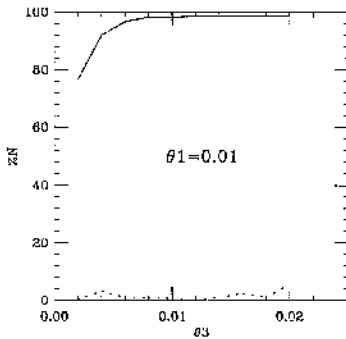
Figure 6.6:

Figure 6.7:
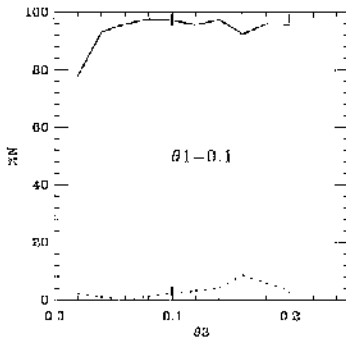

Figure 6.8:

Figure 6.9:

Figure 6.10: SUSY breaking scale=1 TeV. N field percentage in the eigenvectors of the lightest (continuous line) and second lightest (dotted line) neutral Higgs bosons for M_{H^+}=200-800 GeV and different values of θ_1, $\theta_3 = 0 - 2\theta_1$, Fig. 6.6, 6.8.

Figure 6.11: SUSY breaking scale=1 TeV. N field percentage in the eigenvectors of the lightest (continuous line) and second lightest (dotted line) neutral Higgs bosons for $M_{H^\pm}$=55-200 GeV and different values of θ_1, $\theta_3 = 0 - 2\theta_1$, Fig. 6.7, 6.9.
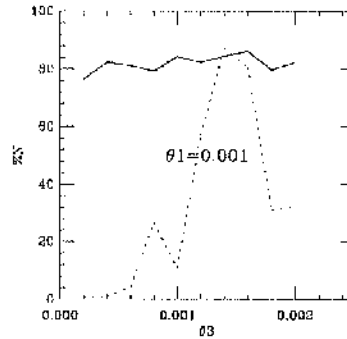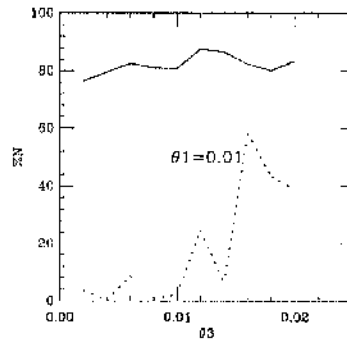
Figure 6.12:

Figure 6.13:

Figure 6.14:

Figure 6.15:

Figure 6.16: SUSY breaking scale=174 GeV. N field percentage in the eigenvectors of the lightest (continuous line) and second lightest (dotted line) neutral Higgs bosons for M_{H^+}=200-800 GeV and different values of θ_1, $\theta_3 = 0 - 2\theta_1$, Fig. 6.12, 6.14.
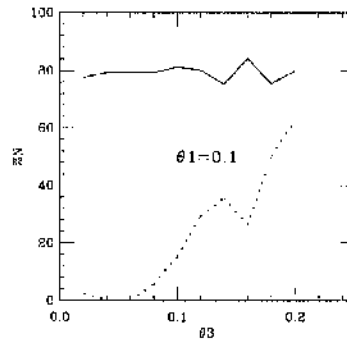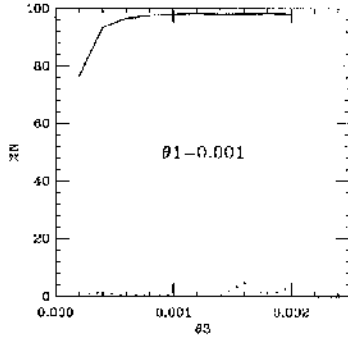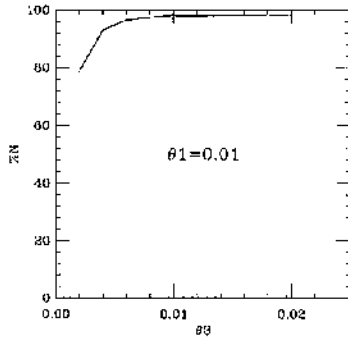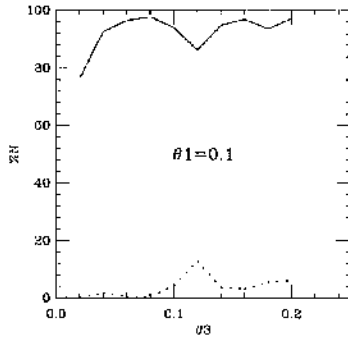
Figure 6.17: SUSY breaking scale=174 GeV. N field percentage in the eigenvectors of the lightest (continuous line) and second lightest (dotted line) neutral Higgs bosons for $M_{H^\pm}$=55-200 GeV and different values of θ_1, $\theta_3 = 0 - 2\theta_1$, Fig. 6.13, 6.15.
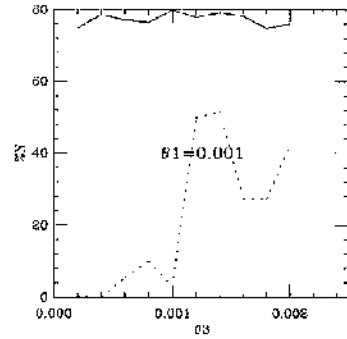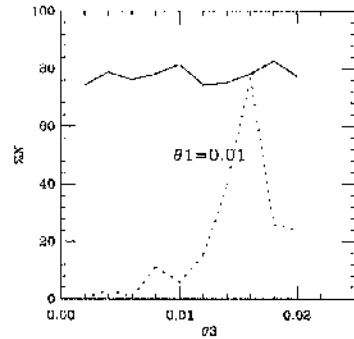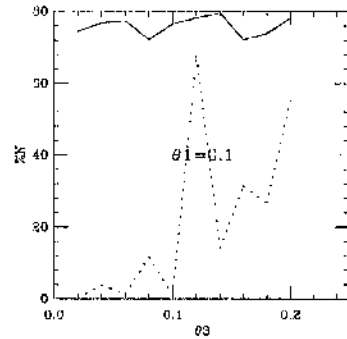
neutralino masses. In particular, we required the lightest chargino to have a mass greater than 91 GeV [42]. As far as the experimental constraint on the lightest neutralino mass is concerned, no experimental limit coming from the MSSM can be applied to the NMSSM, due to uncertain singlet admixture.

LEP1 results imply that the Z boson width should not be affected by the process of eq. (6.3). The corresponding decay width is [32]

$$\Gamma\left(Z \to h_1 h_2\right) = \frac{M_Z}{16\pi} g_{Zh_1h_2}^2 \lambda^{\frac{1}{2}}(1, x_1, x_2) \tag{6.9}$$

where

$$\lambda(x, y, z) \equiv x^2 + y^2 + z^2 - 2xy - 2yz - 2zx$$

$x_i \equiv m_{h_i}^2/M_Z^2$, and

$$g_{Z h_1 h_2} \equiv g_2 \left(cos\beta(a_{12}a_{23} - a_{22}a_{13}) - sin\beta(a_{11}a_{23} - a_{21}a_{13})\right) \tag{6.10}$$

where a_{1j} and a_{2j} (j=1,5) are the eigenvectors of h_1 and h_2 respectively, in the unitary gauge (see Appendix C), with j=1,5 indicating $Re\left(H_1^0\right)$, $Re\left(H_2^0\right)$, $Im\left(H_1^0\right)$ $(=Re\left(H_s^0\right))$, $Re\left(N\right)$ and $Im\left(N\right)$ respectively. The experimental constraint is that $BR(Z \to h_1 h_2) < 10^{-7}$ [33]. Also, the decay width for the process of eq. (6.5) should such that that [32]

$$\Gamma\left(Z \to h_i l^+ l^-\right) < \Gamma^{exp} \tag{6.11}$$

where Γ^{exp} is the experimental upper bound for the corresponding process in the SM, equivalent to $BR\left(Z \to h\, l^+ l^-\right) < 1.30 \times 10^{-7}$ [33] at $m_h = 60$ GeV [2], and

$$\Gamma\left(Z \to h_i\, l^+ l^-\right) = \frac{1}{96\,\pi^3} \frac{g_{ZZh_i}^2 g_{Zl^+l^-}^2}{M_Z} \left(|C_L|^2 + |C_R|^2\right) \tag{6.12}$$

$$\times \int_\rho^{(1+\rho^2/2)} \frac{1 + \rho^2 - 2x}{(\rho^2 - 2x)^2 + \Gamma_Z^2/(4M_Z^2)}(x^2 - \rho^2)^{1/2}dx$$

---

[2]The value of m_h is clearly smaller the the existing lower bound coming from LEP2, as the Z boson is on shell.

where $\rho = m_{h_i}/M_Z$, $x = E_{h_i}/M_Z$, $g_{Zl^+l^-} = 2e/sin(2\theta_W)$,
$C_L = -\frac{1}{2} + sin^2(\theta_W)$, $C_R = sin^2(\theta_W)$, and

$$g_{ZZh_i} = \frac{g_2}{2\,cos\theta_W}\,M_Z\,cos\beta\,(a_{i1} + a_{i2}\,tan\beta)\,. \tag{6.13}$$

We use h_i rather than S_i to differentiate between the SCPV case and
the non SCPV one.

As far as the constraints coming from LEP2 are concerned, we fol-
low the qualitative analysis of [34]. We calculate the total number of
events, using the cross section formulae at the centre of mass energy
for a given total luminosity. We assume, somewhat arbitrarily, an ex-
perimental lower bound of approximately 20 (the discovery limit), that
is to say at least 20 Higgs bosons need to be produced at LEP2 for
certain discovery. Assuming then the maximum center of mass energy
and total luminosity (given by the sum of the luminosities accumulated
by the four experiments at LEP2 for that particular center of mass
energy), it is possible to obtain upper limits on the couplings Zh_ih_j
and ZZh_i, against which the ones coming from the numerical analysis
discussed in the previous chapter can be checked.
In principle one should use a Montecarlo simulation describing the de-
cay of the produced Higgs bosons into channels like $b\bar{b}$ or $\tau\bar{\tau}$. However,
as discussed in [34], the above criterion does give results in good agree-
ment with the more sophisticated LEP2 Montecarlo simulation, as long
as the mass of the produced Higgs boson is not too close to M_Z; this
is going to be certainly the case for m_A and small CP violating phases,
although not necessarily so for the second lightest neutral Higgs boson
mass. We will nontheless stick to this assumption as an easy way to
study qualitatively the impact the experimental constraints can have
on the numerical analysis we discussed in the previous chapter.
The cross sections for the two processes of eq. (6.1) and (6.2) are re-
spectively

$$\sigma\left(e^+\,e^- \to h\,Z\right) = R_h^2 \times \sigma_{SM}\left(e^+\,e^- \to h\,Z\right) \tag{6.14}$$

and

$$\sigma\left(e^+\,e^- \to A\,Z\right) = R_A^2 \times \sigma_{SM}\left(e^+\,e^- \to A\,Z\right) \tag{6.15}$$

where [35]

$$\sigma_{SM} = \frac{\pi\,\alpha\lambda_{Zh}^{1/2}\left(\lambda_{Zh} + 12\frac{M_Z^2}{s}\right)\left(1 + (1 - 4\,sin^2\theta W)^2\right)}{192\,s\,sin^4\theta_W\,cos^4\theta_W\,(1 - M_Z^2/s)^2} \qquad (6.16)$$

is the corresponding SM cross section for a Higgs boson of mass equal to m_h (m_A) respectively, and

$$\lambda_{Zh} = \left(1 - \frac{M_h^2 + M_Z^2}{s}\right)^2 - \frac{4\,M_h^2\,M_Z^2}{s};$$

s is the center of mass energy squared, and R_h (R_A) is the ZZh (ZZA) coupling in units of the SM ZZh coupling.

The cross section for the process of eq. 6.6 is instead the following

$$\sigma\left(e^+e^- \to h\,A\right) = \frac{\alpha\,g_{Zh_1h_2}^2}{24\,s\,sin^2\theta_W\,cos^2\theta_W}\left(|C_L|^2 + |C_R|^2\right) \qquad (6.17)$$

$$\times \frac{\lambda^{3/2}(1, y_1, y_2)}{(1 - y_Z)^2 + \frac{y_Z\Gamma_Z^2}{4s}}$$

where $y_i = m_{h_i}^2/s$ and $y_Z = M_Z^2/s$, $\lambda(x,y,z) = x^2 + y^2 + z^2 - 2xy - 2yz - 2zx$.

The cross sections are calculated for each set of NMSSM parameters which gives real eigenvalues. All the neutral Higgs bosons are considered as being a mixture of the CP odd and even sectors; the processes $Z^* \to h_i\,h_j$ and $Z^* \to Z\,h_j$ are then considered (when the masses are such that the processes can be accessed at LEP2) and the corresponding cross-sections calculated.

The resulting number of events can be then obtained from the relation $\int \mathcal{L} \times \sigma = N$ where σ is the cross section and N is the number of events. If the resulting number of events for a particular set of parameters and for a particular process is bigger than [3] 20 then the set is rejected on the

---

[3]In [34] a number of events equal to 50 is assumed as the discovery limit. However, this number includes all possible Higgs boson available, namely three for the coupling ZZh_i as with no CP violation there is no mixing between the even and odd Higgs sectors; this means that there is no vector-vector-boson coupling with a pseudoscalar Higgs boson and that the only Higgs bosons available are the scalar ones, which are three.

As we consider each channel independently, we assume a discovery limit of twenty events for each particular Higgs boson, not just the whole of them.

basis that the corresponding mass spectrum would have been observed
at LEP2.

We have assumed in the numerical analysis outlined in the next section
$\sqrt{s} = 189$ GeV and $\int \mathcal{L}=175 \times 4\,pb^{-1}$, the four factor being the number
of the experiments at LEP2.

In [34] the NMSSM was discussed without SCPV, with the result that a
lower experimental bound has been established on the (4,4) matrix ele-
ment of the 5×5 neutral Higgs boson mass matrix, namely $(4,4) > 69$
GeV under the assumption that the lightest neutral Higgs boson is
heavier than 12 GeV, so that the decay into $b\bar{b}$ is available [36]. This
added experimental constraint is clearly not valid when SCPV is consid-
ered; however, for small CP violating phases such that the CP odd and
CP even sectors can be considered as decoupled, then one should also
implement this constraint. Unfortunately, when $\theta_1 = 0.001, 0.01\,rad$
the lightest neutral Higgs boson is below 12 GeV so this constraint
does not play any role; for $\theta_1 = 0.1$ rad the parameter space is not
always within the small CP violating phases regime, that is to say the
mixing between the CP odd and CP even part is not negligible (par-
ticularly for high values of v_3).

It should be noted that we have neglected Yukawa type diagrams con-
tributions where the virtual Z couples to a pair of fermions, i.e. $b\bar{b}$
(the top quark is too heavy to be produced at LEP2), with subsequent
radiation of a Higgs boson, which can then decay to a pair of $b\bar{b}$. This
process is important for high values of $\tan\beta$ only, when h_b is not neg-
ligible; through this process a second lightest neutral Higgs boson as
heavy as 180 GeV is kinematically accessible at LEP2, whereas we have
found that an upper bound close to 120 GeV exists [4].

As far as the experimental constraint on the lightest chargino is con-
cerned, the current lower bound on its mass is 91 GeV [42].

6.3.2   Numerical results

We show in Fig. 6.18, 6.20, 6.22 the lightest neutral Higgs boson mass
as a function of θ_3, varied between zero and twice θ_1 (for a total of 10

---

[4]Note however that this upper bound is increased by the inclusion of stop quarks
contributions to the radiative corrections.

points), for fixed values of θ_1 equal to 0.001, 0.01 and 0.1 rad respectively. $M_{H=}$ is randomly varied between 69 (although we have shown graphs for $M_{H+}=55$ GeV, for the experimental constraint we adopt the latest bound of 69 GeV) and 200 GeV, $m_6 = -500 - 0$, the SUSY breaking scale is taken equal to 1 TeV (continuous line) and 174 GeV (dotted line) and $\lambda = k = 0.5$.

Furthermore, in all the graphs, for each of the ten values of θ_3 one hundred thousand random samples of the unfixed parameters of Tab.5.1 were performed.

The squares (SUSY=1 TeV) and diamonds (SUSY=174 GeV) show the corresponding upper bounds obtained when the experimental constraints we discussed above are also imposed (when not present in the graphs, it just means that all the sets are experimentally ruled out), with the corresponding minima of the effective potential being in general local. The y axis is taken to be logarithmic in order to be able to distinguish the curves for different SUSY scales, as they are quite close.

A similar scenario is shown in Fig. 6.19, 6.21, 6.23 where this time $M_{H^\pm}$ is varied between 200 and 800 GeV.

The strongest experimental constraint for a SUSY scale equal to 174 GeV and $M_{H^\pm} = 69 - 200$ GeV turned out to be the one coming from LEP1. The sum of the masses of the lightest and second lightest neutral Higgs bosons is for example always below M_Z when the SUSY scale is equal to 174 GeV and $\theta_1 = 0.001$ rad; however, when the SUSY scale is equal to 1 TeV, the LEP1 constraints can be kinematically avoided, as can be seen in the graph of Fig. 6.18, where some experimental points are present for $\theta_3 < \theta_1$ (squares). It should noted that when θ_3 is increased, the number of sets giving real eigenvalues drops down, so that fewer cases can be tested against the experimental constraints (see chapter 5, section 5.4.)

On the other hand, for the range $M_{H^\pm} = 200 - 800$ GeV we do get sets which pass all the experimental constraints, as this time the number of sets which give real eigenvalues in the first place is bigger, and the upper bound on the sum of the masses of the lightest and second lightest neutral Higgs boson avoids the LEP1 constraint.

We have restricted ourselves to the regime where θ_3 is smaller or of the same order than θ_1; the case when $\theta_1 << \theta_3$ has not been studied as decoupling occurs and the pseudoscalar is almost completely singlet,
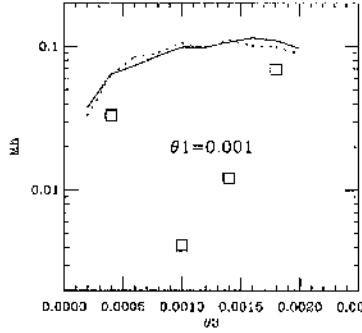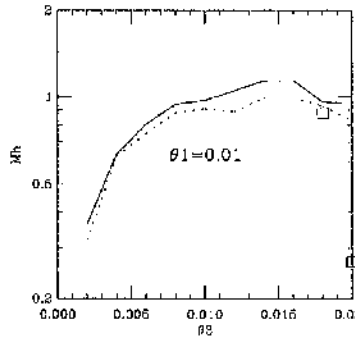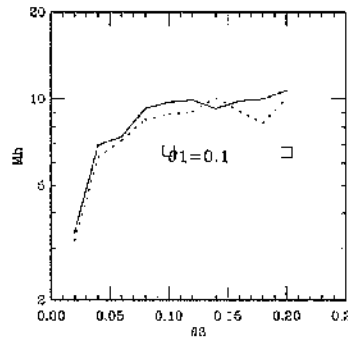
Figure 6.18:

Figure 6.19:

Figure 6.20:

Figure 6.21:

Figure 6.22: Upper bound on the lightest neutral Higgs boson mass as a function of θ_3 for different values of θ_1. $M_{H^\pm} = 69 - 200$ GeV and SUSY breaking scale equal to 1 TeV (continuous line) and 174 GeV (dotted line). Experimental acceptable upper cases are also shown (squares for SUSY=1 TeV).

Figure 6.23: Upper bound on the lightest neutral Higgs boson mass as a function of θ_3 for different values of θ_1. $M_{H^\pm} = 200 - 800$ GeV and SUSY breaking scale equal to 1 TeV (continuous line) and 174 GeV (dotted line). Experimental upper bounds are also shown (squares for SUSY=1 TeV and diamonds for SUSY=174 GeV).
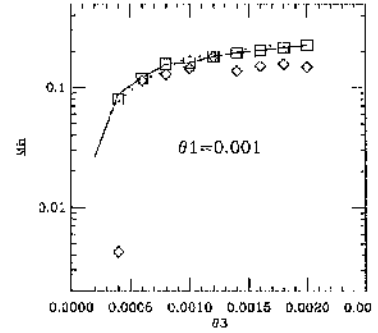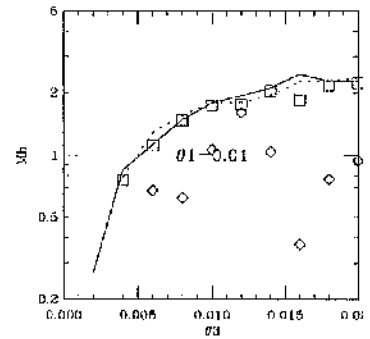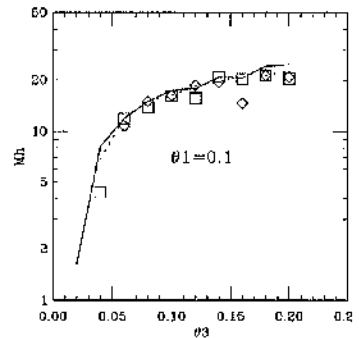
as discussed in 6.2. However, decoupling can be desirable because in this case the second lightest neutral Higgs boson is almost completely in the $H_1 H_2$ sector and therefore detectable without any suppression coming from the N field content in the corresponding eigenvector.

Furthermore, we have not considered the case where λ is taken to be small. Although this allows a much bigger number of sets to have real eigenvalues, it constrains the mass of the second lightest neutral Higgs boson to lower values, implying a stronger suppression coming from the LEP1 constraint.

We have seen that because of the N field presence, the small SCPV scenario cannot be ruled out experimentally; however, we need to assess how much N field does need to be present in the eigenvector of the lightest neutral Higgs boson for this to be the case. This can be seen easily enough taking for example fixed values of θ_1 and θ_3, and plotting m_{h_1} as a function of the N field percentage in the eigenvector. We show in Fig. 6.24, 6.26, 6.25 and 6.27 the cases $\theta_1=0.001$, 0.01 rad, $m_6 = -500 - 0$ GeV, the SUSY scale equal to 174 GeV, and $M_{H^\pm} = 69 - 200$ GeV and $M_{H^\pm} = 200 - 800$ GeV: diamonds are the corresponding points with the experimental constraints satisfied; when no diamond is shown, it just means that all the sets were ruled out.

We draw the obvious conclusion that for the experimental constraints to be satisfied, a high content of the N field in the eigenvector is required, i.e. > 90%, which turns out to be natural. Also, LEP1 constraints play an important role, especially for low values of $M_{H^\pm}$ and exact SUSY.

However, note the number of sets upon which the experimental constraints are imposed must be large, and for $M_{H^\pm}=69\text{-}200$ GeV and a SUSY scale of 174 GeV, turns out to be instead quite small (less than few hundreds per one hundred thousand random parameter sets).

6.3.3 Conclusions

We have discussed in this chapter the issue of whether the weak SCPV scenario within the NMSSM can in any way be tested experimentally by LEP2. The typical processes where a virtual Z couples to one or a pair of neutral Higgs bosons were considered; in particular, we included all the five neutral Higgs bosons in the analysis, if their masses turned

Figure 6.24:

Figure 6.25:

Figure 6.26: $M_{H\pm} = 69 - 200$ GeV, SUSY=174 GeV. Upper bound on the lightest neutral Higgs boson mass vs the N field percentage for two values of $\theta_1 = \theta_3$ (squares) and corresponding experimental points (diamonds).
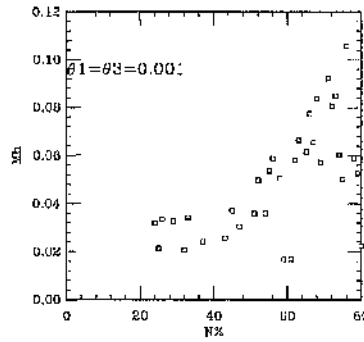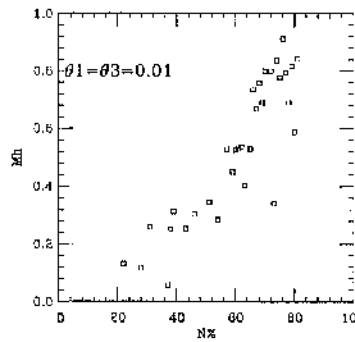
Figure 6.27: $M_{H\pm} = 200 - 800$ GeV, SUSY=174 GeV. Upper bound on the lightest neutral Higgs boson mass vs the N field percentage for two values of $\theta_1 = \theta_3$ (squares) and corresponding experimental points (diamonds).
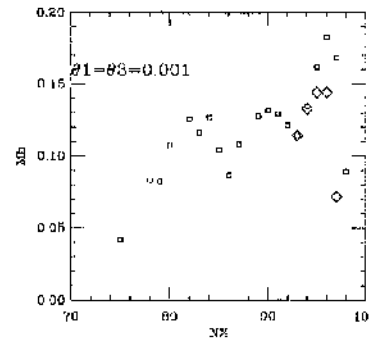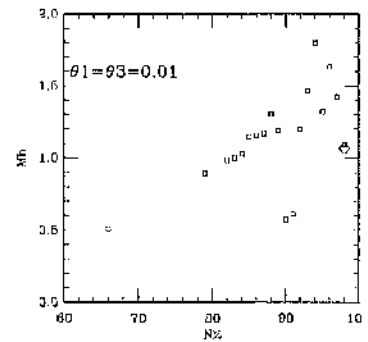
out to be accessible at LEP2.

The discussion presented was qualitative as no realistic montecarlo analysis was considered, but rather the single cross sections were taken, and from them the number of events obtained; the criterion was that if 20 neutral Higgs bosons of the same mass can be produced in the first place, then they would certainly be observed. The analysis is certainly simplistic, but nontheless gives some insight into the possible testing of the model experimentally.

At first sight a light pseudoscalar neutral Higgs boson should be easily accessible at LEP, and indeed within the MSSM a lower bound of about 70 GeV on its mass is reported. However, we have shown that for weak SCPV within the NMSSM, in a vast region of the parameter space the pseudoscalar is to a large extent mainly singlet, so that its coupling is much reduced. The main consequence is that both its production and its decay are much reduced, so that it can easily escape detection. The second lightest neutral Higgs boson in the scenario is a scalar, and in certain areas of the parameter space, where the light pseudoscalar is almost completely singlet, is mainly in the $H_1 H_2$ sector; furthermore, its mass has an upper bound which at the tree level is within the reach of LEP2. Although in general LEP2 cannot rule out the existence of such a particle, and so the scenario as a whole, future colliders like LHC should be able to. Even if one thinks of fine tuning the parameters in such a way that detection of the light pseudoscalar and lightest scalar are hard, LHC should in any case be able to access the other neutral Higgs bosons. The N field presence in itself is extremely important particularly for the pseudoscalar, and in general, to a certain degree, for all the other neutral Higgs bosons as well, but it will not prevent the overall testability of the whole scenario by LHC as, if one particular coupling is suppressed, there will be another one which is enhanced, similarly to what happens within the MSSM with the lightest neutral and pseudoscalar Higgs bosons.

Yukawa type diagrams have been neglected because we have considered small values of $\tan\beta$, for which these diagrams are negligible at LEP2. In the analysis we have also included the constraints coming from LEP1 and imposed the lower bounds on the charginos masses.

However, for simplicity we have not included constraints coming from hadron colliders.

The result, based on the limit coming from LEP2, is that weak SCPV in the NMSSM cannot be ruled out yet, and calls attention to the possibility that a light pseudoscalar neutral Higgs boson can have escaped detection so far.

The result is qualitative, as the space of unknown parameters in the model is large, and on the experimental side it does not take sufficient account of the complexities of decay modes and detector efficiencies.

Note also that a light neutral Higgs boson can actually very well escape detection in other models, such as the two Higgs doublet model [43] [44], so emphasising the need for future experiments to search for light neutral Higgs bosons.

Chapter 7

Neutron and electron dipole moments

7.1 Introduction

In this chapter we study the neutron and electron dipole moments (nEDM and eEDM), as a possible probe of the feasibility of the spontaneous CP violation scenario for the NMSSM, when the CP violating phases are not small. This is necessary in order to establish whether big CP violating phases can be taken, as the small CP violating phases regime might be ruled out by future collider experiments like LHC.
In particular the cancellation mechanism will be investigated.
Large CP violating phases are compatible with LEP but give rise necessarily to a big contribution to the neutron and electron dipole moments. The experimental upper bounds have been decreasing in recent years, and are currently, for the neutron $nEDM < 6 \times 10^{-26} \, e \, cm$ [45] and for the electron $eEDM < 4.3 \times 10^{-27} \, e \, cm$ (see [46]).
It should be noted that within the SM the nEDM is predicted to be of the order of $O(10^{-34}) \, e \, cm$, whereas the eEDM is predicted to be $<< 10^{-50} \, e \, cm$ (see [47] and references therein). Within the SM CP-violation can arise from weak interaction as well as strong interaction (we will not discuss the latter case in this work). In the former case the CP violating phases are those of the Kobayashi-Maskawa (KM) matrix for the quarks, and there are analogous CP violating phases in the lep-

tonic sector if at least two neutrinos are massive (otherwise the electron EDM would be zero, as the CP violating phases can be rotated away). However, the CP violating phases cancel at the one loop level and the resulting EDMs are zero. At the two loop level it is found that the sum of all the contributions is exactly equal to zero, both for the electron and neutron, so that one has to go at least to the three loop level to find non zero EDMs. This in turn explains the smallness of the resulting EDMs, which are well below any possible experimental investigation. Within SUSY theories, limiting ourselves to the KM CP violating phases, we still find that the one loop contributions are equal to zero, and that the sum of the two loop contributions vanishes, as within the SM. However, many other CP violating phases can be present in the model, so that in general one loop contributions will be different from zero. In fact, it is known that in SUSY EDMs are in general bigger than the experimental bounds, unless the CP violating phases are < 0.01 rad.

A study of the neutron and electron EDMs can then provide insight into the physics beyond the standard model.

Our aim is to study numerically the various contributions to the neutron and electron EDM within the NMSSM for the SCPV scenario and see under which conditions there is agreement with the experimental constraints.

In the second section of this chapter we review some of the many papers which have appeared in the last ten years or so about this subject.

In the third section we present the explicit formulas for all the relevant contributions to the electron and neutron EDMs.

In the fourth section we discuss a numerical analysis of the neutron and electron EDMs.

7.2 NDM and EDM: a general review

There are more CP violation sources in supersymmetric theories than in the SM. Although this is an upside as far as baryogenesis is concerned, a possible inconsistency with the neutron and the electron dipole moments experimental upper bounds can arise.

The electric dipole interaction of a spin 1/2 particle f with an electromagnetic field can be described by an effective lagrangian

$$\mathcal{L}_I = -\frac{i}{2} d_f \, \bar{f} \, \sigma^{\mu\nu} \, \gamma_5 \, f \, F_{\mu\nu} \qquad (7.1)$$

where d_f is the EDM of the particle, f is the spin 1/2 field, $F_{\mu\nu}$ is the electromagnetic field, and $\sigma^{\mu\nu} = \frac{i}{2} [\gamma^\mu, \gamma^\nu]$ where γ^μ are the gamma matrices.

It should be noticed that a term like in eq. (7.1) cannot be present at the tree level in a quantum field theory, because it is not renormalizable. However, such a term can occur at the one loop level, if CP violating interactions are present in the theory.

We generalise the idea, so that we can write an effective lagrangian

$$\mathcal{L}_I = \sum_i C_i(Q) \, O_i(Q) \qquad (7.2)$$

where $C_i(Q)$ are Wilson coefficients evaluated at a scale Q, and $O_i(Q)$ are CP violating operators. The coefficients $C_i(Q)$ are effectively the contributions to the EDM at the scale Q, as d_f was in eq. (7.1).

The dimension of O_i has to be bigger than four, as all the operators of dimension smaller than five are automatically CP conserving. The scale dependence of $C_i(Q)$ has to be such that the product $C_i(Q) \, O_i(Q)$ is independent of Q.

We have effectively three operators, namely

$$O_1 = -\frac{i}{2} \bar{f} \, \sigma_{\mu\nu} \, \gamma_5 \, f \, F_{\mu\nu} \qquad (7.3)$$

$$O_2 = -\frac{i}{2} \bar{f} \, \sigma_{\mu\nu} \, \gamma_5 \, T^a \, f \, G^a_{\mu\nu} \qquad (7.4)$$

$$O_3 = -\frac{1}{6} f_{abc} \, G^a_{\mu\rho} \, G^{b\rho}_\nu \, G^c_{\lambda\sigma} \, \epsilon^{\mu\nu\lambda\sigma} . \qquad (7.5)$$

The first two are dimension five operators whereas the third one, first discussed by [49], has dimension six.

We can ignore operators of higher dimension on the ground that their contribution will be negligible compared to the ones given by lower dimension operators. This assumption may turn out to be wrong for

big values of $\tan\beta$ and if the squarks of the third generation are significantly lighter than those of the first two generations, so that the one-loop contributions are suppressed [51].

Higher-loop contributions like those of [50] are found to be one order of magnitude smaller the the one-loop contributions, and so they can be important in the case when the latter are suppressed, i.e. for large squark masses, or in the case of cancellation.

We will nontheless ignore these contributions on the basis that if cancellation is possible, than it can occur also when these new diagrams are included, although these two-loop contributions have the same sign as the one-loop ones.

However, the two-loop six dimension purely gluonic operator O_3 cannot be ignored compared to the five dimension operators, as there are no mass insertions required, which tend to somehow suppress O_1 and O_2, so that its contribution can be quite big, although smaller than the former two.

Once again an effective lagrangian like the one in eq. (7.2) cannot be present at the tree level because it is not renormalizable. However, these terms are generated at the one loop level (C_1 and C_2) and two loop level (C_3). The corresponding Feynman diagrams are shown in Fig. 7.37, 7.38, 7.40, 7.41 at the end of the chapter.

Note that for the chargino there are just two diagrams, i.e. one in which the couplings at the vertices are due to gauge and Yukawa interaction respectively (gaugino-higgsino diagram), and another one where the couplings at the vertices are both due to Yukawa interactions (higgsino-higgsino diagram). For neutralinos there is also the possibility of the couplings at the vertices being both due to the gauge interaction (gaugino-gaugino diagram).

It should be stressed that the operators O_2 and O_3 do not contribute to the electron EDM. As far as the neutron EDM is concerned, all the operators O_i, i=1,2,3 contribute and have to be calculated at the relevant scale Q where all QCD contributions are comparable, namely $Q \approx$ EWS. They have then to be run down using the RGE approach to the scale relevant for the neutron, namely $\Lambda_{QCD} \approx 237$ MeV, in order to be able to compare the theoretical prediction with the experimentally measured value. This has been done in [52] [58] considering the b and c quark thresholds, which tend to enhance the magnitude of the neutron

EDM, as well as the chiral symmetry breaking scale $\Lambda_\chi \approx 1.18$ GeV threshold, which instead tends to suppress the final value of EDM.

In the region between Λ_χ and Λ_{QCD}, QCD is not perturbative, so that dimensional analysis is used instead [48]. The final result is

$$C_i^q(\Lambda_\chi) = \eta_i \, C_i^q(Q) \tag{7.6}$$

where $\eta_1 \approx 1.53$ and $\eta_2 \approx \eta_3 \approx 3.4$.

The dimensional analysis then gives for the EDM d_f of a quark f

$$d_f = C_1^f(\Lambda_\chi) + \frac{e}{4\pi} C_2^f(\Lambda_\chi) - \frac{e\Lambda_\chi}{4\pi} C_3^f(\Lambda_\chi). \tag{7.7}$$

To obtain the neutron EDM from the EDMs of the single quarks, a model of the neutron has to be assumed. It is customary to assume for the neutron the non relativistic quark model, so that

$$d_n = \frac{4}{3}d_d - \frac{1}{3}d_u \tag{7.8}$$

where d_n is the neutron EDM, and d_d, d_u are the d and u quark EDMs respectively. This assumption is known to work very well for the baryon magnetic dipole moments [19].

However, it should be born in mind that one could think of assuming instead the relativistic quark-parton model [55] [56] and in that case the overall normalisation and even sign of the various contributions are different; furthermore, in the latter model we also have a contribution from the s quark, which is completely absent in the non relativistic quark model (see also [57]). However, as long as cancellation occurs mainly within the dominant term which contributes to the nEDM, i.e. the d quark contribution (the u quark contribution is suppressed due to the smaller mass when compared with the d quark), then both the models should give the same qualitative answer.

The six dimension purely gluonic operator was originally found to give by far the biggest contribution of all [54]; however, a subsequent analysis found that this is not the case [58], and that the one loop contributions are bigger, the biggest being those of Fig. 7.37, 7.38. An analysis of this contribution and of the others to the neutron EDM within the context of SUSY theories can be found in [52] and [53].

In particular, in [52], the QCD correction factors to the various Wilson operators contributing to the nEDM are studied, and the order of magnitude for the resulting nEDM within the supergravity inspired MSSM has been assessed. For a generic CP violating phase ϕ, the result is that $d_n^{ED} \approx 9.7 \times 10^{-23} \sin\phi\, e\, cm$, $d_n^{CD} \approx 2.1 \times 10^{-23} \sin\phi\, e\, cm$ and $d_n^{G} \approx 4.6 \times 10^{-24} \sin\phi\, e\, cm$ where d_n^{ED} is the quark electric dipole moment contribution, d_n^{CD} is the quark colour dipole moment contribution and d_n^{G} is the six dimension purely gluonic operator contribution. In [53] it is shown that in the limit where supersymmetry is exact, all the contributions to the neutron and electron EDMs have to vanish because they are not supersymmetric. An analysis of the various contributions within the context of the supergravity inspired MSSM, with the CP violation coming from an explicit CP violating phase attached to the gluino mass, has given the following results: $|d_n^{E}| \approx 3.2 \times 10^{-23} \sin\phi\, e\, cm$, $|d_n^{C_1}| \approx 2.1 \times 10^{-23} \sin\phi\, e\, cm$, $|d_n^{C_2}| \approx 3.4 \times 10^{-24} \sin\phi\, e\, cm$ where d_n^{E} is the quark EDM contribution associated to the Feynman diagrams in Fig. 7.37, 7.38, $d_n^{C_1}$ and $d_n^{C_2}$ are the quark colour dipole moment contributions and ϕ is the CP violating phase. There are two colour dipole moment operators as the quark masses are not on shell, so that the quarks in the neutron are not taken to be free: this is done for the sake of generality as otherwise the second operator reduces to the first one. For the six dimension purely gluonic operator the result is that its contribution to the nEDM is approximately equal to $4.6 \times 10^{-24} \sin\phi\, e\, cm$. The single contributions are all bigger than the current experimental upper bound on the NDM, so that either $sin\phi$ is small or the squark masses are very large (the possibility of cancellation will be discussed later).

The latter idea is further discussed in [59] within the framework of the supergravity inspired MSSM, where the one loop order terms contributing to the neutron EDM and electron EDM are studied. No chromoelectric or two loop order terms are considered, as supposed to be smaller than the one loop terms, and the non relativistic quark model for the neutron is assumed (see eq. (7.8)). The CP violation is taken to come from explicit CP violating phases attached to m_H and A_f, the first one being the (2,2) term of the chargino mass matrix, and the second one being the tri-linear term which enters the squark mass matrix (the f refers to the flavour). This is just an assumption as more phases

can be present in the model.

The result obtained is that when squarks are heavier than few TeV, the one loop contributions are under control. In fact, the single contributions actually get smaller and smaller for heavier squark masses; even when the soft masses are taken to be independent, heavy squarks still imply a smaller neutron EDM.

It was also found that there are regions in the parameter space where the electron EDM is bigger than the neutron EDM, therefore representing a stronger constraint.

However, squark masses bigger than 1 TeV means that the hierarchy problem reappears, so that a possible alternative solution is wanted.

In [60] an analogous study is pursued, this time employing the RGE, and in particular the two loop order gauge and Yukawa coupling constants RGE. The μ and B parameters of the MSSM are determined by minimising the full one loop potential. No CP violation other than the one coming with the Yukawa coupling constants is assumed; however, because the tri-linear terms A_i depend on the Yukawa coupling constants, CP violating phases are induced at low energy, so that the one loop diagram amplitudes are not equal to zero.

The value of A_0, which is the common value of the tri-linear terms at the unification scale, is constrained so that no colour breaking minima occur. It is found numerically that the neutron EDM lies in the range 10^{-33}, 10^{-29} $e\,cm$, therefore far below the experimental lower bound.

This study does not assume any unnatural constraint on the magnitude of the phases. However, more phases can be present in the model, therefore raising the magnitude of the neutron and electron EDMs.

In [61] a possible cancellation mechanism is proposed among all the possible terms contributing to the final expression of neutron and electron EDMs. The model considered is the MSSM within the framework of supergravity theories, with the one loop correction to the tree level potential including contributions from top, stop, bottom and sbottom squarks. The RGE are used to fix the soft-terms, starting from the value at the unification scale for A_0 and m_0, these being the common values of the tri-linear and soft-breaking masses respectively. Both the one and two loop order diagrams contributing to the EDMs are considered and the non relativistic quark model for the neutron is assumed (see eq.(7.8)).

The CP violating phases are attached to μ_0 and A_0 at the unification scale. The RGE then make all the A_i ($i = t$, b, τ, u, d, e) at low energy complex; the phase of μ instead does not run.

The conclusion is that cancellation occurs significantly among the different contributions for a SUSY spectrum in the limit of $O(1)$ TeV, so that even for big phases (of the order of $O(1 - 10^{-1})$) there can still be agreement with the experimental bounds. The destructive interference among the different contributions can be such that the upper limit on electron EDM can be a more stringent constraint than the neutron EDM.

However, any significant cancellation needs the two phases to have opposite sign.

In [62] a similar analysis is pursued, considering this time all the possible phases in the model, namely the phase attached to the μ parameter in the superpotential, two phases attached to two of the the gaugino mass terms, and the four phases attached to the four tri-linear soft terms A_u, A_d, A_t and A_e. Any other phase can be rotated away (SCPV is not considered because the model is the MSSM).

A numerical analysis is then discussed for both the electron and neutron EDMs.

As far as the electron EDM is concerned, cancellation seems to occur between the chargino contribution and the gaugino-higgsino mixing diagrams (we mean by this that in the relevant loop diagram, one vertex will be given by a gauge coupling and the other one by a Yukawa coupling) of the neutralino contribution quite naturally, due to the opposite sign of the phase attached to the μ parameter entering the contributions, as long as the chargino and neutralino contribution are of the same magnitude. In general neutralino contributions are smaller than chargino's, because of the smaller values of the function $B(x)$ compared to $A(x)$ (see the next section) due to the fact that the photon in the chargino one-loop diagram is emitted by a fermion field, whereas in the neutralino diagram it is emitted by a scalar field; also, in the neutralino sector there are two gaugino states, compared to only one for the chargino, and therefore the imaginary part of the matrices diagonalizing the neutralino mass matrix will be smaller than chargino ones (i.e. U and V, see D).

Taking big values of μ has the effect of suppressing the chargino-higgsino

contribution and increasing the gaugino-gaugino one.

On the other hand cancellation between gaugino-gaugino and chargino contributions occurs if certain relations among the various phases are satisfied; it is found nontheless that this is indeed the case in a large part of the parameter space, bigger values of μ being preferred as in this way the size of the gaugino-gaugino and chargino contributions is comparable (in general neutralino contributions are smaller than any other contribution) and cancellation is easier to achieve. As far as the neutron EDM is concerned, cancellation is easier to obtain than in the electron EDM case, as there are more diagrams contributing. Chromoelectric contributions coming from charginos and neutralinos can be safely neglected, together with the neutralino contribution associated to the diagram of Fig. 7.37. The six dimension purely gluonic operator on the other hand is not suppressed, and has then to be included.

The overall conclusion of the numerical analysis is that indeed cancellation is a general feature and occurs quite naturally due to certain approximate relations among the mass parameters and phases. These relations among the mass parameters are claimed to be natural, and not a kind of fine tuning.

7.3   Electron and neutron EDMs

We present in this section the explicit formulas for the single contributions to the neutron and electron EDMs at the one and two loop level. Let us start with those diagrams where a photon is emitted, namely those of Fig. 7.37, 7.38.

The gluino contribution is (see Fig. 7.37)

$$d^E_{q-gluino}/e = \frac{-2\alpha_s}{3\,\pi} m_{\tilde{g}}\, Q_{\tilde{q}}\, Im(\Gamma^{11}_q) \tag{7.9}$$

$$\times \left(\frac{1}{M^2_{\tilde{q}1}} B\left(\frac{m^2_{\tilde{g}}}{M^2_{\tilde{q}1}} \right) - \frac{1}{M^2_{\tilde{q}2}} B\left(\frac{m^2_{\tilde{g}}}{M^2_{\tilde{q}2}} \right) \right)$$

where $\Gamma^{ik}_q = D_{q2k}\, D^*_{q1k}$, $\alpha_s = \frac{g^2_s}{4\,\pi}$, $m_{\tilde{g}}$ is the gluino mass and

$$B(x) = \left(2(x-1)^2 \right)^{-1} \left(1 + x + 2\,x\,ln\left(x(1-x)^{-1} \right) \right).$$

The D matrices are unitary matrices which diagonalise the squark mass matrix squared, and are shown in detail in the appendix D together with the squark mass matrices squared, whose eigenvalues are $M_{\tilde{q}_1}^2$ and $M_{\tilde{q}_2}^2$. The index q in the formula refers to the quark whose EDM is calculated, so that for the neutron the d and u quarks have to be considered. The final EDM will be given by eq. (7.8). Gluinos do not couple to leptons so that no contribution of this kind arises for the electron.

For the chargino we have the diagram of Fig. 7.37 as well as the one of Fig. 7.38 contributing. For the u quark EDM [61]

$$d_{u-chargino}^E/e = \frac{-\alpha_{EM}}{4\,\pi\,sin(\theta_W)^2} \sum_{k=1}^{2} \sum_{i=1}^{2} Im\left(\Gamma_{uik}\right) \frac{\tilde{m}_{\chi_i^+}}{M_{\tilde{d}k}^2} \left(Q_{\tilde{d}}\, B\left(\frac{\tilde{m}_{\chi_i^+}^2}{M_{\tilde{d}k}^2}\right) + \tag{7.10}$$

$$+ (Q_u - Q_{\tilde{d}})\, A\left(\frac{\tilde{m}_{\chi_i^i}^2}{M_{\tilde{d}k}^2}\right) \right)$$

where $A(r) = 2(1-r)^{-2}\left(3-r+2\,ln\left((1-r)^{-1}\right)\right)$ and

$$\Gamma_{uik} = k_u\, V_{i2}^\star\, D_{d1k}\left(U_{i1}^\star\, D_{d1k}^\star - k_d\, U_{i2}^\star\, D_{d2k}^\star\right) \tag{7.11}$$

and

$$k_u = \frac{m_u}{\sqrt{2}m_W sin\beta}\ ,\ \ k_d = \frac{m_d}{\sqrt{2}m_W cos\beta} \tag{7.12}$$

where $\tilde{m}_{\chi_i}$, i=1,2 are the chargino mass matrix eigenvalues. The U and V matrices (shown in detail in the appendix D) are the two unitary matrices required to diagonalise the chargino mass matrix; they are different, contrary to the squark case, as the chargino mass matrix is complex and not symmetric. The electron EDM contribution is then given by

$$d_{e-chargino}^E/e = \frac{\alpha_{EM}}{4\pi\,sin^2\theta_W} m_{\tilde{\nu}_e}^2 \sum_{i=1}^{2} \tilde{m}_{\chi_i^+} Im\left(\Gamma_{ei}\right) A\left(\frac{\tilde{m}_{\chi_i^+}^2}{m_{\tilde{\nu}_e}^2}\right) \tag{7.13}$$

where $\Gamma_{ei} = k_e\, U_{i2}^\star\, V_{i1}^\star = |k_e|\, U_{R2i}^\star\, U_{L1i}$.

Note that in the case of no mixing in the squark sector, i.e. when the off-diagonal elements of the squark mass matrices are neglected, and

when terms in k_u^2 and k_d^2 are neglected, it can be shown [59] that the chargino contribution is proportional to

$$\frac{1}{\left(m_{w_2}^2 - m_{w_1}^2\right)}.\qquad(7.14)$$

For the neutralino we have just the diagram in Fig. 7.37, as for the gluino; the contribution is given by

$$d_{f-neutralino}^E/e = \frac{\alpha_{EM}}{4\pi\,sin^2\theta_W}\sum_{k=1}^{2}\sum_{i=1}^{4} Im(\eta_{fik})\frac{\tilde{m}_{\chi_i^0}}{M_{\tilde{f}_k}^2}\,Q_{\tilde{f}}\,B\left(\frac{\tilde{m}_{\chi_i^0}^2}{M_{\tilde{f}_k}^2}\right)\quad(7.15)$$

where

$$\eta_{fik} = \left(a_0 X_{1i}D_{f1k}^\star + b_0 X_{2i}D_{f1k}^\star + k_f X_{bi}D_{f2k}^\star\right)\left(c_0 X_{1i}D_{f2k} - k_f X_{bi}D_{f1k}\right)\qquad(7.16)$$

and $\tilde{m}_{\chi_i^0}$, i=1,5 are the neutralino mass matrix eigenvalues.
The D matrix is the one which diagonalises the neutralino mass matrix, and X are the corresponding eigenvectors. The electron EDM contribution will be similar to the d quark EDM contribution, but with the relevant physical quantities of the d quark replaced by those of the electron.
We then have the chromoelectric operator contributions, induced by the dimension five operator

$$\mathcal{L}_I = -\frac{i}{2}\tilde{d}^C\,\bar{q}\sigma_{\mu\nu}\,\gamma_5\,T^a\,q\,G^{\mu\nu a}\qquad(7.17)$$

and whose corresponding Feynman diagrams are shown in Fig. 7.39, 7.40. The resulting gluino, neutralino and chargino dipole moment $\tilde{d}_c$ contributions are, respectively

$$\tilde{d}_{q-gluino}^C = \frac{g_s\alpha_s}{4\pi}\sum_{k=1}^{2} Im(\Gamma_q^{1k})\frac{m_{\tilde{g}}}{M_{\tilde{q}_k}^2}C\left(\frac{m_{\tilde{g}}^2}{M_{\tilde{q}_k}^2}\right)\qquad(7.18)$$

$$\tilde{d}_{q-chargino}^C = \frac{-g^2\alpha_s}{16\pi^2}\sum_{k=1}^{2}\sum_{i=1}^{2} Im(\Gamma_{qik})\frac{\tilde{m}_{\chi_i^+}}{M_{\tilde{q}_k}^2}B\left(\frac{\tilde{m}_{\chi_i^+}^2}{M_{\tilde{q}_k}^2}\right)\qquad(7.19)$$

$$\tilde{d}^C_{q-neutralino} = \frac{g_s g^2}{16\pi^2} \sum_{k=1}^{2} \sum_{i=1}^{4} Im(\eta_{qik}) \frac{\tilde{m}_{\chi_i^0}}{M_{\tilde{q}_k}^2} C\left(\frac{\tilde{m}_{\chi_i^0}^2}{M_{\tilde{q}_k}^2}\right) \qquad (7.20)$$

where

$$C = \frac{1}{6(1-x)^2}(10x - 26 + \frac{2xln(x)}{1-x} - \frac{18ln(x)}{1-x}) \qquad (7.21)$$

and

$$B = \frac{1}{2(1-x)^2}(1 + x + \frac{2xln(x)}{1-x}). \qquad (7.22)$$

Finally, we have the CP violating dimension six purely gluonic operator

$$\mathcal{L}_I = -\frac{1}{6} d^G f_{\alpha\beta\gamma} G_{\alpha\mu\rho} G^\rho_{\beta\nu} G_{\gamma\lambda\sigma} \epsilon^{\mu\nu\lambda\sigma} \qquad (7.23)$$

where $f_{\alpha\beta\gamma}$ are the Gell-Mann coefficients, $\epsilon^{\mu\nu\lambda\sigma}$ is the totally antisymmetric tensor with $\epsilon^{0123} = +1$, and $G_{\alpha\mu\nu}$ is the gluon field strength. The relevant diagram is shown in Fig. 7.41 and the associated contribution is given by

$$d^G = -3\alpha_s \left(\frac{g_s}{4\pi \, m_{\tilde{g}}}\right)^3 \left(m_t(z_1^t - z_2^t) Im\left(\Gamma_t^{12}\right) H\left(z_1^t, z_2^t, z_t\right) + \qquad (7.24)$$

$$+ m_b(z_1^b - z_2^b) Im\left(\Gamma_b^{12}\right) H\left(z_1^b, z_2^b, z_b\right)) $$

where

$$\Gamma_q^{1k} = D_{q2k} D^\star_{q1k}, \quad z_\alpha^q = \left(\frac{M_{\tilde{q}_\alpha}}{m_{\tilde{g}}}\right)^2, \quad z_q = \left(\frac{m_q}{m_{\tilde{g}}}\right)^2 \qquad (7.25)$$

and

$$H(z_1, z_2, z_3) = \frac{1}{2} \int_0^1 dx \int_0^1 du \int_0^1 dy, x(1-x)u \frac{N_1 N_2}{D^4} \qquad (7.26)$$

with

$$N_1 = u(1-x) + z_3 x(1-x)(1-u) - 2ux(z_1 y + z_2(1-y)) \qquad (7.27)$$

$$N_2 = (1-x)^2(1-u)^2 + u^2 - \frac{1}{9}x^2(1-u)^2 \qquad (7.28)$$

$$D = u(1-x) + z_3 x(1-x)(1-u) + ux(z_1 y + z_2(1-y)). \qquad (7.29)$$

Note that the formulas above are for the MSSM. The corresponding ones for the NMSSM are just the same, but of course the squarks, charginos and neutralinos mass matrices will be different. Also, the number of neutralinos in the NMSSM is five instead of four, as in the MSSM.

As far as the CP violating phases are concerned, we just consider SCPV, in which we have only two phases, whereas a general MSSM has seven. These phases will enter the off-diagonal elements of all the mass matrices, as well as the (2,2) element of the chargino mass matrix. Also, we will consider small values of $\tan\beta$, so that the b quark contribution can be safely ignored.

As far as the determination of the relevant physical quantities at the M_Z scale is concerned, we will use the Standard Model RGE for the quark masses from the GeV scale up to the M_Z scale, whereas the two Higgs doublet model RGE are used to obtain the top quark mass, starting from the pole mass value of 174 GeV [52] [63]. All the coupling constants are also given at the M_Z scale. However, the electron electric dipole moment should be calculated at the zero scale, where $\alpha_{EM} = 1/137.035$.

Notice also that the assumed values of the current quark masses at low energy scale play an important role. However, we have verified that the overall conclusions coming from the numerical analysis presented in the next section, do not change when m_u and m_d are two times bigger than the currently reported values [27].

7.4 Numerical analysis

In the first chapters we have discussed SCPV within the NMSSM, comparing the results with the relevant limits set experimentally by LEP1 and LEP2.

We now want to assess what the resulting electron and neutron EDMs are, as a result of the presence of the CP violating phases coming from SCPV. We will not discuss the most general case where explicit phases are also considered.

The analysis of the electric dipole moments is largely independent of our analysis of the Higgs sector, as the only quantities which enter the

expressions of the nEDM and eEDM are λ, k, $\tan\beta$, v_3, θ_1, θ_3 and μ, whereas all the other soft parameters introduced in the previous chapters enter only the Higgs sector. We can then confine our attention to these seven quantities, as the other parameters can be chosen to give a suitable Higgs spectrum compatible with the experimental constraints already discussed, as well as make sure that the resulting minima of the effective potential are absolute ones (this in particular implies taking μ different from zero for small CP violating phases, see chapter 5, section 5.4).

The parameters v_3 and μ are varied randomly, within the same ranges as in Tab. 5.1, i.e. μ=-500-500 GeV and v_3=10-510 GeV, throughout all the analysis discussed in this section.

The other parameters are the squark soft-terms, whose corresponding terms, which appear in the lagrangian, are (only one generation is shown)

$$\mathcal{L}_{soft} \supset -M_Q^2\,\tilde{Q}^*\,\tilde{Q} - M_u^2\,\tilde{U}^*\,\tilde{U} - M_d^2\,\tilde{D}^*\,\tilde{D}- \tag{7.30}$$

$$\left(A_u\,h_u\,\tilde{Q}\,H_2\,\tilde{U} + A_d\,h_d\,H_1\,\tilde{Q}\,\tilde{D} + h.c.\right)$$

where M_Q is the left-handed doublet soft-term, M_u and M_d are the corresponding right-handed ones, A_u and A_d are the tri-linear couplings, $\tilde{Q} = \begin{pmatrix} \tilde{u}_L \\ \tilde{d}_L \end{pmatrix}$ is the doublet field, $\tilde{U} = \tilde{u}_R^*$ and $\tilde{D} = \tilde{d}_R^*$ are the corresponding right-handed fields, H_1 and H_2 are the Higgs doublet fields, and h_u and h_d are the Yukawa coupling constants. Similar terms can be written for the s-leptons, with the difference that there are no right-handed neutrinos and s-neutrinos. The squark and slepton mass matrices will also contain terms depending on μ, λv_3 and $k v_3$, because corresponding terms appear in the F term of the effective potential (see Appendix D).

As far as the CP violating phases are concerned though, it makes a difference whether we take these phases with positive or negative signs, whereas the Higgs spectrum analysis does not change. So we will allow θ_1 and θ_3 to be either positive or negative; in particular we take the values of θ_1, analogously with what we did for the Higgs spectrum, equal to 0.001, 0.01, 0.1, 1 rad and -0.001, -0.01, -0.1, -1 rad for a total of eight cases, with θ_3 varied for each case between zero and $2\theta_1$ and between $-2\theta_1$ and zero. Note that the cases with θ_1 negative are ex-

pected to be equivalent to the ones with θ_1 positive, as the soft terms are themselves allowed to take positive as well as negative values. We will refer to this as case (A).

However, we will also consider case (B), where all the soft terms are fixed to given values, and case (C) where the soft terms m_i are taken equal to m_0, A_i are taken equal to A_0 and the gaugino masses are taken to be

$$(g^2/g_s^2)M_g = M_2 = (3g^2/5g'^2)M_1.$$

The parameters m_0, A_0 and M_2 are then varied randomly.

Cases (B) and (C) are considered for comparison with the Supergravity analysis, where all the soft-terms are fixed through the RGE; in principle then the corresponding Higgs sector should be considered too. In our case, we just make assumptions on the squark sector, so that the Higgs sector once again is unchanged. We of course expect cancellation to occur preferably for case (A), as compared to cases (B) and (C), because of the bigger number of parameters varied.

7.4.1 Case (A)

Let us start considering case (A), where, as well as μ and v_3, eleven soft terms in the squark mass matrices, the gluino mass term and the gauginos are picked at random, within ranges chosen such that squarks, gluinos and gauginos are not much heavier than 1 TeV, with preference to masses below 1 TeV. More precisely, two different ranges were considered, as can be seen in Tab. 7.1, the first one with bigger top squark and gauginos masses than the second one.

The soft terms of Tab. 7.1 are chosen at random for each value of θ_3. The number of sets considered for each value of θ_3 was 100. This number, although small, was chosen to speed up the numerical computations, as a double integral within the expression of the six dimension purely gluonic operator is to be computed every time.

We plot the number of sets as a function of the corresponding $log_{10}|\text{nEDM}|$ where the x axis is divided in bins, we have Fig. 7.1, 7.2 for the first set of Tab. 7.1, and Fig. 7.3, 7.4 for the second set: the squares, diamonds, bursts and crosses correspond to $|\theta_1|$=0.001, 0.01, 0.1, 1 rad respectively.

Table 7.1: Case (A). Ranges within which the parameters are randomly
varied.

	light $\bar{q}$	heavy $\bar{q}$
M_{Q_1}	100-600 GeV	500-1000 GeV
M_{u_1}	100-600 GeV	500-1000 GeV
M_{d_1}	100-600 GeV	500-1000 GeV
M_{Q_t}	500-1000 GeV	1000-1500 GeV
M_t	500-1000 GeV	1000-1500 GeV
M_E	100-600 GeV	500-1000 GeV
M_e	100-600 GeV	500-1000 GeV
A_u	-500-500 GeV	-1000-1000 GeV
A_d	-500-500 GeV	-1000-1000 GeV
A_t	-100-100 GeV	-100-100 GeV
A_e	-500-500 GeV	-1000-1000 GeV
M_g	174-674 GeV	1000-1500 GeV
M_1	174-674 GeV	1000-1500 GeV
M_2	174-674 GeV	1000-1500 GeV

The curves in general show a peak around a certain value of the nEDM. We can clearly see that even for $\theta_1 = 1$ rad (θ_3 is not small either) cases can be found for which the resulting neutron EDM is far below the experimental limit, suggesting that cancellation is occurring. However, the number of sets for which this is true is always small, confirming our expectations that for large phases the cancellation mechanism as a way to avoid the experimental constraints, is not natural.

Notice also that for the first set of parameters squarks are lighter ($\approx 500 GeV$) than for second one ($\approx O(1\text{TeV})$), so that the corresponding values of the nEDM are consequently bigger, as it should be expected.

It is of interest to assess what are the important contributions between which cancellation occurs. For this purpose, we have studied a specific example (see Tab. 7.2), and considered all the single different contributions to the final values of the nEDM and eEDM. We have chosen the values for the various parameters in a way to have a value of the nEDM and eEDM in agreement with the experimental constraint, for the light $\bar{q}$ ($\bar{l}$). In general, we have found that the relevant parameters for cancellation are M_2, M_{Q_1}, M_{d_1} and M_g. M_1 in fact just enters the neutralino mass matrix, which gives a smaller contribution when compared to the chargino and gluino ones, and the neutron EDM varies weakly with M_{u_1} and A_i for i=u, d.

The stop soft terms enter only in the gluonic operator contribution, which is found to be always negligible compared to the other contributions. In Fig. 7.5, 7.6, 7.7 and 7.8 we can see the nEDM as a function of the relevant parameters for cancellation, i.e. we have varied one single parameter each time and kept fixed the others, for the set 7.2.

To better understand what contributions are more relevant, and whether cancellation really takes place, we need to plot the single contributions as a function of one of the above four parameters, which are the ones to which cancellation is more sensitive. The graphs in Fig. 7.9, 7.10, 7.11 and 7.12 show the ratio of the contributions normalised to the experimental upper bound on nEDM, and plotted as a function of M_2. The dotted lines show $\pm d$, where d is the experimental bound on the magnitude.

The behaviour of the chargino contribution is explained referring to 7.14; it is clear that there are regions of the parameter space, when
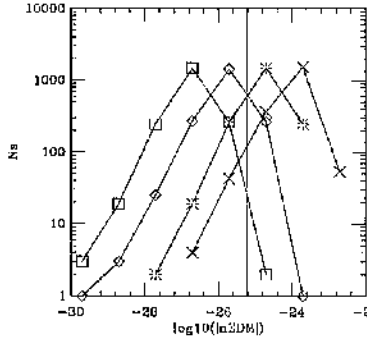
Figure 7.1: Tab. 7.1, light squark case. Number of sets vs $log_{10}(|nEDM|)$ for $\theta_1=0.001$ rad (squares), 0.01 rad (diamonds), 0.1 rad (bursts) and 1 rad (crosses). The experimental constraint is also shown.
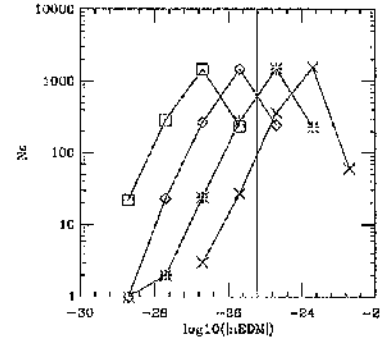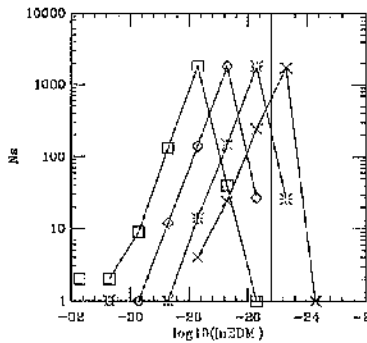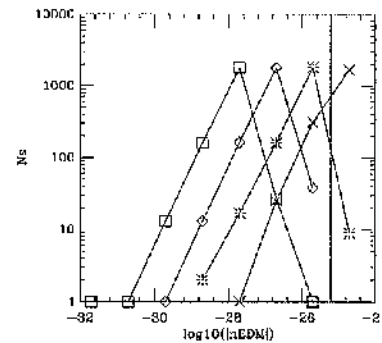

Figure 7.2: Tab. 7.1, light squark case. Number of sets vs $log_{10}(|nEDM|)$ for $\theta_1=-0.001$ rad (squares), -0.01 rad (diamonds), -0.1 rad (bursts) and -1 rad (crosses). The experimental constraint is also shown.

Figure 7.3: Tab. 7.1, heavy squark case. Number of sets vs $log_{10}(|nEDM|)$ for $\theta_1=0.001$ rad (squares), 0.01 rad (diamonds), 0.1 rad (bursts) and 1 rad (crosses). The experimental constraint is also shown.

Figure 7.4: Tab. 7.1, heavy squark case. Number of sets vs $log_{10}(|nEDM|)$ for $\theta_1=-0.001$ rad (squares), -0.01 rad (diamonds), -0.1 rad (bursts) and -1 rad (crosses). The experimental constraint is also shown.

Table 7.2: Case (A). A particular case with cancellation.

μ	88.758 GeV
M_{Q_1}	563.579 GeV
M_{u_1}	254.357 GeV
M_{d_1}	128.123 GeV
M_{Q_t}	727.729 GeV
M_t	996.014 GeV
M_E	330.501 GeV
M_c	426.348 GeV
A_u	16.880 GeV
A_d	-462.039 GeV
A_t	24.548 GeV
A_e	355.591 GeV
M_g	203.128 GeV
M_1	475.509 GeV
M_2	370.373 GeV
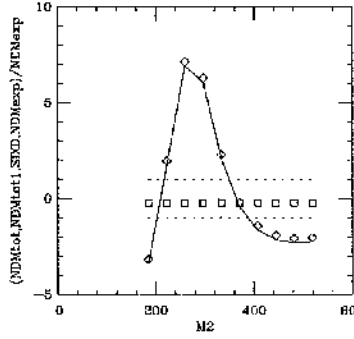
Figure 7.5: Tab. 7.2. Total NDM (continuous line), purely gluonic dimension six operator (squares) and one loop+chromoelectric operator contribution (diamonds), normalised with the experimental upper bound (dotted lines), as a function of M_2.
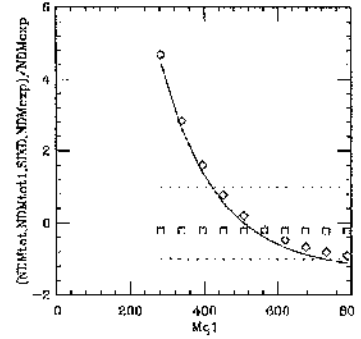
Figure 7.6: Same as in Fig. 7.5, as a function of M_{Q_1}.
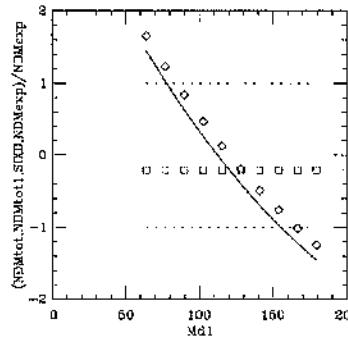
Figure 7.7: Same as in Fig. 7.5, as a function of M_{d_1}.
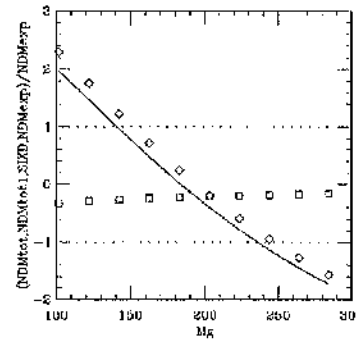
Figure 7.8: Same as in Fig. 7.5, as a function of M_g.
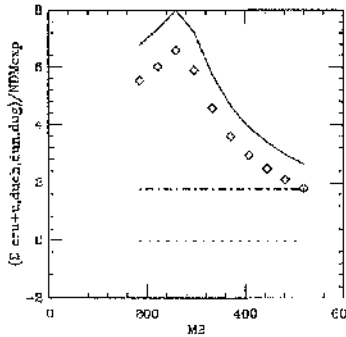
Figure 7.9: Tab.7.1. Chargino u quark contribution (duch) (continuous line), neutralinos u quark contribution (dun) (dotted line), gluino u quark contribution (dug) (dot-dashed line) and u quark one loop +chromoelectric contribution (diamonds), normalised with the experimental upper bound, as a function of M_2.
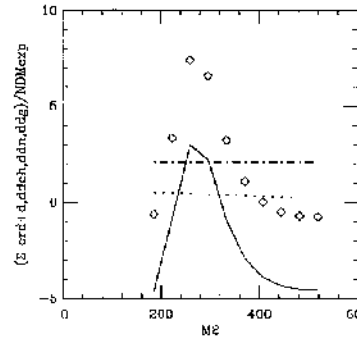
Figure 7.10: Same as in Fig. 7.9, but for the d quark contribution.
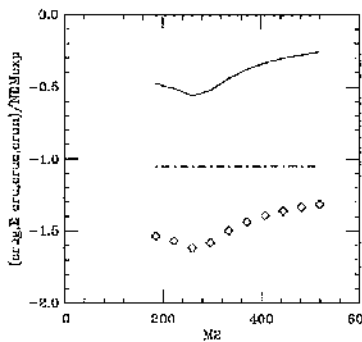
Figure 7.11: Tab.7.1. u quark chromoelectric chargino contribution (cru) (continuous line), u quark chromoelectric neutralino contribution (crun) (dotted line), u quark chromoelectric gluino contribution (crug) (dot-dashed line) and u quark total chromoelectric contribution (diamonds), normalised with the experimental upper bound, as a function of M_2.
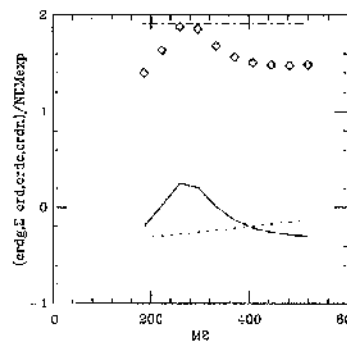
Figure 7.12: Same as in Fig. 7.11, but for the d quark contribution.

M_2 is O(100 GeV), where the u and d quark chargino contribution will
have a peak, when there is a high degeneracy between the two chargino
eigenvalues. We have seen that this does not occur for high values
of M_2, as it should be expected. Also, the d quark contribution can
be smaller than the u quark contribution, despite the fact that the d
quark is twice as heavy than the u quark, due to the various terms
which enter the final expression of $d^E_{u-chargino}$ and $d^E_{d-chargino}$. This in
turn explains the fact that for the specific example shown cancella-
tion occurs between the d and u quark contributions. For this to be
possible, the d quark contribution must be suppressed in order to be
comparable to the smaller u quark contribution, and also because the
former one contributes 4 times more than the latter one. The d quark
contribution is reduced due to the cancellation between the one-loop
electromagnetic contribution and the chromoelectric one, especially as
far as the charginos diagrams are concerned.
The gluonic operator, on the other hand, is always small. In fact, a
region of the parameter space can always be chosen so that this is true,
as the stops soft terms do not enter the other contributions.
Those sets which minimize the neutron EDM do not necessarily do
so for the electron EDM and vice versa. However, sets can be found
for which both nEDM and eEDM are below the experimental lower
bounds, as for the case of Tab. 7.2. The number of sets for which this
is possible is always very small compared to the overall number of sets
(< 100 out of 2000), hinting to the need for a high fine tuning.

As already said, the μ parameter is varied randomly together with
v_3; it is of some interest to see which values of these two parameters are
preferred for cancellation to occur. We show in Fig. 7.13, 7.14, 7.15,
7.16 the values of μ against θ_3 for case (A) and the two sets of Tab.
7.1; we will just consider $\theta_1=1$, -1 rad respectively, and those sets such
that the nEDM is below the experimental upper limit; the diamonds
and squares refer to values of v_3 smaller and bigger than 250 GeV re-
spectively.
   The graphs for $\theta_1=-1$ rad and $\theta_1=1$ rad are one the reversal of the
other, with respect to the $\theta_3=0$ axis, as expected. Also, v_3 does not
seem to be of any importance, as diamonds and squares are equally
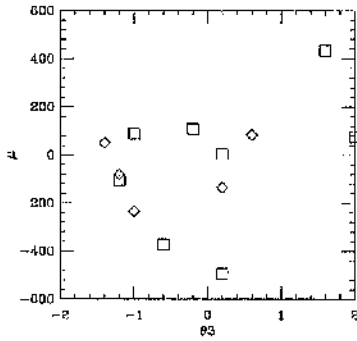present. However, there are preferred regions of μ values. This again

Figure 7.13: Light $\tilde{q}$ $(\tilde{l})$ case. Values of μ vs θ_3 for $\theta_1{=}1$ rad and nEDM<exp.upper limit. Squares are for v_3 >250 GeV, and diamonds are for v_3 <250 GeV.
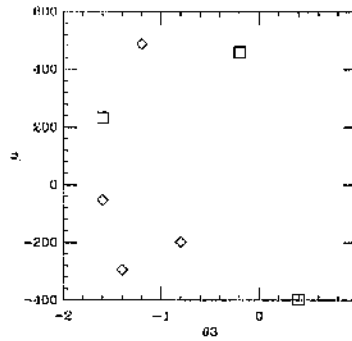

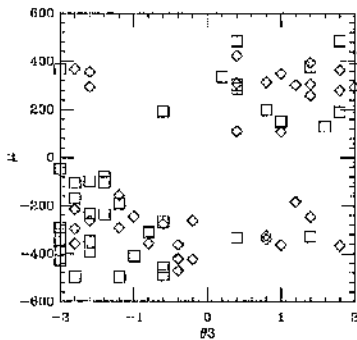Figure 7.14: Same as in Fig. 7.13, but for $\theta_1{=}{-}1$ rad.

Figure 7.15: heavy $\tilde{q}$ $(\tilde{l})$ case. Values of μ vs θ_3 for $\theta_1{=}1$ rad and nEDM<exp.upper limit. Squares are for v_3 >250 GeV, and diamonds are for v_3 <250 GeV.
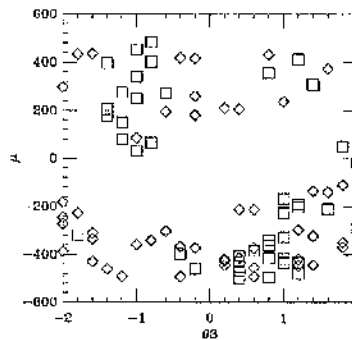
Figure 7.16: Same as in Fig. 7.15, but for $\theta_1{=}{-}1$ rad.

Table 7.3: Case (B)

M_{Q_L}	M_{Q_R}	M_{E_L}	M_{E_R}	A_0	$M_{\tilde{g}}$	M_1	M_2
340	360	195	225	250	250	75	85

is due to the fact the chargino contribution, for which μ is a crucial parameter, is bigger than the others.

Similar graphs are given for the eEDM in Fig. 7.17, 7.18, 7.19, 7.20. Notice that the light $\tilde{q}$ ($\tilde{l}$) case gives fewer sets in agreement with the experimental upper bound on nEDM (eEDM) than for the heavy $\tilde{q}$ ($\tilde{l}$) case, as expected.

7.4.2   Case (B)

So far we have just varied randomly all the parameters entering the mass matrices. Let us now consider the case (B), where all the soft terms are fixed to the values of Tab. 7.3, taken from [62], where for the left-handed squarks soft terms, $M_{Q_i} = M_{Q_L}$, for the right-handed squarks soft terms $M_{q_i} = M_{Q_R}$, and analogously for the sleptons, $M_{E_i} = M_{E_Q}$ and $M_{e_i} = M_{E_R}$; also, for all the trilinear couplings, $A_i = A_0$. We obviously expect a smaller degree of cancellation, as the only parameters varied are v_3 and μ; however, these parameters are quite important as far as the chargino contribution is concerned, and so we still expect cancellation to be possible. This does occur, but in only about one tenth as many cases as case (A).

We once again plot the number of sets as a function of the corresponding nEDM, as in the previous analysis, in Fig. 7.21, 7.22, and the ones for eEDM in Fig. 7.23, 7.24. We show in Fig. 7.25, 7.26, 7.27 and 7.28 the values of μ which give cancellation, for the nEDM, as given before, and found that, as in case (A), negative values of μ are preferred.

7.4.3   Case (C)

Let us now consider case (C). The parameters m_0, A_0 and m_2 are varied within the ranges 200-800 GeV, -100-100 GeV and 200-800 GeV
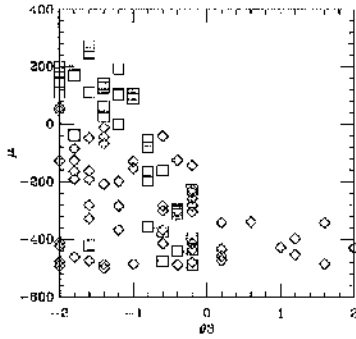
Figure 7.17: Light squark case. Values of μ vs θ_3 for $\theta_1=1$ rad and eEDM<exp.upper limit. Squares are for v_3 >250 GeV, and diamonds are for v_3 <250 GeV.
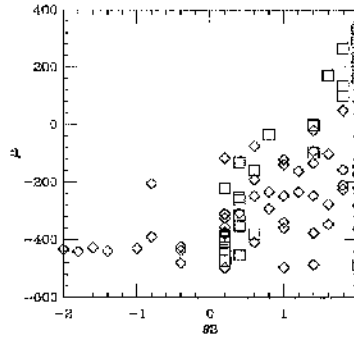

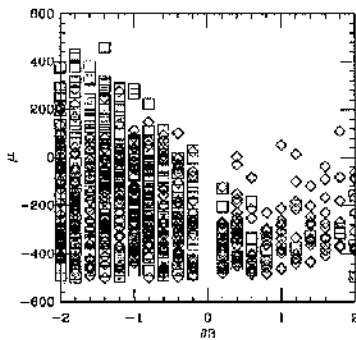Figure 7.18: Same as in Fig. 7.17, but for $\theta_1=-1$ rad.

Figure 7.19: Heavy squark case. Values of μ vs θ_3 for $\theta_1=1$ rad and eEDM<exp.upper limit. Squares are for v_3 >250 GeV, and diamonds are for v_3 <250 GeV.
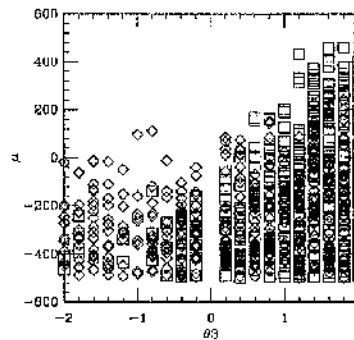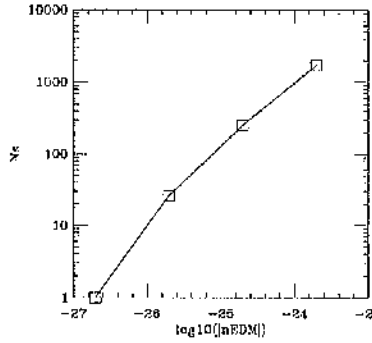

Figure 7.20: Same as in Fig. 7.15, but for $\theta_1=-1$ rad.

Figure 7.21: Case (B). Number of sets vs $log_{10}(|nEDM|)$ for $\theta_1 = 1$ rad.
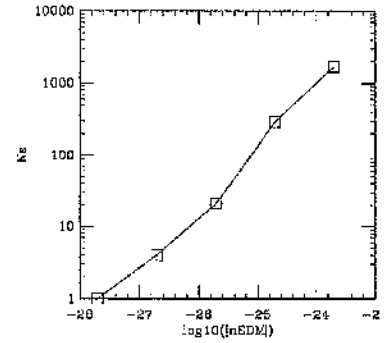
Figure 7.22: Case (B). Number of sets vs $log_{10}(|nEDM|)$ for $\theta_1 = -1$ rad.
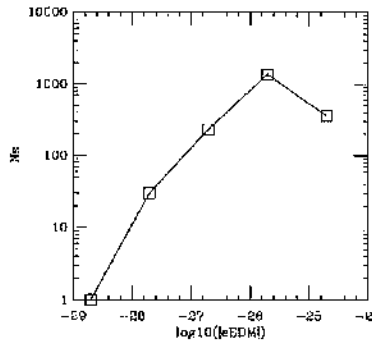
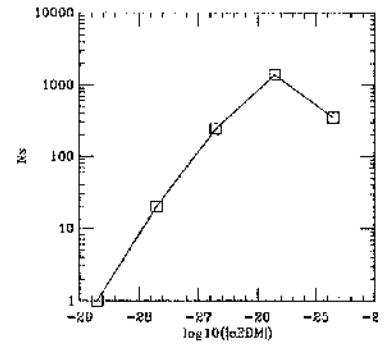Figure 7.23: Case (B). Number of sets vs $log_{10}(|eEDM|)$ for $\theta_1 = 1$ rad.

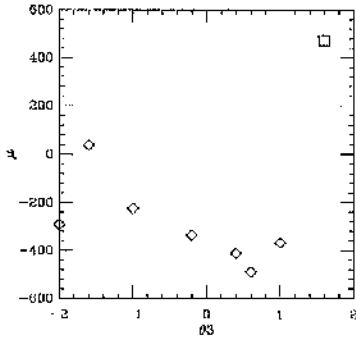Figure 7.24: Case (B). Number of sets vs $log_{10}(|eEDM|)$ for $\theta_1 = -1$ rad.

Figure 7.25: Case (B). Values of μ vs θ_3 for θ_1=1 rad and nEDM<exp.upper limit. Squares are for v_3 >250 GeV, and diamonds are for v_3 <250 GeV.

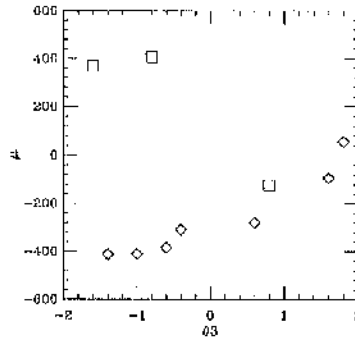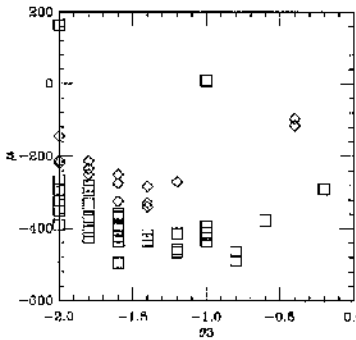Figure 7.26: Same as in Fig. 7.25, but for θ_1=-1 rad.

Figure 7.27: Case (B). Values of μ vs θ_3 for θ_1=1 rad and eEDM<exp.upper limit. Squares are for v_3 >250 GeV, and diamonds are for v_3 <250 GeV.
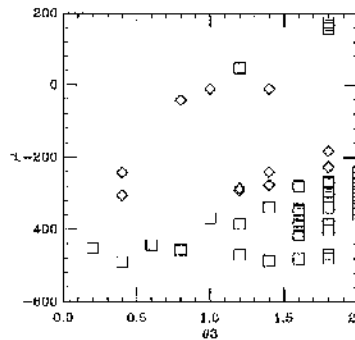

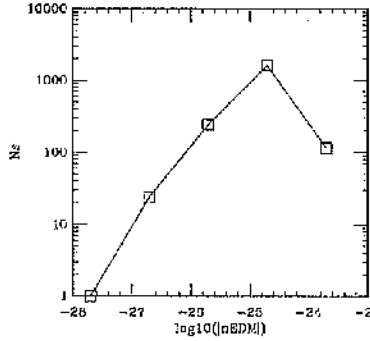Figure 7.28: Same as in Fig. 7.25, but for θ_1=-1 rad.

Figure 7.29: Case (C). Number of sets vs $log_{10}(|nEDM|)$ for θ_1=1 rad.
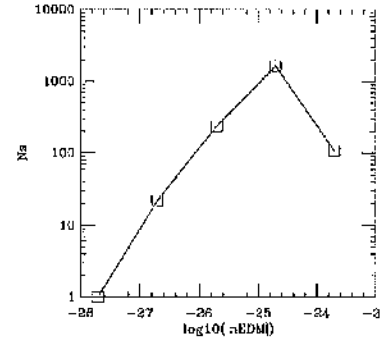
Figure 7.30: Case (C). Number of sets vs $log_{10}(|nEDM|)$ for θ_1=-1 rad.

respectively. A_0 is restricted to such a small range in order to avoid the stop masses squared from becoming negative, which would correspond to a colour breaking solution.

The results are shown in Fig. 7.29 and 7.30 for the nEDM, and 7.31, 7.32 for the eEDM. There are about five times as many acceptable cases as in case (B).

Again, we show in Fig. 7.33, 7.34, 7.35, 7.36, the values of μ which give cancellation, for the nEDM and eEDM, as given before. We notice that this time we were able to find more cases which gave an eEDM below the experimental upper constraint, because of the bigger number of parameters being varied randomly, as compared with case (B).

The conclusion is again that, even for large phases, θ=O(1), it is possible to obtain cancellation such that the resulting values of nEDM and eEDM are smaller than the current upper limits. However, this is in general not easy to achieve (few tens of cases out of two thousand), and requires extreme fine tuning of the parameter space.

The aim of the analysis presented in this chapter was to study whether big CP violating phases are acceptable or not. This case must be studied as the weak SCPV scenario may be ruled out by future experiments,
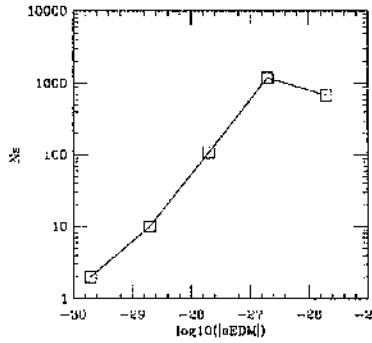
Figure 7.31: Case (C). Number of sets vs $log_{10}(|eEDM|)$ for $\theta_1 = 1$ rad.
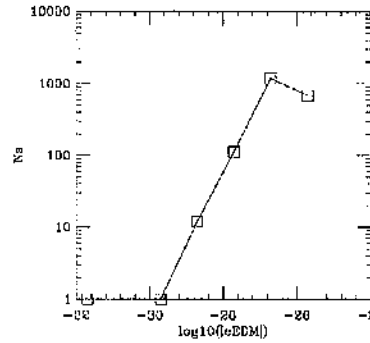
Figure 7.32: Case (C). Number of sets vs $log_{10}(|eEDM|)$ for $\theta_1 = -1$ rad.

placing constraints on the smallness of θ_1 and θ_3.

The conclusion of the whole analysis is that SCPV within the NMSSM, with the assumptions we have discussed, requires, unless the sparticle masses are very large, CP violating phases to be of the order of $O(10^{-1})$ or smaller, in order to have the nEDM and eEDM smaller than the experimental upper limits, over a wide area of the parameter space. This in turn requires the lightest neutral Higgs boson to have a mass smaller than M_Z.
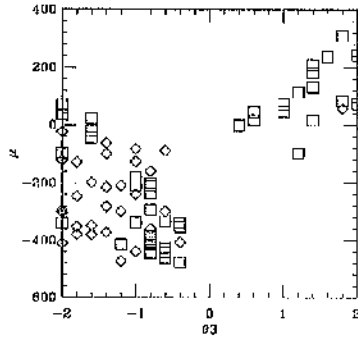
Figure 7.33: Case (C). Values of μ vs θ_3 for $\theta_1=1$ rad and nEDM<exp.upper limit. Squares are for $v_3 >250$ GeV, and diamonds are for $v_3 <250$ GeV.
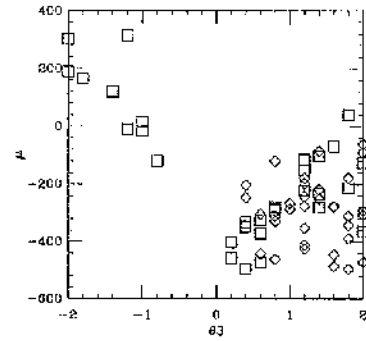
Figure 7.34: Same as in Fig. 7.33, but for $\theta_1=-1$ rad.
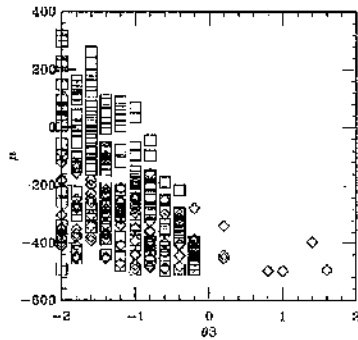
Figure 7.35: Case (C). Values of μ vs θ_3 for $\theta_1=1$ rad and eEDM<exp.upper limit. Squares are for $v_3 >250$ GeV, and diamonds are for $v_3 <250$ GeV.
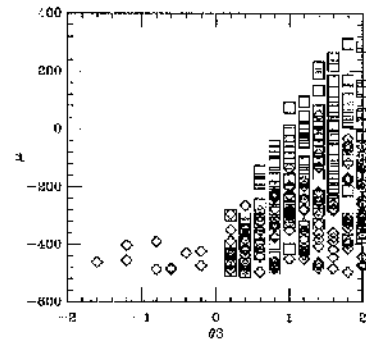
Figure 7.36: Same as in Fig. 7.35, but for $\theta_1=-1$ rad.
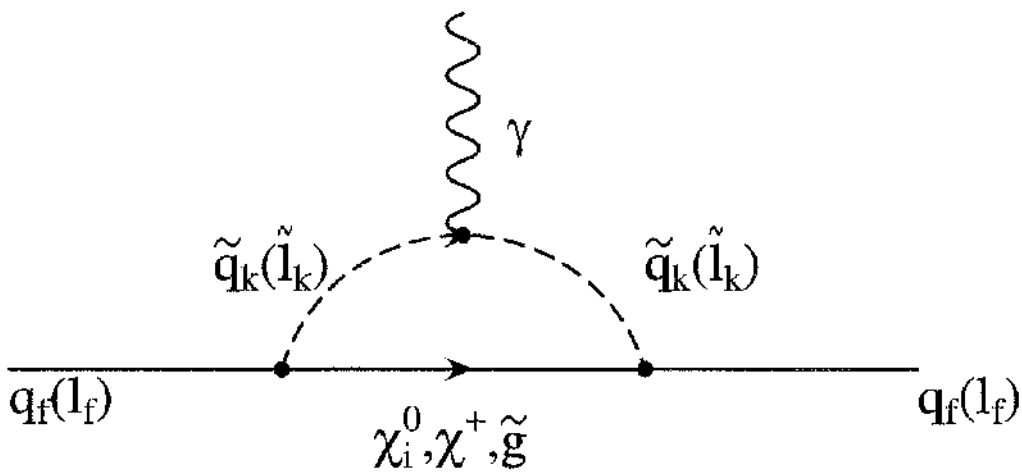
Figure 7.37: χ_i^0 are the neutralinos, $\chi^\pm$ are the charginos, and $\tilde{g}$ are gluinos.
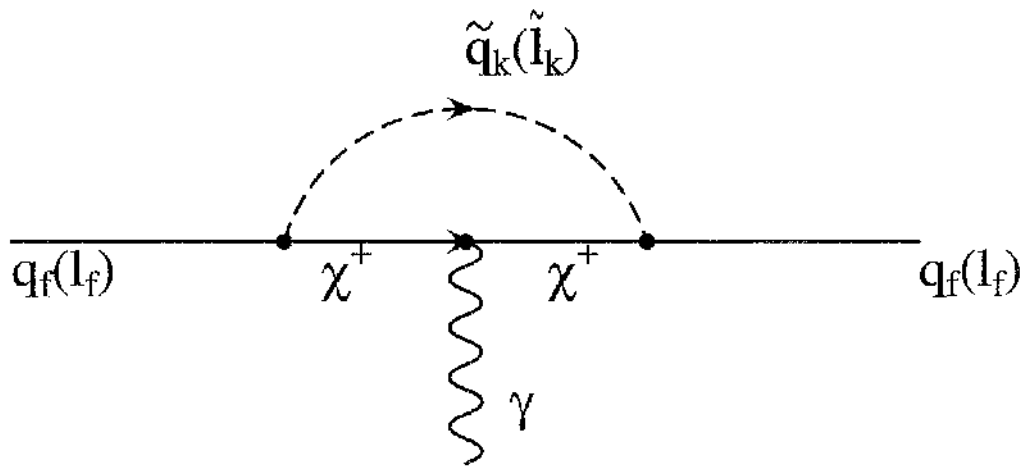
Figure 7.38: γ is the photon, q_f (l_f) are quarks (leptons) and $\tilde{q}_k$ ($\tilde{l}_k$) are squarks (sleptons).

Figure 7.39: g are gluons and $\tilde{g}$ are gluinos.

Figure 7.40:
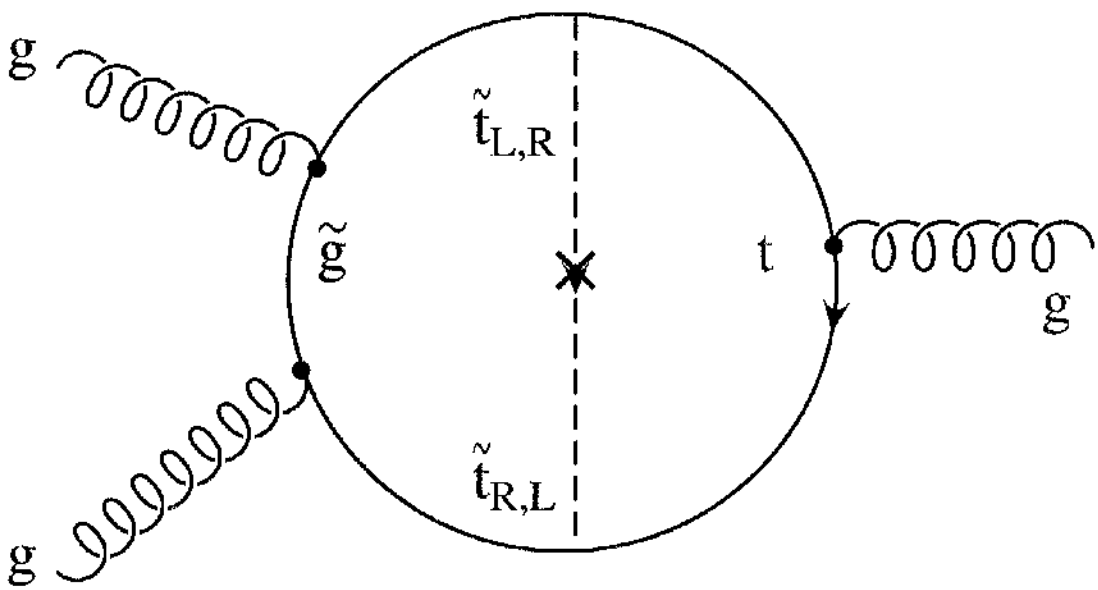
Figure 7.41: $t\tilde{}_{R,L}$ are right-handed and left-handed stops.

Chapter 8

Conclusions

In this thesis we have discussed Spontaneous CP Violation within the Next-to-Minimal Supersymmetric Standard Model. We have considered the most general superpotential, with no assumptions on the values the soft-terms present in the corresponding effective potential. This results in a model with many independent parameters.
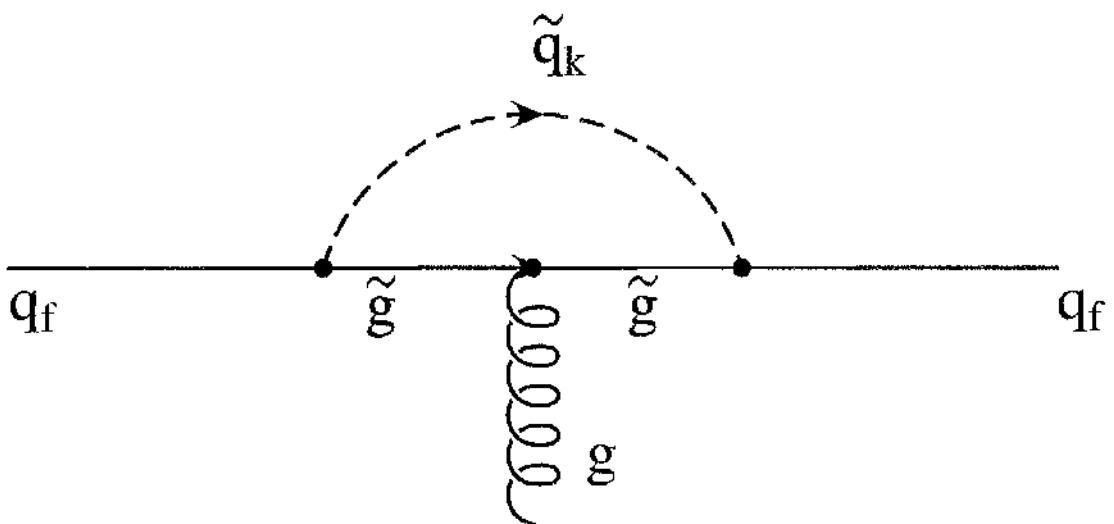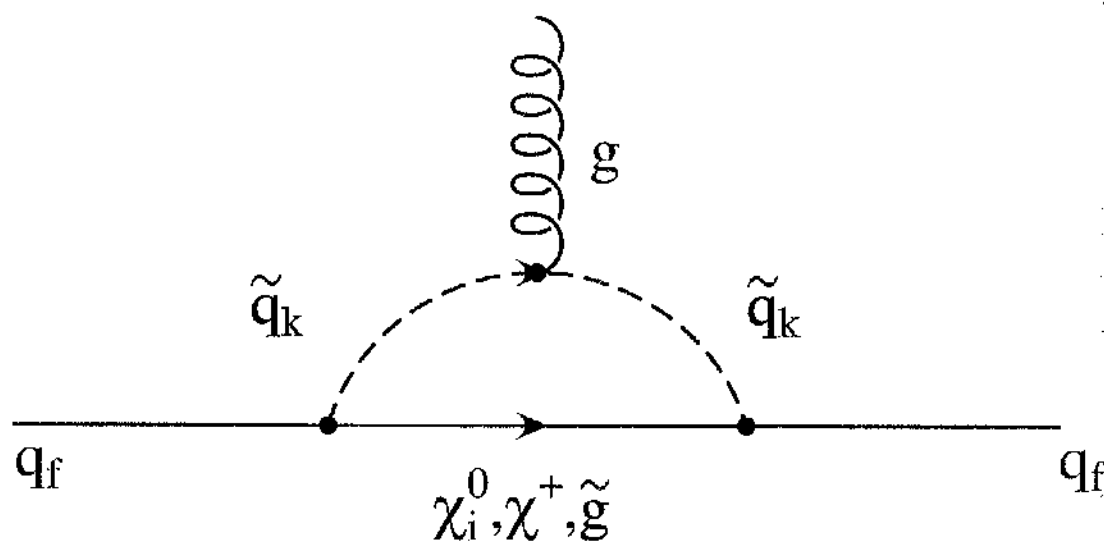
We have conducted a systematic analysis of the parameter space, and studied the resulting Higgs spectrum. We have discovered a behaviour similar to the one predicted by the Georgi-Pais theorem, i.e. for weak SCPV a light Higgs pseudoscalar is present. However, unlike what happens in the MSSM, this light pseudoscalar can be naturally highly singlet, and so invisible at the present colliders, as we have seen with regard to LEP2.

We have also studied the constraints coming from the upper limits on the neutron and electron electric dipole moments, in connection with the case where the CP violating phases are large. We have found that the resulting nEDM and eEDM can be quite small, due to cancellation among the various terms contributing, but that this is not a natural occurrence, suggesting that fine tuning of the parameter space is required. In view of this result, the SCPV scenario we outlined stands only for small or relatively small phases ($\theta_1\,\theta_3 < 0.1$ rad) with the consequence of a Higgs boson lighter than M_Z, which, as already noted, would be a pseudoscalar and predominantly singlet in a wide region of the parameter space. The predicted Higgs spectrum is likely to be tested by future colliders such as LHC, thanks to the much higher luminosity and

125

centre of mass energy.

Appendix A

Coefficients in the RG equations

The f_i coefficients which appear in the right-hand side of the two doublets RG equations are, including also the b quark contribution, the following:

$$f_1 = 12\,Y_1^2 - Y_1\,(9\,g_2^2 + 3\,g_1^2) + 2\,Y_5^2 - 4\,Y_3^2 + 4\,Y_3\,Y_4 + 2\,Y_4^2 +$$
$$+ \frac{1}{4}(9\,g_2^4 + 6\,g_2^2\,g_1^2 + 3\,g_1^4) + 12\,Y_1\,h_b^2$$

$$f_2 = 12\,Y_2^2 - Y_2\,(9\,g_2^2 + 3\,g_1^2) + 2\,Y_6^2 + 12\,(Y_2\,h_t^2 - h_t^4) + 4\,Y_3^2 + 4\,Y_3\,Y_4 + 2\,Y_4^2 +$$
$$+ \frac{1}{4}(9\,g_2^4 + 6\,g_2^2\,g_1^2 + 3\,g_1^4)$$

$$f_3 = 2\,(Y_1 + Y_2)\,(3\,Y_3 + Y_4) - Y_3\,(9\,g_2^2 + 3\,g_1^2) + 6\,Y_3\,h_t^2 + 4\,Y_3^2 + 2\,Y_5\,Y_6 + 2\,Y_4^2 +$$
$$+ \frac{1}{4}(9\,g_2^4 - 6\,g_2^2\,g_1^2 + 3\,g_1^4) - 12\,h_t^2\,h_b^2$$

$$f_4 = 2\,Y_4\,(Y_1 + Y_2 + 2\,Y_4 + 4\,Y_3) + 4\,Y_7^2 - Y_4\,(9\,g_2^2 + 3\,g_1^2) + 3\,g_2^2\,g_1^2 +$$
$$+ 6\,Y_4\,h_t^2 + 12\,h_t^2\,h_b^2$$

$$f_5 = 2\,Y_5\,(3\,Y_1 + 2\,Y_5 + 4\,Y_8) + 2\,Y_6\,(2\,Y_3 + Y_4) + 8\,Y_7^2 -$$
$$- \frac{1}{2}(9\,g_2^2 + 3\,g_1^2)\,Y_5 + 6\,Y_5\,h_b^2$$

$$f_6 = 2\,Y_6\,(3\,Y_2 + 2\,Y_6 + 4\,Y_8) + 2\,Y_5\,(2\,Y_3 + Y_4) + 8\,Y_7^2 -$$

$$-\frac{1}{2} Y_6 \left(9 g_2^2 + 3 g_1^2\right) + 6 Y_6 h_t^2$$

$$f_7 = 2 Y_7 \left(Y_3 + 2 \left(Y_4 + Y_5 + Y_6 + Y_8\right)\right) - \frac{1}{2} Y_7 \left(9 g_2^2 + 3 g_1^2\right) + 3 Y_7 \left(h_t^2 + h_b^2\right)$$

$$f_8 = 2 Y_5^2 + 2 Y_6^2 + 4 Y_7^2 + 20 Y_8^2$$

where g_1, g_2, g_3 are the gauge coupling constants.

Appendix B

Mass matrices

We assume a generic SUSY breaking scale, take the most general super-potential as well as take all the soft masses as independent parameters. We take the the basis

$$(Re(H_1), Im(H_1), Re(H_2), Im(H_2), Re(N), Im(N)).$$

The neutral Higgs bosons mass matrix at the tree level is then the following

$$M^2(1,1) = 4\,Y_1\,v_1^2\,cos(\theta_1)^2 + 2\,Y_1\,v_1^2 + 2\,(Y_3 + Y_4)\,v_2^2 + 2\,Y_5\,v_3^2 + 2\,\mu^2 +$$

$$+4\,\mu\,k\,v_3\,cos(\theta_3) + 2\,m_1^2$$

$$M^2(1,2) = 4\,Y_1\,v_1^2\,sin(\theta_1)\,cos(\theta_1)$$

$$M^2(1,3) = 4\,(Y_3 + Y_4)\,v_1\,v_2 cos(\theta_1) + 2\,Y_7\,v_3^2\,cos(2\theta_3) - 2\,m_{12}^2 +$$

$$+2\,m_5\,v_3\,cos(\theta_3)$$

$$M^2(1,4) = 4\,(Y_3 + Y_4)\,v_1\,v_2 cos(\theta_1) - 2\,m_5\,v_3\,sin(\theta_3) + 2\,Y_7\,v_3^2\,sin(2\theta_3)$$

$$M^2(1,5) = 4\,Y_7\,v_3\,v_2\,cos(-\theta_3) + 4\,Y_5\,v_1\,v_3\,cos(\theta_1)\,cos(\theta_3) + 2\,m_5\,v_2 + 4\mu\,k\,v_1\,cos(\theta_1)$$

$$M^2(1,6) = 4\,Y_5\,v_3\,v_1\,sin(\theta_3)\,cos(\theta_1) + 4\,Y_7\,v_2\,v_3\,sin(-\theta_3)$$

$$M^2(2,2) = 4\,Y_1\,v_1^2\,sin^2(\theta_1) + 2\,Y_1\,v_1^2 + 2\,(Y_3 + Y_4)\,v_2^2 + 2\,Y_5\,v_3^2 + 2\mu^2 + $$
$$+ 4\mu\,k\,v_3\,cos(\theta_3) + 2\,m_1^2$$

$$M^2(2,3) = -4\,(Y_3 + Y_4)\,v_1\,v_2\,sin(\theta_1) - 2\,Y_7\,v_3^2\,sin(2\theta_3) + 2\,m_5\,v_3\,sin(\theta_3)$$

$$M^2(2,4) = -4\,(Y_3 + Y_4)\,v_1\,v_2 + 2\,Y_7\,v_3^2\,cos(2\theta_3) - 2\,m_{12}^2 + 2\,m_5\,v_3\,cos(\theta_3)$$

$$M^2(2,5) = 4\,Y_7\,v_2\,v_3\,sin(-\theta_3) - 4\,Y_5\,v_3\,v_1\,cos(\theta_3)\,sin(\theta_1) - 4\mu\,k\,v_1\,sin(\theta_1)$$

$$M^2(2,6) = -4\,Y_7\,v_3\,v_2\,cos(-\theta_3) - 4\,Y_5\,v_3\,sin(\theta_3)\,v_1\,sin(\theta_1) + 2\,m_5\,v_2$$

$$M^2(3,3) = 4\,Y_2\,v_2^2 + 2\,Y_2\,v_2^2 + 2\,(Y_3 + Y_4)\,v_1^2 + 2\,Y_6\,v_3^2 + 2\mu^2 + $$
$$+ 4\mu\,k\,v_3\,cos(\theta_3) + 2\,m_2^2$$

$$M^2(3,4) = 0$$

$$M^2(3,5) = 4\,Y_7\,v_1\,v_3\,cos(\theta_1 - \theta_3) + 4\,Y_6\,v_2\,v_3\,cos(\theta_3) + 4\mu\,k\,v_2 +$$

$$+2\,m_5\,v_1\,cos(\theta_1)$$

$$M^2(3,6) = 4\,Y_7\,v_1\,v_3\,sin(\theta_1 - \theta_3) + 4\,Y_6\,v_2\,v_3\,sin(\theta_3) - 2\,m_5\,v_1\,sin(\theta_1)$$

$$M^2(4,4) = 2\,Y_2\,v_2^2 + 2\,(Y_3 + Y_4)\,v_1^2 + 2\,Y_6\,v_3^2 + 2\mu^2 + 4\mu\,k\,v_3\,cos(\theta_3) + 2\,m_2^2$$

$$M^2(4,5) = -4\,Y_7\,v_1\,v_3\,sin(\theta_1 - \theta_3) + -2\,m_5\,v_1\,sin(\theta_1)$$

$$M^2(4,6) = 4\,Y_7\,v_1\,v_3\,cos(\theta_1 - \theta_3) - 2\,m_5\,v_1\,cos(\theta_1)$$

$$M^2(5,5) = 4\,Y_7\,v_1\,v_2\,cos(\theta_1) + 2\,Y_8\,(4\,v_3^2\,cos(\theta_3)^2 + 2\,v_3^2) +$$
$$+2\,(Y_5\,v_1^2 + Y_6\,v_2^2) + 2\,m_3^2 + 4\,m_4^2 + 4\,m_6\,v_3\,cos(\theta_3)$$

$$M^2(5,6) = 4\,Y_7\,v_1\,v_2\,sin(\theta_1) + 8\,Y_8\,v_3^2\,sin(\theta_3)\,cos(\theta_3) - 4\,m_6\,v_3\,sin(\theta_3)$$

$$M^2(6,6) = -4\,Y_7\,v_1\,v_2\,cos(\theta_1) + 8\,Y_8\,v_3^2\,sin^2(\theta_3) + 4\,Y_8\,v_3^2 +$$
$$+2\,(Y_5\,v_1^2 + Y_6\,v_2^2) + 2\,m_3^2 - 4\,m_4^2 - 4\,m_6\,v_3\,cos(\theta_3).$$

For the neutralinos, in the basis

$$\left(-i\lambda_2, -i\lambda_1, \psi_{H_1}^0, \psi_{H_2}^0\right)$$

where λ_2 and λ_1 are the SU(2) and U(1) gaugino fields, $\psi_{H_1}^0$ and $\psi_{H_2}^0$ are the Higgsino fields, and ψ_N is the sfield corresponding to the N

field, the mass matrix is

$$Mn(1,1) = M_2 \qquad\qquad Mn(1,2) = 0$$

$$Mn(1,3) = -\frac{g_2}{\sqrt{2}}\, v_1\, e^{\theta_1}/\sqrt{2} \quad Mn(1,4) = \frac{g_1}{\sqrt{2}}\, v_2/\sqrt{2}$$

$$Mn(1,5) = 0 \qquad\qquad Mn(2,2) = M_1$$

$$Mn(2,3) = \frac{g_2}{\sqrt{2}}\, v_1\, e^{\theta_1}/\sqrt{2} \qquad Mn(2,4) = -\frac{g_2}{\sqrt{2}}\, v_2\, e^{\theta_1}/\sqrt{2}$$

$$Mn(2,5) = 0 \qquad\qquad Mn(3,3) = 0$$

$$Mn(3,4) = k\, v_3\, e^{\theta_3} + \mu \qquad Mn(3,5) = k\, v_2$$

$$Mn(4,4) = 0 \qquad\qquad Mn(4,5) = k\, v_1\, e^{\theta_1}$$

$$Mn(5,5) = -2\lambda\, v_3\, e^{\theta_3}$$

where M_2 is the SU(2) gaugino mass and M_1 is the U(1) gaugino mass. For the charginos, in the basis

$$\left(-i\lambda^{\pm}, \psi_{H_2}^{|}\right)$$

where $\lambda^{\pm}$ are the winos, and $\psi_{H_1}^{\pm}$ are the higgsinos[1], the mass matrix is

$$Mc(1,1) = M_2 \qquad Mc(2,2) = -\mu - \lambda\, v_3\, e^{\theta_3}$$

$$Mc(1,2) = \frac{g_2}{\sqrt{2}}\, v_2 \quad Mc(2,1) = \frac{g_2}{\sqrt{2}}\, v_1\, e^{\theta_1}.$$

---

[1]Note that $\psi_{H_2}^{+} = \left(\psi_{H_1}^{-}\right)^{*}$

Appendix C

Neutral Higgs boson mass matrix in the unitary gauge

In a general gauge the two neutral Higgs boson fields and the N field are defined as

$$H_1^0 = Re(H_1^0) + i\,Im(H_1^0) \tag{C.1}$$

$$H_2^0 = Re(H_2^0) + i\,Im(H_2^0) \tag{C.2}$$

$$N = Re(N) + i\,Im(N) \tag{C.3}$$

In the unitary gauge the two neutral Higgs boson fields are instead defined

$$H_1^0 = v_1\,e^{i\theta_1} + e^{i\theta_1}\,(S_1 - i\,(G\,cos\beta - A\,sin\beta)) \tag{C.4}$$

$$H_2^0 = v_2 + S_2 + i\,(G\,sin\beta + A\,cos\beta) \tag{C.5}$$

where S_1, S_2 and A are the two scalar fields and the pseudoscalar one respectively, and G is the Goldstone boson field. The N field does not play any role in this transformation, as the Goldstone boson is in the $H_1\,H_2$ sector.

We can then reexpress the imaginary and real parts of H_1^0 and H_2^0 in terms of S_1, S_2, G and A through the orthogonal transformation whose matrix is

$$P = \begin{pmatrix} A & B \\ B & C \end{pmatrix}$$

where

$$A = \begin{pmatrix} P(1,1) = cos\theta_1 & P(1,2) = -sin\beta sin\theta_1 & P(1,3) = 0 \\ P(1,2) & P(2,2) = sin\beta cos\theta_1 & P(2,3) = 0 \\ P(1,3) & P(2,3) & P(3,3) = 1 \end{pmatrix}$$

$$B = \begin{pmatrix} P(1,4) = 0 & P(1,5) = 0 & P(1,6) = cos\beta sin\theta_1 \\ P(2,4) = 0 & P(2,5) = 0 & P(2,6) = -cos\beta cos\theta_1 \\ P(3,4) = 0 & P(3,5) = 0 & P(3,6) = 0 \end{pmatrix}$$

and

$$C = \begin{pmatrix} P(4,4) = 0 & P(4,5) = 0 & P(4,6) = sin\beta \\ P(4,5) & P(5,5) = 1 & P(5,6) = 0 \\ P(4,6) & P(5,6) & P(6,6) = 0 \end{pmatrix}$$

in the basis

$$\left(Re(H_1), Im(H_1), Re(H_2), Im(H_2), Re(N), Im(N) \right).$$

The matrix P transforms the original 6x6 neutral Higgs boson mass matrix squared, M_6^2, into a 6x6 with the sixth colum and row made of noughts, M_5^2, i.e.

$$P^T M_6^2 P = M_5^2.$$

This transformation is necessary when the real couplings among neutral Higgs bosons (for example the ZhA coupling), given by the products of the corresponding physical eigenvectors, are required, so that the Goldstone boson component is rotated away.

Alternatively, one might work out the neutral Higgs boson mass matrix squared directly in the unitary gauge.

Appendix D

Diagonalization of squarks, sleptons and chargino mass matrices

The general squark mass matrix is

$$
\begin{pmatrix}
M_{11}^2 & M_{12}^2 \\
M_{21}^2 & M_{22}^2
\end{pmatrix}
$$

where the matrix elements are in our case, for the up squarks

$$M(1,1) = m_{Q_3}^2 + m_u^2 + \Delta_u \, , \qquad\qquad M(2,2)^2 = m_{\tilde{u}_3}^2 + m_u^2 + \Delta_{\bar{u}}$$

$$M(1,2)^2 = H_u(A_u v_2\, e^{i\theta_2} + \mu\, v_1\, e^{i\theta_1} + \lambda\, v_3\, e^{i(\theta_1 + \theta_3)}) \, , \quad M(2,1)^2 = M_{1,2}^*$$

where

$$\Delta_u = (T_3^u - Q_{EM}^u sin^2\theta_W)cos2\beta\, M_Z^2$$

and

$$M(1,1) = m_{Q_3}^2 + m_d^2 + \Delta_d \, , \qquad\qquad M(2,2)^2 = m_{\tilde{d}_3}^2 + m_d^2 + \Delta_{\bar{d}}$$

$$M(1,2)^2 = H_d(A_d v_1\, e^{i\theta_1} + \mu\, v_2\, e^{i\theta_2} + \lambda\, v_3\, e^{i(\theta_2 + \theta_3)}) \, , \quad M(2,1)^2 = M_{1,2}^*$$

for the down squarks, where

$$\Delta_d = (T_3^d - Q_{EM}^d sin^2\theta_W)cos2\beta\, M_Z^2.$$

135

This matrices are diagonilized by the unitary transformation

$$D_q^\dagger M_{\tilde{q}}^2 D_q = diag(\lambda_1, \lambda_2)$$

with

$$D_q = \begin{pmatrix} cos\frac{\theta_q}{2} & -sin\frac{\theta_q}{2}e^{-i\phi_q} \\ sin\frac{\theta_q}{2}e^{i\phi_q} & cos\frac{\theta_q}{2} \end{pmatrix}.$$

The phase θ_q is given by $tan\theta_q = \frac{2|M_{21}^2|}{M_{11}^2 - M_{22}^2}$ whereas ϕ_q is such that $M_{21}^2 = |M_{21}^2|e^{i\phi_q}$.

For the sleptons we have analogous formulas, with corresponding soft-terms. However, there are not right-handed neutrinos and s-neutrinos.

The chargino mass matrix is not hermitian, not symmetric and not real, so that two unitary matrices are required to diagonilize it, i.e.

$$U'^* M_C V^{-1} = M_D$$

with M_D diagonal but not real. The matrices U' and V satisfy the relation

$$V(M_C^\dagger M_C)V^{-1} = M_D M_D^* = U'^*(M_C M_C^\dagger)(U'^{*-1})$$

and can be taken to be

$$U' = \begin{pmatrix} cos\frac{\theta_1}{2} & -sin\frac{\theta_1}{2}e^{-i\phi_1} \\ sin\frac{\theta_1}{2}e^{i\phi_1} & cos\frac{\theta_1}{2} \end{pmatrix}$$

and

$$V = \begin{pmatrix} cos\frac{\theta_2}{2} & -sin\frac{\theta_2}{2}e^{-i\phi_2} \\ sin\frac{\theta_2}{2}e^{i\phi_2} & cos\frac{\theta_2}{2} \end{pmatrix}.$$

Writing $S_1 = M_C^* M_C$ and $S_2 = M_C M_C^\dagger$, the phases θ_1, θ_2, ϕ_1 and ϕ_2 are given by

$$tan(\theta_1) = \frac{2\sqrt{S_1(21)S_1^*(21)}}{S_1(11) - S_1(22)}$$

$$tan(\theta_2) = \frac{2\sqrt{S_2(21)S_2^*(21)}}{S_2(11) - S_2(22)}$$

and

$$tan(\phi_1) = \frac{Im(S_1(12))}{Real(S_1(12)}$$

$$tan(\phi_2) = \frac{Im(S_2(21))}{Real(S_2(21)}.$$

We can redefine the matrix U' so that the eigenvalues of M_C are also real; this is done multipling U' by the matrix H, so that we have now

$$U = H \times U'$$

with

$$H = \begin{pmatrix} e^{i\gamma_1} & 0 \\ 0 & e^{i\gamma_2} \end{pmatrix}$$

where γ_1 and γ_2 are the phases of the diagonal elements in M_D.

Bibliography

[1] D. Bailin, A. Love, Supersymmetric Gauge Field Theory and String Theory, Bristol: Institute of Physics, 1994.

[2] Mohapatra, R.N. Nath, Unification and Supersymmetry, The Frontiers of Quark-Lepton Physics, New York; London: Springer, 1986.

[3] J. Wess, Supersymmetry and Supergravity, Princeton, N.J., Princeton University Press, 1992.

[4] S.P. Martin, A Supersymmetry Primer, in "Perspectives on Supersymmetry", ed. G.L. Kane, World Scientific, 1998.

[5] P. Srivastava, Supersymmetry, Superfields and Supergravity: an Introduction. General Editor: D. F. Brewer.

[6] Supersymmetry, a decade of development, edited by Peter West, 1986.

[7] J. F.Gunion, H. E.Haber, G. Kane, S. Dawson, The Higgs Hunter's Guide, Frontiers in Physics, 1990.

[8] J.F.Gunion, H.E.Haber, *Nucl. Phys. B* **272**, 1 (1986).

[9] A. Pomarol, *Phys. Rev. D* **47**, 273 (1993).

[10] H. Nilles, M. Srednicki, D. Wyler, *Phys. Lett. B* **120**, 346 (1983).

[11] R.Arnowitt, P. Nath, *Phys. Rev. D* **46**, 3981 (1992).

[12] J.-M. Frere, D.R.T.Jones and S.Raby, *Nucl. Phys. B* **222**, 11 (1983).

[13] A.Barroso and J.C.Romão, *Phys. Lett. B* **158**, 51 (1985).

[14] N. Maekawa, *Phys. Lett. B* **282**, 387 (1992).

[15] T. D. Lee, *Phys. Rev. D* **8**, 1226 (1973).

[16] Y. Zeldovich, I. Kobzarev and L. Okun, Sov. Phys. JETP 40 (1974) 1.

[17] L.M. Krauss and Soo-Jong Rey, *Phys. Rev. Lett.* **69**, 1308 (1992).

[18] A. Pomarol, *Phys. Lett. B* **287**, 331 (1992).

[19] H. Georgi and A. Pais, *Phys. Rev. D* **10**, 1246 (1974).

[20] A.T. Davies, C.D. Froggatt and A. Usai, *Proc. of the Conference of Strong and ElectroWeak Matter*, 1998, World Scientific.

[21] J.C. Romão, *Phys. Lett. B* **173**, 309 (1986).

[22] A.T. Davies, C.D. Froggatt, G. Jenkins and R.G. Moorhouse, *Phys. Lett. B* **372**, 88 (1996).

[23] A.T. Davies, C.D. Froggatt and A. Usai, *Proc. of the International European Conference on High Energy Physics*, Jerusalem (1997), Eds. D. Lellouch, G. Mikenberg and E. Rabinovici , Springer-Verlag (1998),p891.

[24] D. Comelli, M. Pietroni and A. Riotto, *Phys. Rev. D* **50**, 7703 (1994).

[25] K.S. Babu and S.M. Barr, *Phys. Rev. D* **49**, 2156 (1994).

[26] Opal collaboration, CERN-EP-2000-055, April 25, 2000.

[27] Particle Data Group, July 1998, C. Caso et al., Springer.

[28] E. H. Thorndike, CLEO Collaboration, Proc. at XXVII Int. Conf. on High Energy Physics, Glasgow, Instituc of Physics, Bristol 1995. *Phys. Rev. Lett.* **74**, 2885 (1995).

[29] N. Haba, M. Matsuda and M. Tanimoto, *Phys. Rev. D* **54**, 6928 (1996).

[30] Asatrian H.M., Eguian G.K., Mod. Phys. Lett. A10(1995) 2943.

[31] T. Elliott, S.F. King, and P. L. White *Phys. Rev. D* **49**, 2435 (1994).

[32] N. Haba, 6th KEK meeting on CP violation and its origin (1998).

[33] Particle Data Tables, *Phys. Rev. D* **54**, 1 (1996).

[34] S. F. King and P. L. White, *Phys. Rev. D* **53**, 4049-4062 (1996).

[35] S. Dawson, Perspective on Higgs Physics II, World Scientific Publishing, 1997.

[36] M. Boonekamp, V. Ruhlmann-Kleider, Preliminary, DELPHI Collaboration, Paper submitted to the HEP'99 Conference Tampere, Finland, July 15-21.

[37] G. K. Yeghiyan, Acta Physica Slovaka 49 (1999) 823.

[38] G.L. Kane, C. Kolda, and J. D. Wells *Phys. Rev. Lett.* **70**, 2686 (1993).

[39] Asatrian H.M., Eguian G.K. Preprint hep-ph/9605458.

[40] M. Carena, J.R. Espinoza, M. Quiros and C.E.M. Wagner, *Phys. Lett. B* **355**, 209 (1995).

[41] The OPAL Collaboration, G. Abbiendi et al hep-ex/9809031.

[42] The OPAL Collaboration, hep-ex/9809031 30 Sep. 1998.

[43] S. Heinemeyer, W. Hollik and G. Weiglein, *Phys. Rev. D* **58**, 091701 (1998); *Phys. Lett. B* **440**, 296 (1998); Eur. Phys. J. C9 343 (1999).

[44] R.-J.Zhang, *Phys. Lett. B* **447**, 89 (1999).

[45] Harris et al., *Phys. Rev. Lett.* **82**, 904 (1999).

[46] I.S. Altarev et al., *Phys. Lett. B* **276**, 242 (1992).

[47] S. M. Barr, W. J. Marciano, CP violation, editor C. Jarlskog, World Scientific.

[48] A. Mahonar and H. Georgi, *Nucl. Phys. B* **234**, 1984 (.)

[49] S.Weinberg, *Phys. Rev. Lett.* **63**, 2333 (1989).

[50] M. Aoki et al., 6th KEK meeting on CP violation and its origin (1998).

[51] D.Chang, W.Y.Keung and A.Pilaftis, *Phys. Rev. Lett.* **82**, 900 (1999).

[52] R.Arnowitt, Jorge L.Lopez, and D. V. Nanopoulos, *Phys. Rev. D* **42**, 2423 (1990).

[53] R.Arnowitt and M. J. Duff, *Phys. Rev. D* **43**, 3085 (1991).

[54] J.Dai, H.Dykstra, R.G.Leigh, S.Paban, A.Dicus, *Phys. Lett. B* **237**, 216 (1990).

[55] J.Ellis, R.A.Flores, *Phys. Lett. B* **377**, 83 (1996).

[56] A.Bartl, T.Gajdosik, W.Porod, P.Stockinger and H.Stremnitzer, *Phys. Rev. D* **60**, 073003 (1999).

[57] S.Pokorski, J.Rosiek and C.A.Savoy, *Nucl. Phys. B* **570**, 2000 (8)1.

[58] E. Braaten, C.S. Li, and T.C. Yuan, *Phys. Rev. Lett.* **64**, 1709 (1990).

[59] Y.Kizukuri, N.Oshimo, *Phys. Rev. D* **46**, 3025 (1992).

[60] S. A. Abel, W. N. Cottingham and I. B. Whittingham *Phys. Lett. B* **370**, 106 (1996).

[61] T. Ibrahin and P. Nath, *Phys. Lett. B* **418**, 98 (1998); T. Ibrahim and P. Nath, *Phys. Rev. D* **57**, 478 (1998); Erratum ibid. **D58** 019901 (1998); T. Ibrahim and P. Nath, *Phys. Rev. D* **58**, 111301 (1998); Erratum ibid. **D60** (1999) 099902.

[62] M. Brhlik, G. J. Good and G.L. Kane, *Phys. Rev. D* **59**, 115004 (1999).

[63] H. Arason, D.J. Castaño, B. Kesthely, S. Mikaelian, E. J. Piard, P. Ramond, and B.D. Wright, *Phys. Rev. D* **46**, 3945 (1992).